POLITECNICO DI MILANO

School of Industrial and Information Engineering
Master of Science in Electronics Engineering
Department of Electronics, Information and Bioengineering

Development of an optogenetic stimulation system for bionic tactile prostheses

Supervisor: **Prof. Andrea Ivano MELLONI**

Co-supervisor: **Dr. Calogero ODDO**

Master thesis of:

Simone Scaduto

No.863762

Academic year 2017-2018

Abstract

In the last two decades, we have witnessed to the development of a new opto-genetic technology, that has given the possibility to manipulate neuronal cells with light. Precisely, optogenetics is a technique capable of activating or inhibiting the action potential of neuronal cells, genetically modified, by sending light to them at a given wavelength. Recent discoveries and developments of this technique, have highlighted new potential fields of use for the stimulation of the central nervous system, by means of optical stimulation of the peripheral pathways. The key to the development of this methodology lies on the advantages this technique has brought with respect to traditional electrical stimulation, such as: stimulation selectivity, bi-stable behavior (polarization and depolarization of cell), better biocompatibility and longer life time of the implanted prostheses.

This thesis presents (demonstrates) the development of an optogenetic stimulation system for tactile prostheses, with the aim of restoring the sense of touch to an amputated patient. This system includes: an artificial fingertip able to convert tactile stimuli into electrical signals, a real time module for acquisition and data processing in addition to an optical projection system, that makes use of DMD device (Digital Micromirror Device), for manipulating projection patterns. The innovative and unique part of this thesis is the development of an elaborated system for decoding tactile stimuli into neural opto-physiological signals and the design choice of using a MEMS device similar to the DMD, for the implementation of neuronal stimulator, able to project the required patters of light, in order to stimulate axons in peripheral nerves.

Characterization tests on the implemented optical setup and on the prototype have been carried out. In particular, we analyzed the system ability to differentiate different stimuli applied to the artificial fingertip. In addition, an in vitro experiment on cell culture has been performed, to demonstrate the potential use of this setup as a cell optical stimulator in optogenetic applications.

Furthermore, two new optical stimulator architectures system have been proposed, scaled to the anatomical dimension of the peripheral nerves associated with the sense of touch, presenting a first feasibility test and simulating the optical properties of the two models.

Sintesi

Negli ultimi due decenni, abbiamo assistito allo sviluppo di una nuova tecnologia opto-genetica, che ha dato la possibilita' di manipolare cellule neuronali con la luce. Precisamente, l'optogentica e' una tecnica capace di attivare o inibire il potenziale d'azione delle cellule neuronali, geneticamente modificate, inviando su di esse luce ad una determinata lunghezza d'onda. Le recenti scoperte e sviluppi di questa tecnica, hanno messo in evidenza nuovi potenziali utilizzi per la stimolazione del sistema nervoso centrale, attraverso la stimolazione ottica delle vie periferiche. La chiave di sviluppo di questa metodologia sta nei vantaggi che questa tecnica ha apportato rispetto alla tradizionale stimolazione elettrica, come ad esempio: la selettivita' di stimolazione, il comportamento bi-stabile (polarizzazione e depolarizzazione cellulare), migliore biocompatibilità e maggiore durata delle protesi impiantate.

Questa tesi presenta (dimostra) lo sviluppo di un sistema di stimolazione optgenetica per protesi tattili, con lo scopo di ripristinare il senso del tatto ad un paziente amputato. Questo sistema include: un polpastrello artificiale capace di trasdurre stimoli tattili in segnali elettrici, un modulo real time per l' acquisizione ed elaborazione dei dati e un sistema di proiezione ottico, che fa uso del dispositivo DMD (Digital Mircromirror Device), per la manipolazione dei pattern di proiezione. La parte innovativa ed unica di questo lavoro di tesi e' lo sviluppo di un sistema elaborato per la decodifica di stimoli tattili in segnali opto-fisiologici neuronali e la scelta progettuale di utilizzare un dispositivo MEMS simile al DMD, per l'implementazione dello stimolatore neuronale, in grado di proiettare specifici pattern di luce, con lo scopo di stimolare gli assoni dei nervi periferici.

Sono stati effettuati dei test di caraterzzazione sul setup ottico e di validazione del prototipo. In paricolare, abbiamo analizzato la capacita' del sistema di differenziare diversi stimoli applicati al dito artificiale. Inoltre, e' stato effettuato un esperimento in vitro su una coltura cellulare, per dimostrare il potenziale uso di questo setup come stimolatore ottico cellulare per applicazioni optogenetiche.

In aggiunta, sono state proposte due nuove architetture di stimolatore ottico, scalati alla dimensione anatomica dei nervi periferici associati al senso del tatto, presentando una prima prova di fattibilita' e simulando le proprieta' ottiche dei due modelli.

Contents

List of Figures

List of Tables

List of Acronyms

ISI: Interstimulus Interval

ChR2: Channelrhodopsin 2

DMD: Digital Micromirror Device

MEMS: Micro Electro-Mechanical Systems

NA: Numerical aperture

f/#: f-Number

NIR: Near Infrared

2P: Two photon

PNS: Peripheral Nervous System

FPGA: Field Programmable Gate Array

ADC: Analog to digital converter

FIFO: First In First Out

DMA: Direct Memory Access

RT: Real Time

DLP: Digital Light Processing

SOM: System on Module

FWHM: Full Width Half Maximum

PWM: Pulse Width Modulation

Ringraziamenti

Questo lavoro di tesi mi ha dato una grande opportunita‘ di crescita professionale e personale. Per questa ragione, vorrei ringraziare tutte le persone, che in un modo o nell’ altro, mi hanno guidato e sostenuto durante il mio percorso di studi, conclusosi con la stesura di questa tesi.

Ringrazio il Professor Andrea Melloni, per la sua disponibilita‘, professionalita‘ e per i suoi preziosi consigli.

Grazie al Professor Calogero Oddo, per avermi fatto conoscere il mondo dell’optogenetica, per l’aiuto che mi ha dato in questi mesi e per la conoscenza trasmessami. Un ringraziamento particolare va a tutti i ragazzi del suo laboratorio dell’Istitituto di Biorobotica del Sant’Anna.

Un ringraziamento, anche al Professor Mauro Tonelli e ai dottorandi del dipartimento di Fisica dell’Universita‘ di Pisa, per aver messo a disposizione il laboratorio e tutti i dispositivi per l’implementazione del setup ottico.

Grazie al Professor Leonardo Ricotti e a Federica Iberite del Laboratorio di Biologia del Sant’Anna, per avermi offerto la possibilita‘ di condurre esperimenti biologici con colture cellulari.

Grazie a tutti gli amici, che per mia fortuna ho conosciuto e con i quali ho avuto modo di condividere esperienze indimenticabili.

Infine, tutta la mia riconoscenza va alla mia famiglia, motore delle mia vita. Grazie Mamma e Papa‘ per avermi supportato, sopportato e dato tutto quello di cui avevo bisogno per condurre e portare a termine con serenita‘ i miei studi.

1 An Introduction to Optogenetics

This chapter presents the emergent Optogenetics technology on the border between genetics and optics able to manipulate neuronal cells with light. We would like to show how this latest technology can help in modern implementations of bionic devices, learning the knowledge needed to face the next challenges. Particular attention is given to the differences between electrical and optical stimulation and finally a brief summary on the innovations brought by this thesis work is presented.

1.1 Work goals and Optogenetics technique

Our work is devoted to the development of bionic prosthesis for regeneration of the sense of touch in patients without upper limb. To do this, we are going to combine two different techniques: the already used electrical tactile sense perception and the optogenetics stimuli delivery for neuronal cell stimulation. In particular, we deal with an electrical tactile sensor and an optical patterns projection system for peripheral nervous system stimulation. In this thesis work we have addressed the various critical issues of the problem, finding a solution that we considered optimal for our specifications. Furthermore, we implemented a linking protocol between the two technologies, developing an optogenetic stimulation system for bionic tactile prostheses.

Optogenetics is a technique able to stimulate and inhibit the action potential of neuronal cells. The responsible for cellular depolarization and hyperpolarization is a light-sensitive channel protein, injected genetically into the cell. A substantial introduction of the optical stimulation technology will be given in the next sections.

1.1.1 Light-sensitive channel protein

As already mentioned, those directly involved in neurons stimulation are light-sensitive channel proteins in the visible wavelengths, that are part of the first family of opsins, called microbial opsin type I. Three branches of this family have found utility in optogenetics [1]-[2]: the bacteriorhodopsins, an inhibitory proton pump able to expel protons to the extracellular space, the halorhodopsin, an inhibitory hydrochloric pump able to allow the passage of the chlorine ion inside

the cell, and finally the channelrhodopsin , cation-conducting channel that allows the depolarization of the cell thanks to the passage of positive ions inside it (see Figure 1.1.A). and The photon absorption isomerizes the retinal linked with the opsin protein (this structure is called rhodopsins) from the all-trans to the 13-cis configuration (see Figure 1.1.B). This excited state of the retina leads to the initiation of a series of physiological reactions, which cause the aperture of the channel and thus, the ions transport mechanism. After stimulation, the activated retinal associated with its opsin protein thermalizes to the all-trans state again, causing the closure of the channel. Unfortunately, this reversible reaction does not occur rapidly and it does not allow to achieve high frequency neuronal activity modulation [3]. Some of these proteins are ion selective pumps capable to pump ions even in the opposite direction to the gradient concentration, thus able to generate a drift current, instead, other are simple membrane channel protein that allow the transport of cations by natural diffusion due to the difference ions concentration between extracellular and intracellular environment, thus able to generate a diffusion current.

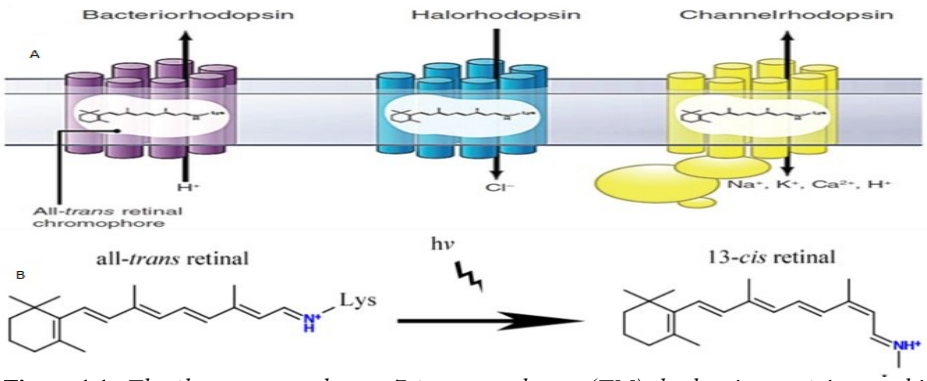

Figure 1.1: *The three mayor classes, 7-transmembrane (TM) rhodopsins proteins used in optogenetics*
(A) The left and the center protein are used for cell inhibition (proton pump), the last one is a light gated ion used for cell activation (cation-conducting). (B) Absorption of a photon excites the retinal from the all-trans to the 13-cis configuration, triggering a physiological process that makes possible ion conduction. From [1].

1.1.2 Transfection and cell membrane conductance modulation

It is important to understand how these proteins are expressed within the cell. Thanks to genetics evolutions, we are getting the possibility to apply the optogenetics technique on every part of the nervous system [4]. Different methodologies are used to transfect neuronal cells, depending on where transfection occurs.

Regarding the central nervous system, the opsin protein is encoded in biosafety viral vector and viral injected in the specific area of the brain (in vivo) or in a dissociated neuronal culture (in vitro). The promoter of viral vector is able to target a specific type of neuron cell. After targeting, in a couple of weeks, opsin is

expressed in the cell membrane, becoming an integral part of it (see Figure 1.2). Opsin are regenerated by the neuron forever. It is important to note, that the neuronal cell is already equipped with channel proteins used for natural conduction of ions. The difference between the two protein is that the opsin gives the possibility to be externally activate with light.

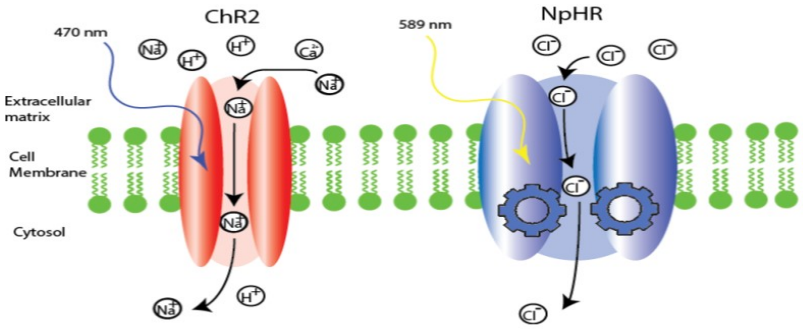

Figure 1.2: *Schematic illustration of ChR2 and NpHR in the cell membrane*
ChR2 is a gate for cations, the gradient between outside and inside the cell generate diffusion current. NpHR is a selectively pump ion chloride, able to pump ions against the gradient, generating a drift current. The two protein are activated at two different wavelengths. From [2].

In case of peripheral transfection [5], AAV6 viral vector is injected under control of the neuron promoter (specificity in targeting different neuronal cells) into the muscle of rats at distance of 10cm from the body of the neurons, delivering the ChR2 transgene to the corresponding neuron, thanks to a retrograde specific transport. In practice, the promoter can trace the entire neuron axon up to the cell body. The opsin gene will be processed and synthesized by both the body and the axon of the cell. The efficiency of retrograde transport is high (85% cells expressed ChR2) with really high specificity. The result is that ChR2 is strongly expressed long the nerve. Therefore, the Ranvier nodes of the axons (Myliated axon) can also be transfected by the photosensitive proteins (see Figure 1.3).

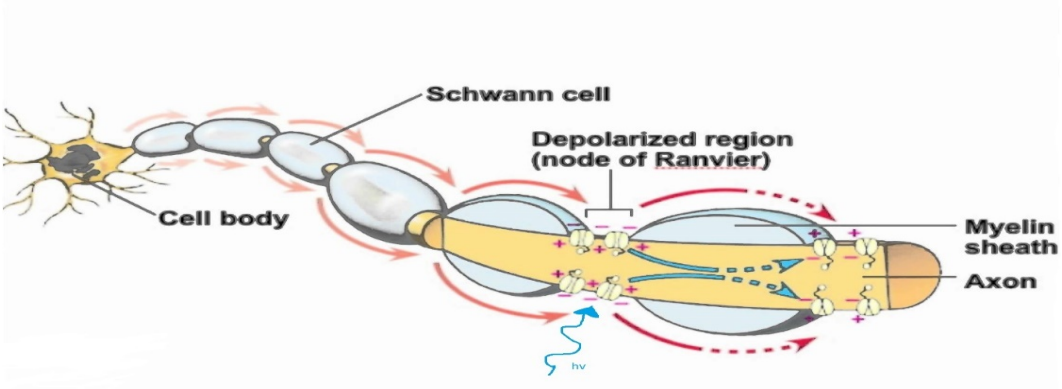

Figure 1.3: *Myliated axon*
The Ranvier node is the only region where depolarization can take place. In fact, myelin is an insulating material (lipid) that does not allow passage of ions. Note that, the Ranvier nodes contain ion channels as well as the neuronal cellular body also before transfection.

The different ions concentration between the internal and external cell environment provides a gradient and thus, a voltage drop on the membrane, called resting potential [6]. This potential can be calculated from the Nernst equation:

$$E_x = \frac{RT}{z_x F} ln[c_x^o]/[c_x^i], \tag{1.1}$$

where RT/z_x is the thermal voltage, R is the molar gas constant, T is the temperature in Kelvin, z_x is the number of exchanged charges (1 for, K^+, N_a^+ and C_l^-), and F is the Faraday constant. The superscripts "i" and "o" indicate the ion concentration inside and outside the cell, respectively. In case of neuronal cell, the resting potential is around -70mV. The electric time variant potential V_M on the cell membrane can be calculated by the Goldman–Hodgkin–Katz:

$$V_M = \frac{RT}{F} ln \frac{[K_o]P_K(t)+[Na_o]P_{Na}(t)+[Cl_i]P_{Cl}(t)}{[K_i]P_K(t)+[Na_i]P_{Na}(t)+[Cl_o]P_{Cl}(t)}, \tag{1.2}$$

As we can see, the ions concentrations are weighted with the magnitudes of their time dependent transmembrane permeability constants P. The permeability gives an estimation of how easily an ion can cross a unit area of a membrane driven by a one-molar difference in concentration; It is proportional to the number of open ion channels and the number of ions that each channel can conduct per second. The Optogenetics capability is the possibility to time modulate the transmembrane permeability constants P providing light to the cell. The modulation result gives a variation of the cell membrane potential. If this reaches a certain threshold value, the action potential is triggered. Figure 1.4 shows an electrical model of cell membrane expressed photosensitive proteins.

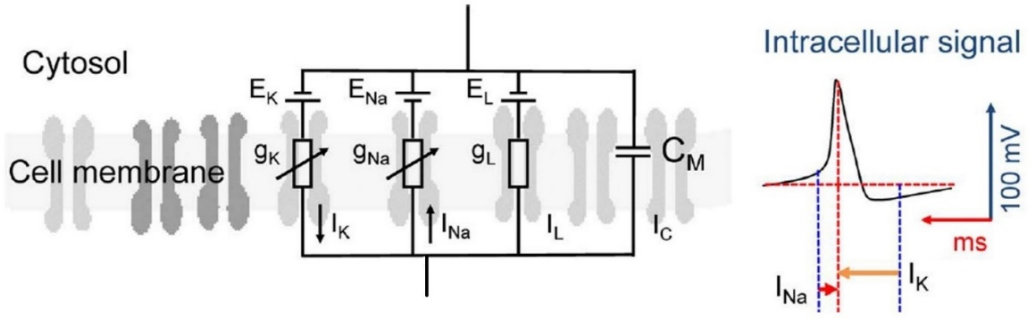

Figure 1.4: *Electrical model of membrane neuronal cell*
In the figure is possible to see the equivalent gradient potential electrical model and the time modulation of the conductance of the cellular membrane. Notice that, the trigger to the modulation is given with light stimulation of the channel proteins. I_L and g_L are the contributions of the minority ions. On the right, we can see the evolution in time of the action potential and the current involved in process. The stimulation is in the order of ms. From [6].

When the cell is stimulated with light, the channel proteins open a gate for the sodium ion diffusion current, with direction towards the inside of the cell. The cell

will be depolarized and this process allows the opening of channels that lead to an increase of the potassium conductance, thus favoring a potassium ion diffusion current, with direction towards the outside of the cell. In this way, the cell will be polarized and the equilibrium will be restored. After one cycle, new optical stimulation can be applied and action potential can be evoked again. The current formula involved in this process is:

$$I_M = C_M \frac{dV_M}{dt} + \sum_x I_x = C_M \frac{dV_M}{dt} + \sum_x g_x\,(V_M, t)(V_M - E_x), \tag{1.3}$$

where C_M is the membrane capacitance, and V_M is the membrane potential. The different ions conductance depends on time and membrane potential. The order of magnitude of the current is around hundreds of (pA). In few words, optogenetics is the trigger of the action potential in neuronal cell.

1.1.3 Absorption spectrum

As we have seen, we have different channel proteins, some of them are selective proton pumps, others are cation access ports to the cytoplasm of the cell. To stimulate each of these, light at different wavelength is needed (see Figure 1.2). This means that, if the same neuronal cell is transfected with proteins useful for activation or inhibition and if we have available the right light sources at different wavelengths, then we would have to be able to activate or deactivate the neuronal activity of the same cell. This is an important key point that makes optogentics also used as a pain-relieving therapy, using it as an inhibitor for high neuronal cells activity. The Figure 1.5 and Table 1.1 are going to give a complete overview on wavelength absorption and application of such proteins. It may also be curious to know the absorption cross-section of the retinal opsin. A detailed discussion of this topic can be found in [7].

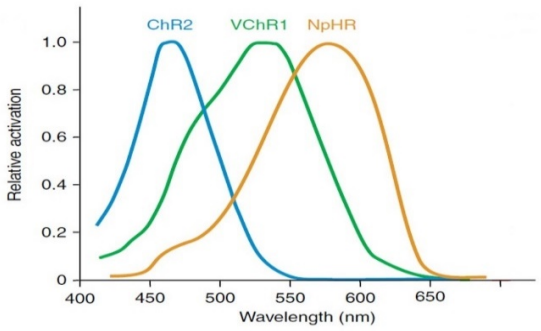

Figure 1.5: *Opsins absorption wavelength*
The picture shows the peaks and activation bands for the three main important photosensitive proteins, we are in the visible spectrum. From [10].

Opsin	Host organism	Wavelength sensitivity	Control Mode	Modulatory capabilities	Experimental systems tested
ChR2, ChETA	Chlamydomonas reinhardtii	470 nm (maximum activation)	Depolarizing	Rapid on/off, best used for precise activation of neurons on the millisecond timescale. Can be used to evoke single spikes or defined trains of action potentials over a range of frequencies	In vitro: dissociated neuron culture In vivo: C. zebrafish, chicken, mouse, rat, primate
VChR1	Volvox carteri	535 nm (maximum activation)	Depolarizing	Red-shifted action spectrum relative to ChR2. Similar to ChR2, VChR1 can be used to drive reliable action potential firing over a range of frequencies.	In vitro: dissociated neuron culture
NpHR, eNpHR	Natronomonas pharaonis	589 nm (maximum activation)	Hyperpolarizing	Light-activated chloride pump. Can be used to hyperpolarize neurons with high temporal precision; capable of inhibiting single action potentials within high frequency spike trains (up to 30 Hz). Also can be used to mediate sustained inhibition of neurons over many minutes	In vitro: dissociated neuron culture and mouse brain slice In vivo: C. elegans and mouse

Table 1.1: *Optogenetic proteins at glance*
The table describes almost the photosensitive proteins used for in vitro e in vivo optogenetics stimulation. From [8].

1.1.4 Temporal dynamic activation

Another important parameter to take into consideration is the temporal dynamics activation of neuronal stimulation. Neuronal activity is based on the generation and transmission of electrical signals called spikes with a certain temporal duration and with a time variant interval ISI (Interstimulus Interval) between them. In the worst case, the time duration between two spikes is in the order of a few ms. An analogy can be done between neuronal and digital signal. In both case the information is decoded in two levels 0 and 1 but in digital the transmission signal is segmented in clock period, instead, neuronal activity has, if we can say, an arbitrary clock period. What we would like to achieve is an optical stimulation speed of neuronal cells in the order of the natural temporal dynamics of neuronal activation. First generation protein synthesized for optogenetics experiments were slow and presented some artifact like: doublet of spikes due to a single photo-stimulation and missing spike after photo-stimulation occurred. Thanks to the genetics progress, we have now very fast and efficient proteins, that allow a real time stimulation of neurons with the same natural dynamics of the cells [9]. As already discussed in the section 1.1.1, the critical point to have a fast photo-stimulation response is the speed with which the retinal thermalizes from the 13-cis configuration to the all-trans configuration. Unfortunately, the closure of ions channels after photo-stimulation is still quite slow and it is the most inductive process involved during the stimulation, responsible for the prolonged depolarization of the cell. Genetic mutations have been made to achieve better performance and more reliability in the opsin protein and nowadays spikes train can be generated with frequency up to at least 200Hz (see Figure 1.6).

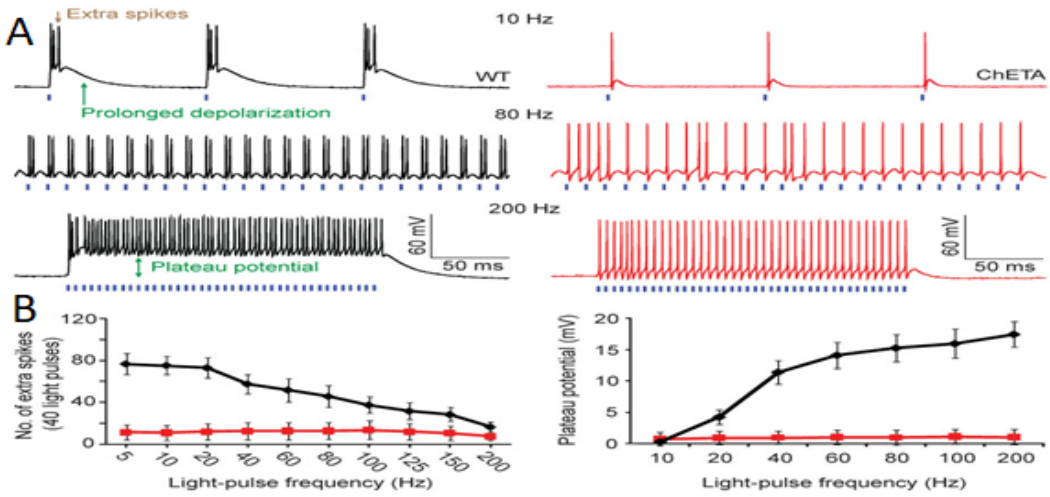

Figure 1.6: *Spikes generation with photo-stimulation*
(A) Comparison between two different ChR2 protein at different frequency stimulation. As we can see, for the genetic improved protein no double spike is present anymore and also depolarization effect is almost zero for all the stimulation frequency, blue dots indicate the photo-stimulation.
(B) The two graphs show the improvement with the last generation protein for the overall stimulation frequencies. From [7].

Improving the τ_{off}, hyperpolarization time, thanks to a fast thermalisation of the retina, optogenetics can achieve good result in terms of fast decay response, coming to imitate the natural speed of spikes generation.

1.2 Optical Stimulation Devices

So far we have seen what are the tools that allow the photo-stimulation of neuronal cells, how these are inserted into, what is their place once expressed and how they work. Now we are going to show which devices are used for the photo-stimulation of the body and axon of the neuron cell in vivo e in vitro. Regarding in vivo experiments, the stimulation devices are implanted and tested on animals like rats or primates, instead, for what concern the in vitro experiments, devices are used to optical stimulate cell cultures. Several works are carrying out studies on the stimulation of different parts of the nervous system. We are focus on the tactile regeneration and so, on the stimulation of the peripheral nerves but other people are working to regenerate the sight sense, the hearing sense and to study pathologies, discovering and analyzing neuronal circuits from every part of the brain. It is easy to understand how optogenetics can have many outlets on different problems that share the same medium, the neuronal matter. In the next subsections, we give an overview of which are the most used optical stimulation devices.

1.2.1 Optical fiber implant and Optoelectrode

One of the first method of analysis has been an optical interrogation of the brain, studying the behavioral state of the animals. To perform this experiment, the animal undergoes a surgical operation in which an iron cannula is implanted inside the skull. After a fiber is inserted inside the cannula, through an external laser source, coupled with the fiber, light is deliver at the wavelength desired for the optogenetic stimulation [1]. Same work has been done to stimulate the spinal cord circuits, even here surgery to insert a cannula into the spine has been done in order to bring the fiber closer to the vivo tissue of the nervous system [10]-[11]-[12].

To record spikes activity while opto-stimulation occurs, an electrode next to the fiber has been used. Unfortunately, this is not an efficient way to record physiological signals. In fact, unwanted interactions can occur and the electrode can also act as an obstacle to the light and thus, limit the volume of stimulated tissue. To overcome this problem, a new device has been developed, the opto-electrode. Different opto-electrodes are present in literature, two different design are the most important for in vivo and in vitro stimulation.

Regarding in vitro stimulation, an array of opto-electrode has been designed [8], giving the possibility to photo-stimulate the cell culture and to record the signal activity at the same time (see Figure 1.7). The light is coupled into the system by means of a grating coupler and with a waveguide is carried near the electrode. At the output of the waveguide, there is another grating coupler, used as an output gate for the light. Above the outputs couplers, there is the cell culture, thus in this way, opto-stimulation occurs from below. The light is provided by a Laser Led mounted on a moving platform in order to be displaced over each input grating, placed in the edge of the chip. The electrical recording is done with an electrode in TiN (Titanium nitride) with a diameter of 60µm, linked externally to the chip with a via of Al and the electrical signal is recovered by an external readout circuit. In this way, it is possible to do sequential photo-stimulation and electrical recording, without any interferences, on different parts of the sample.

Regarding the in vivo stimulation, a different device has been designed, to allow penetration in tissue [13]. In particular, a tapered needle composed of dual core is employed. One core is used as an optical channel (fiber) and the other hollow core is filled with an electrolyte to be used like an extracellular recording electrode. A layer of metal cover the external cladding of the fiber in order to provide an extracellular recording electrode (see Figure 1.8). With this device, it is not possible to have spatial modulation, in fact, only a given portion of volume can be optically stimulated and studied, making a local electrophysiology of the tissue.

To have the possibility of optically stimulate more points of the tissue, a new integration design has been done [14]. The cladding of a fiber has been removed on its termination and the core has been coated with metallic material not transparent to the light, leaving small windows (in the order of few micrometer side) without coverage, so that the light can come out and stimulate different region of the tissue.

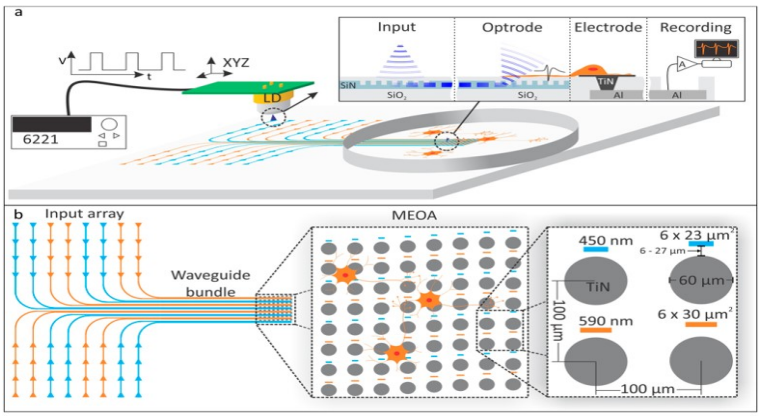

Figure 1.7: *Optoelectrode array for in vitro stimulation*
The width of the waveguides is different according to wavelength that travels through. Each electrode has a corresponding associated waveguide and the pitch between two different optrode is 100µm. The two different wavelength are used to activate and inhibit the culture cells. From [8].

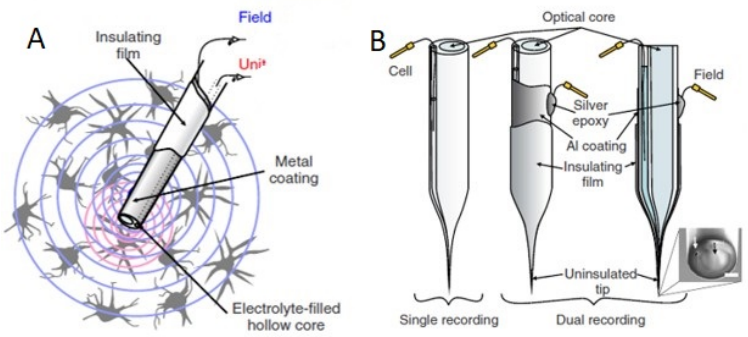

Figure 1.8: *Optoelectrode for in vivo stimulation*
(A) Show in detail the optoelectrode tip and (B) give three different large scale view of the same device. Extracts from [13].

1.2.2 Near-field wireless optoelectronics Led

In order to have the possibility to stimulate animals without any disturbance by hardware components that act as a link between the source and the optogenetic stimulator, wireless power transmitters and receivers are desirable to power up micro LED's implanted in the anatomic tissue. This technology opens the door for optogenetics experiments in which animals are able to behave freely while stimulation of the nervous system occurs [15]-[16].

This wireless system is able to produces sufficient light power for optogenetics stimulation. This type of device exploits inductive coupling in near field wireless power transmission. The RF power transfer is carried at frequency of tens MHz. The electrical interface [15] (see Figure 1.9.C) consists of a pair of metallic guides, shifted level and arranged in the perimeter of the stimulation area, connected to each other with a voltage generator, in order to generate a source electromagnetic field which will coupling to a separate RF transmission loop antenna operating at 13.56 MHz. The wireless system has an embedded circuit made by: a capacitor that provides impedance matching, a Schottky diode to rectify the received RF signals to yield a current source for the two LED's, the blue LED used for optogenetics stimulation and the red LED for signal of system activation. The portable system is also covered with PDMS to make it biocompatible for an in vivo implantation.

In [16] another work like this one has been made. The only difference is the integration capabilities of the system. In fact, an additional model adaptable to the stimulation of the peripheral nervous system have been designed The on board components are practically the same.

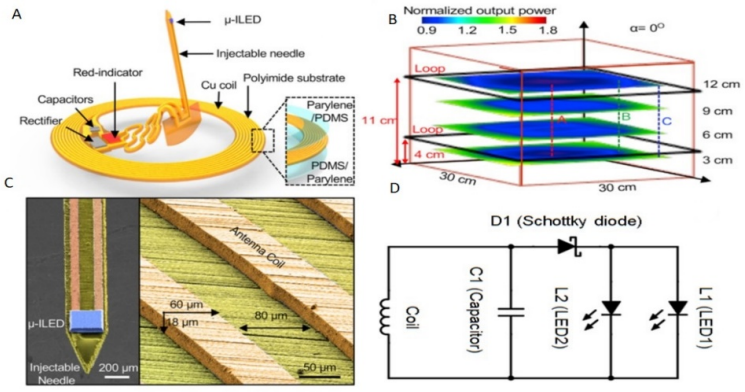

Figure 1.9: *Near-field optoelectronic system*
(A) Overall view of the portable system, PDMS covers the coil to make it biocompatible. (B) Electromagnetic power source is provided by two metal line linked together with a voltage generator with a carrier frequency of 13.56MHz. (C) Under Microscope view of the coil and μ-LED. (D) Circuit embedded on the portable system device. From [15].

1.2.3 Parallel patterns photo-stimulation using DMD

The need to optical stimulate different regions of the sample led to the development of new stimulation systems such as the opto-electrodes array, already seen in the previous section. Although, it has given this possibility, it does not allow a parallel lighting of the sample. As a matter of fact, with this device we can study different regions sequentially. Moreover, because of the diffraction of the output beam coming out from the waveguide, it is not possible to achieve a precise stimulation of the specimen.

The introduction of the DMD (Digital Micromirror device), as a tool for optogenetic stimulation, has led to exceeding these limits.

A DMD is an optical micro-electrical-mechanical system (MEMS) consisting of an array of aluminum micromirrors with (±12) degree tilt angle states. The DMD has bi-stable operation, allowing two stable micro-mirror states dependent on its geometry and the electrostatics force carried out from the electrodes. The DMD pixel is an opto element for the capability to determine the direction of the reflected light, acting like a spatial light modulator and a mechanical element for the physical structure that it has. The Figure 1.10.A shows a micromirror in the unpowered state. DMD chips are often used for high speed industrial, lithography, medical, and advanced display applications [17].

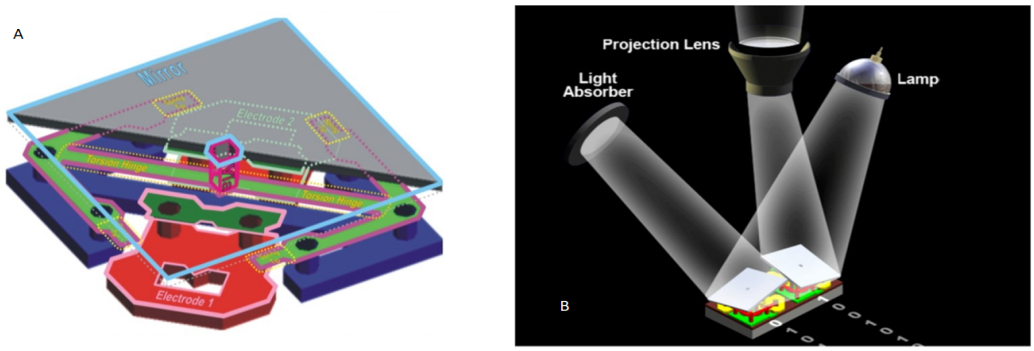

Figure 1.10: *DMD basic structure and operation principle*
(A) Illustration of DMD internal structure. A via supports the mirror on a torsion hinge, two electrodes generate electrostatic forces to allow the out of plane torsion of the mirror. (B) Operating principle of the DMD when the light affects with a certain angle and the two micromirrors are in the two different states, ON state light goes in the optical axis direction, OFF state light is absorbed and not transmitted. From [17].

Thanks to these powerful features, the DMD gives the possibility to project light patterns directly on the cell sample, simultaneously stimulating more regions. Since the light source is still a laser or a LED, also the temporal modulation is preserved. In [18], the DMD is used like a spatial multiplexer. The light reflected from different points of the DMD is coupled with different optical fibers implanted in the in vivo tissue. In this way, using a single light source, it is possible to spatially multiplex the light in more optical fibers, and thus stimulate multiple regions in parallel. In others works [19]-[20], the light reflected by the DMD is processed by an optical system, in order to be coupled with a microscopes, to study the effects of optogenetic stimulation through imaging.

The electrical recording of the optical stimulation using DMD is done with the help of two techniques: Voltage Clamp and Whole cell patch-clamp. Both technique exploit the variation of ionic concentration in extra and intra cell environment due to the photo-stimulation, recording ionic current involved in the process. Surely the use of DMD leads to more cumbersome and less portable setup compared to the integration of hybrid circuits that include the optical stimulation part and the electric cellular reading. In this thesis, we will see, how this device has all the potentiality, to be used as a stimulator for a peripheral nervous system.

1.2.4 Active and passive optical cuff

In here we are going to present two different stimulators device, both used for in vivo stimulation of the sciatic nerve in rats [5].

The first topology is an Active Optical Cuff made by 28 microLEDs attached to outside glass capillary pipette and externally wired to the power supply (see Figure 1.11.A). This device wraps the nerve (see Figure 1.12.) and send light from

longitudinal section without having the possibility to discriminate every single axon. The stimulator is arranged approximately at 10cm from the neuron body, almost at the same height as where the cell transfection took place. The amount of light sent is above the activation stimulation threshold. Thanks to the not toxic properties of the glass and of the PDMS materials, this device is completely biocompatible with the nerve. Furthermore, being the stimulator implanted externally to the nerve, this type of stimulation has the advantage to be less invasive than the traditional electrical one, where the electrode passes through the nerve section.

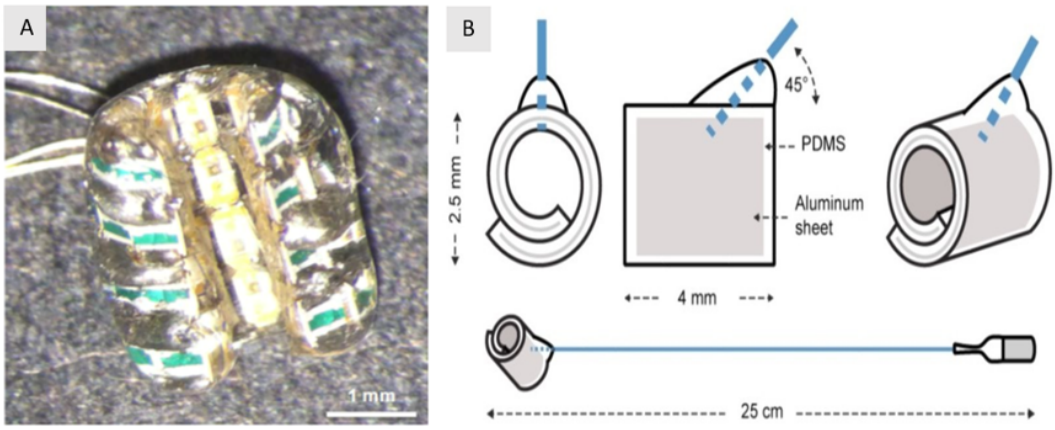

Figure 1.11: *Active and Passive Cuff*
(A) The Active cuff device is approximately long 2mm and 28 blue microLEDs are encapsulated inside a glassy material, making it a biocompatible system. (B) The passive spiral cuff is made in polydimethylsiloxane (PDMS), containing a sheet of aluminum, coupled with a silicon-based optical fiber in turn coupled with a diode laser source at 470nm. From [5].

The second topology is a Passive Optical Cuff made by a sheet of aluminum encapsulated inside PDMS material and coupled with an optical fiber at 45 degrees. Once the light guided by the fiber reaches the aluminum it is spread on the surrounding material and part of it is absorbed by the nerve (see Figure 1.11.B). The operating mode is the same as the active cuff.

The cuffs are wide enough to wrap a significant amount of Ranvier nodes in order to increase the stimulation probability. Both topologies illuminate all the nerve's bundles simultaneously, without any spatial discrimination. Nevertheless, time modulation is possible, indeed, light pulses are sent and muscle electrical activity is recorded to study how stimulation effects the animal.

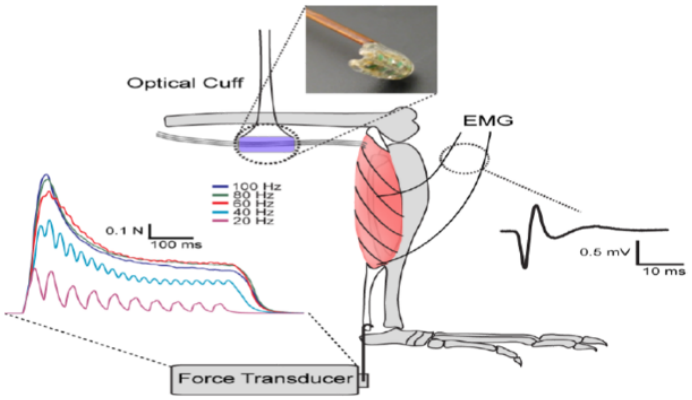

Figure 1.12: *Overall stimulation setup*
Nerve stimulation with an optical cuff (passive or active) and EMG (Electromyography) recording muscle. Train of pulse is sent at multiple frequency and transduction is done between EMG and strength developed by the muscle. From [5].

An interesting result came out from this experiment, the possibility of tuning the muscle force by changing the stimulation frequency.

These two works in the literature, give us the opportunity to experience a new stimulator, which has better characteristics than those already seen, adaptable to the sense of touch.

1.3 Light propagation in tissue

As we have seen in the previous section, most of the time, optogenetics technology has to deal with light propagation in tissue. In fact, almost all the methods of visualization of opsin-expression and optical stimulation of opsin channels are combined with matter and propagation through it. Actually, understanding how light propagate in the medium is very important.

Unluckily, we get attenuation of light during propagation in neural tissue due to medium absorption and multiple scattering [21]. The attenuation depends on the wavelength of light, smaller wavelength higher attenuation. Intensity of light at particular wavelength can be simulated using absorption and scattering properties. The Beer–Lambert (1.4) equation can be used to estimate light attenuation during propagation in tissue:

$$I(z) = I_0 e^{-\mu_t(\lambda)z}, \tag{1.4}$$

where I(z) is the light intensity after a distance z, I_0 is the initial light intensity before propagation, and μ_t is the extinction coefficient. This coefficient can be calculated

from the absorption and scattering coefficient in biological tissue, $\mu_a(\lambda)$ and $\mu_s'(\lambda)$, respectively:

$$\mu_t = \mu_a(\lambda) + \mu_s'(\lambda), \tag{1.5}$$

Both $\mu_a(\lambda)$ and $\mu_s'(\lambda)$ depend on the wavelength λ. It is important to note, that the scattering of light in tissue is anisotropic. It means that light will scatter with preferential angles. The value μ_s' takes into account also the anisotropic factor, g:

$$\mu_s' = \mu_s(1 - g), \tag{1.6}$$

Extinction coefficients and anisotropic factors for brain tissues (white and gray matters) are listed in Table 1.2.

Wavelength	Layer	$\mu_a\ (mm^{-1})$	$\mu_s(mm^{-1})$	g	n
480 nm	Grey matter	0.37	11.0	0.89	1.37
	White matter	0.35	43.0	0.8	1.37
590 nm	Grey matter	0.19	9.7	0.89	1.36
	White matter	0.19	41	0.83	1.38

Table 1.2: *Optical properties of in vivo tissue*
The table highlights the optical properties of white and gray matter both contained in the central and peripheral nervous system.
From [21].

In case of peripheral nervous system stimulation, such as the median nerve, we deal with white matter. In fact, the axons are coated with myelin, an insulating lipid coating of white color. Since we are trying to design a new optical stimulator for peripheral nerve, we performed the attenuation of the light intensity in the white matter.

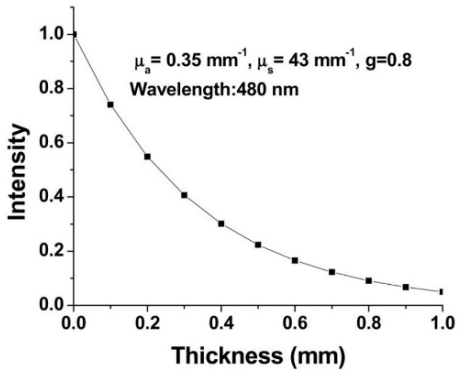

Figure 1.13: *Optical intensity attenuation in tissue*
The power decrease exponential with the propagation distance, absorption and scattering are taken into account.

As we can see from the Figure 1.13, after traveling through a depth of 1 mm, the intensity of the blue light beam is attenuated by 90%. This intensity decay is less, when light at higher wavelength is used for stimulation of targeted neurons (vChR1). Using light at visible range, it is possible reach neurons at larger depths by increasing the power light incidents in the tissue. However, this approach could significantly damage neurons closer to the source, especially for long-term stimulation studies. Light intensity of 100mW/mm^2 is safe for in vivo tissue [13].

An important parameter to know is the minimum intensity of light necessary to activate the action potential, by means of optogentics stimulation.

The expression density of photosensitive proteins depends on many factors and it is not easy to establish before transfection. Thanks to many measurements on whole cell conductance and cell membrane capacitance, an estimation has been done [22]. The result has shown an ChR2 expression density around 2000channels/μm^2. For neuron activation with same expression density, the threshold light intensity value to evoke the action potential is approximately 1mW/mm^2

From the result on light propagation, we have seen, that light with an intensity of 100mW/mm^2 reaches a depth of 1mm, from the point where stimulation take place, with an intensity of 10mW/mm^2. This shows that only a small region of the tissue receives light above the threshold intensity. Even the threshold is variable, dependent on: the type of stimulation protocols used, the stimulation duration and repetition rate. If light is sent to the tissue using optical fibers, we can make improvements, shaping the final tip of it and choosing different NA (Aperture Number), in order to get different angle of light propagation and increase the spatial resolution, but single cell activation is still far.

Nevertheless, recent optogenetics applications aim to study neuronal connectivity mapping, establishing the critical number of neurons that controls a specific behavior, investigating the spatio-temporal neuronal activity. The common characteristic of all these experiments is the need to have a more sophisticated lighting systems. Indeed, we need lighting precision on the single cell.

To obtain this specification, two-photon stimulation can give the right solution to the problem (see Figure 1.14) [23]-[24].

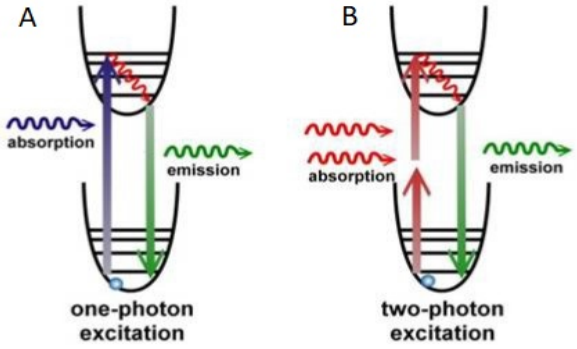

Figure 1.14: *1 and 2 photon fluorescent protein Band Diagram*
(A) Shows the band diagram of 1 photon stimulation opsin and (B) shows the band diagram of two photon stimulation. From [24].

This technique allows us to improve the penetration depth, through the use of longer wavelength and to enhance the axial resolution, due to the non-linearity of the two photon effect. In fact, while the single photon absorption is proportional to the light intensity, the two-photon absorption is proportional to the square of the intensity. Being a second-order effect with a low probability of stimulation, the resolution is intrinsically high, because it occurs only where photons intensity is very high and thus, in the beam waste of the incident light in the tissue.

The area affected by the stimulation is so small (sub cell size), that it does not allow the opening of a sufficient number of channels to reach the activation threshold. The reasons are the small conductance of a single membrane protein (40-80fS) [25] and low density expression of channel ¨protein (2000 channels/ μm^2) [26]. In order to increase the lightened volume, different techniques of light delivering are used, like: spiral scanning with low NA beam, parallel and scanning and parallel illumination with computer generated holography.

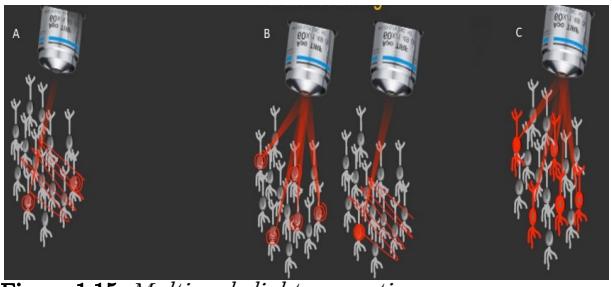

Figure 1.15: *Multi scale light generation*
(A) Laser spiral scanning with low NA beam, (B) parallel and spiral scanning, (C) parallel illumination computer generated holography. From [24].

Holography gives the possibility to modulate the wave front of the incident light beam, creating 3D interference patterns in the anatomical tissue. Since we need high power laser source in NIR, a femtosecond laser (mode locking) is required in order to generate really short pulse at high intensity photons. The power threshold required for two photon opsin activation is more or less (0.3-0.5mW/μm^2), much higher than power density threshold required for one single photon activation. Femtosecond laser are really expensive compare with the CW laser and no portable device at all.

Nevertheless, as we already said, two photon stimulation can penetrate deeper in the tissue making it less invasive for in vivo experiment (see Figure 1.16). Furthermore, millisecond temporal resolution and sub-millisecond temporal precision can be achieved independently on the opsin used. 2P-parallel illumination combined with fast opsin enables sub-millisecond temporal precision. Another advantage is the stimulation wavelength, being larger than that used for single-photon stimulation, it is also less toxic for neuronal cells. Future steps could be done to enhance the opsin expression density and conductivity, in order to stimulate single cell without use of femtosecond laser but using fiber laser, less expensive and more portable.

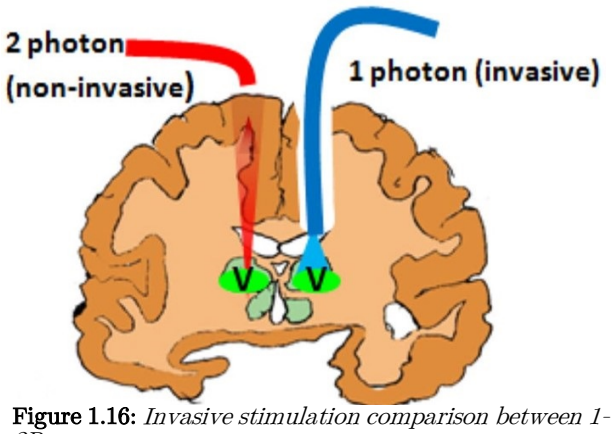

Figure 1.16: *Invasive stimulation comparison between 1-2P*
The possibility to penetrate more deep in the tissue for NIR radiation make 2P stimulation less invasive. From [21].

1.4 Optogenetics advantages versus Electrical Stimulation

In the previous sections, we have introduced the tools to understand how optogentics works, how it is currently used in experiments in vivo and in vitro, what are the critical aspects and what they will be the directions to improve the whole technique. Now, we would like to highlight what are the advantages brought by this technique, comparing it with traditional electrical stimulation. A list of critical points shows the superiority of the optical stimulation.

- Specificity

The electrical stimulation is able to excite a neuron thanks to an exchange of electric charge between electrode and the external ions surrounding the cell. Charge exchange on a fairly large volume may pose a risk for the activation of other neurons close to that area and thus, single neurons selectivity is not preserved anymore. Instead, optical stimulation has the only function to activate channels protein able to conduct ions between the intra and extra neuron environment, and consequentially, to trigger the action potential of the single cell that receive light at a certain wavelength. Furthermore, having the possibility to activate channel proteins at different wavelengths, we can stimulate selectively more neurons, illuminating them with light at different frequencies. Surely there will be a correlation between the stimulation of individual neurons but this is a field of interest for neuroscience and for those who study neuronal networks.

- Bi-stable Modulation Function

Another important characteristic that distinguishes optical with electrical stimulation is the bi-stable behavior of the photosensitive proteins. As said for the specificity, electrical stimulation is based on a charge exchange between the external cell environment and the electrode, thus only neuronal excitation is possible and not de-excitation. Instead, with the optical stimulation we have the possibility to do both the operation. As we have already seen, we have more than one type of photosensitive proteins able to depolarize or polarize the cell, activated at different wavelengths of light. This means that, if the same neuron is transfected with photosensitive proteins having this features, illuminating it with light at two different wavelengths, it is possible activate or inhibit neuronal activity of the cell.

- Side effects and biocompatibility

Most of the time, an electrical stimulation is provided thanks to the intra-fascicular implanted electrodes inside the nerve. This is a really invasive surgery and the nerve can be finally damaged. Moreover, if the amount of charges sent to the nerve are too many, the patient can perceive pain, like a shock sensation.

Someone is trying to design new electrodes less invasive and more biocompatible for the human body but that is still a challenge and many studies are going for that. The invasiveness of the optical stimulation depends on the area in which the stimulation occurs. In peripheral system (see 1.2.4), optical stimulation is certainly less invasive than electrical one. Furthermore, optical stimulator can be covered by biocompatible materials like PDMS or glass (insulators), making them not toxic for the human body. Also the shock sensations are less.

- Duration and stability

Inserting an electrode inside the nerve can lead to electrical instability. The organism could consider the electrode as a foreign object and consequently, acts defensively on this, isolating it from the organic matter of the nerve itself. This biological phenomenon can bring to time variant impedance. It means that, a periodically manual tuning of the amount of charges sent to nerve has to be done. If the electrode, somehow is not biocompatible at all, it could be completely isolated and charges transport is not perceived anymore. Instead, optical stimulation does not take into account matching impedance over the time, indeed, the responsible for activation is light and not charges. Moreover, once the neuronal cells are transfected, the protein expression will always be an integral part of the cells, that can open an ethical discussion on optogentics. Nevertheless, other challenge has to be face, most of them are deal in this thesis work other of them are going to be the continuation for future works.

1.5 Contribution and Summary of thesis work

In this last section could be interesting make the reader understand what are the contributions given by this thesis, presenting a brief summary of what has been done. This thesis work has led to the design and development of a completely new model of prosthetic regeneration of touch sensation for amputated patients. This system includes the sensing of tactile stimuli, data processing and decoding of neuronal signal and the design of a new model of nervous optical stimulator, based on the activation of neuronal cells, through the use of the optogenetics technique. All the scientific materials introduced in this chapter have been studied, in order to obtain the project specifications of our system. In particular, two works make this thesis innovative and unique, the development of a new neuronal decoding signal and the design choice of using MEMS devices for the implementation of neuronal stimulator.

Regarding the signal conditioning, the electric tactile stimulus signal coming out from an artificial fingertip has been decoded into a physiologic signal suitable for neuronal stimulation and then, based on that information, patterns of light are

consequently generated and projected, with the aim of stimulating a precise site of the nerve.

Acquisition and decoding of the electrical signals is developed in FPGA and Real Time Module and patterns generation is managed at a high level, computer station.

Concerning the development of the optical setup for pattern projection, we have studied and assembled modern components, like light-interacting MEMS devices, in order to obtain an unscaled demonstrator of peripheral nervous system stimulator.

Characterization tests have been done on it. In addition, we performed validation tests of the whole prototype, analyzing the results and opening new horizons for further development and study that will lead to a scaled stimulator model and self-sufficient prostheses for the sense of touch.

In addition, we designed two new models of optical stimulator for peripheral nervous system, demonstrating the feasibility of prototypes. Further simulation on the optical properties of the devices have been performed.

Therefore, this thesis work includes: an electronics part for the conditioning of analog signals, data acquisition and processing on Real Time module, high level software management, active study and use of modern devices, dealing also with their management software, development and characterization of an optical setup, processing and data analyze.

Finally, we can say that this thesis has developed a powerful system of tactile prosthesis facing challenges and opening the road to future goals, like scale down the dimensions comparable with the anatomic size and reduce power consumption. The next chapters explain in detail what has just been introduced.

2 Tactile Prosthesis Design

In this chapter, we present two new design of peripheral nerve optical stimulator, that could be used to restore tactile sensation to an amputee patient. We also provide in detail, the specifications and the criteria, followed during the project. Next, we move on to introduce all the devices used to implement an innovative tactile prosthesis system. Moreover, we illustrate all the procedures for the implementation of an optical setup, that has been used to characterize and validate the system. Finally, we show the applied neuronal model to simulate neurons activity.

2.1 Proposed architectures for peripheral nerve stimulator

So far, we have seen how optogenetics technique is used to stimulate neuronal cell from the body and the axons (see section 1.2). This last possibility opens new scenarios and applications for peripheral nervous system stimulation [4].

Since we are interested to rehabilitate the tactile sense of an amputee patient, these last new evolutions are giving us the possibility to think to a new implementation of optical stimulator, suitable for the median and ulnar nerves, which are the responsible for neuronal signal transmission from the mechanoreceptors of the hand to the first order neurons, located in the spinal cord.

This new approach leads us to face new challenges, such as:

1. How to get an optical spatial resolution in the order of axon diameter to illuminate each individual axon in the nerve (single neuron excitation).
2. Which type of electric tactile sensor to couple with the optical stimulator.
3. How to decode tactile sensor electrical signals into neural opto-physiological signals.
4. System integration (portability).
5. Safe surgery (less invasive).
6. No toxic for longer implantation duration (biocompatibility).

Axon stimulation probability depends not only on the density of the photosensitive proteins expressed but also on the physical conformation of the axon and how light is sent to the nerve. Indeed:

- Small diameter axons have Ranvier nodes much closer one of each other and they have a higher probability to be stimulated than the axons with a big diameter.

- Stimulation probability increases, if the distance of light source respect to the axon decreases and if many Ranvier nodes receive light.

The stimulation selectivity, given by optogenetics (see section 1.4), could be a benefit to confine resolution problem to the only nerve bundles. As a matter of fact, the possibility to use different neuron promoters, able to transfect different neuron cells, allows the activation of the photosensitive proteins at different bandwidth of light. Moreover, the possibility to transfect axons neurons at 10 cm (see section 1.1.2) distance from the cell body, makes this technique less invasive and safer for a future direct application on amputee patients [5].

Before moving forward in proposing new topologies of stimulator, it is necessary to define the specifications of the project that were our guidelines for the tactile prosthetic design.

Here the list:

- Spatial Resolution in the same order of the axon diameter, single neuron excitation (5÷15)μm [27].
- Stimulate one or more than one axon simultaneously, Spatial Modulation.
- High temporal resolution in the order of neurons temporal spikes activity, few milliseconds.
- Possible closest distance between stimulator and nerve.
- Focusing light to go deeper in the medium and avoid scattering.
- Signal decoding from electrical to neuronal (Izhikevich model).

In order to match most of these specifications, we have designed a couple of new possible optical peripheral nerve stimulator topologies for tactile sense restore. The two topologies presented in the next section are integrated with calculations and simulations. The physical realization of these two stimulator can be developed in future works.

2.1.1 Longitudinal DMD stimulator

Trying to comply with the specifications given in the previous section, we have developed a type of stimulator, which use the DMD as main device (see section 1.2.3). Indeed, it gives the possibility to get at the same time spatial-temporal modulation and high optical spatial resolution, projecting different patterns of light on the nerve.

Since the transversal section of the severed nerve of an amputated patient is closed, the most efficient way to access into it, is from its longitudinal section. This explains why the DMD is placed laterally (see Figure 2.1). A light source incident with a precise angle ϑ_i on the DMD chip is needed and it can be provided from outside (Fiber-Coupled Laser source) or internally generated (LEDs). Our model exploits the first possibility. From Figure 2.1, we can see, how a multiple outputs optical fiber [14] is inserted inside the system with a certain angle, so that ϑ_i remains fixed at a certain value. Of course, the fiber angle depends on the output light emitted angle. Another possibility can be the generation of light, internally, by a matrix of LEDs. The light reflected by each single micromirror is sent to the nerve with the goal to stimulate single or multiple axon, in order to activate tactile stimuli to an amputee patient. The reflection angle ϑ_r depends on the tilt DMD angle.

The nerve-DMD coupling could be settled in two ways. First idea (see Figure 2.1), less invasive, is simply send the reflected light by DMD micromirros towards the nerve, illuminating only a part of its section, with a certain depth. The second idea, more sophisticated and more invasive is coupling the DMD with a matrix of opto-needles with different length able to penetrate the nerve in different points. The light reflected by DMD coupled with this matrix is guided into the nerve to reach a specific stimulation point. This gives us also the possibility to go deeper in the tissue and thus, get higher stimulation probability and higher spatial modulation.

Optionally, an absorber is placed below the DMD, in order to absorb the light not sent to the nerve and the DMD wires are taken out from the same insert of the fiber. The DMD data could be also transmitted wireless. Everything is mounted in a glass support and covered by PDMS material in order to make it biocompatible and safe for the patient.

The DMD can stimulate multiple Ranvier nodes of the same axon, with high spatial resolution. Being positioned in the transversal section, it can physically illuminate a broad region of nerve, thus increasing the stimulation probability. The possibility to tune the optical output power of a Lasers Led, allows to modulate the penetration depth of the light and thus, to select the number of axons to be stimulated. In order to access to other regions of the nerve, many of these systems can be arranged circularly around the perimeter of the nerve, ensuring a complete stimulation of it.

Nowadays, electronics technology is going to really high speed processing and generate multiple pattern in a short period of time is something already possible, most likely, a dedicated ASIC will be designed to optimize the performances and make the whole system design smaller. All that will give us the possibility to have

a fast device, able to generate high frequency patterns (high spatial-temporal modulation) with excellent resolutions, limited of course, by diffraction.

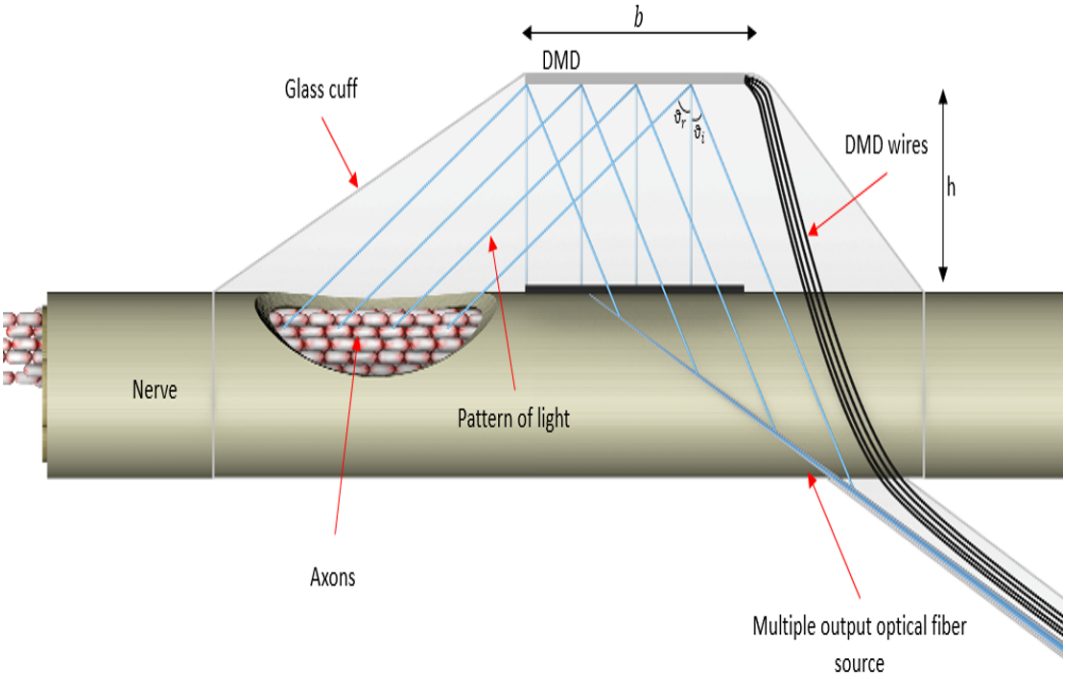

Figure 2.1: *Longitudinal DMD Nerve Stimulator*
In the figure is represented the longitudinal nerve stimulator coupled with the median nerve. All the components are encapsulated inside glass and polymeric material. Also the nerve is inside the box and everything is fixed thanks to anchor points with the surrounding muscles. A fiber brings the light internally with a certain angle of incidence with the DMD. Light should be spread on the overall DMD area thanks to its dispersion. DMD is powered and data transfer is given by external wires. A Diode Laser at 470nm light source and a digital logic circuit control for DMD are required externally to the system.

The stimulator size should be scaled down to fit the size of the nerve. Usually the median nerve cross-section is around (9-12)mm^2 [28], with a diameter around 2mm. If we consider an incident light angle ϑ_i= 24° and a DMD tilt angle of 12°, the reflection angle is ϑ_r=48° (Snell Low). Assuming to have a DMD long b=10mm, the stimulator height is h=9mm. These dimensions allow a possible integration of this device for real application.

A focusing optics has to be internally arranged along the optical way to reduce resolution problem given by diffraction. Another possibility could be hologram pattern generation by the DMD. As a matter of fact, the DMD has the capability to reshape the wavefront of the incident light and to perform a real time focusing through a scattering medium.

2.1.2 Piezo-fiber squeeze stimulator

In this new topology of PNS, we are able to focus light and tune real time, the focal length of the fibers. In fact, as we can see from Figure 2.2.A, a glass ring structure grabs the nerve, and multiple glass fibers are inserted inside cannulas. Each fiber tip is already lens shaped. This form of the fiber tip allows to focus the outgoing light at a certain distance and thus, to stimulate the region of the nerve subtended by the fiber. Furthermore, since the fiber is coupled with a laser able to generate light pulses, high temporal modulation can be achieved without any problem.

To obtain spatial modulation, something more could be added to the system. Inside the cannula a pair of piezoelectric device could be implanted. When high voltage is applied to piezoelectric, the mechanical displacement of them squeezes the fiber in the middle, changing the radius of the lens on the tip and thus, also the fiber focal length (see the green and blue light in the Figure 2.2). The presence of multiple fibers and piezoelectric elements, along the circular section of the nerve, consents the access on different nerve sites. This feature can be exploit, to spatial modulate the optical stimulation. By tuning the optical power laser of the gives us also the possibility to control the penetration depth in the medium.

In order to illuminate more Ranvier nodes, many of that systems can be placed in parallel along the longitudinal section of the nerve (see Figure 2.2.B). Mismatch of optical fibers and mechanical system can give problems in the specificity of the stimulation. Furthermore, high voltage should be applied for the mechanical displacement of the piezoelectric device and that is not safe for the patient. A good isolation and alignment can definitely improve the system performances.

For this topology, we would like to integrate a simulation of how light propagates in nerve tissues. A model presented in [29]-[13] is used to describe how the outgoing light from a non-shaped fiber tip spreads in the matter, also taking into account absorption and scattering. A MATLAB script has been implemented to perform exactly the formulas involved in the model (see Table A.1: 2D Irradiance Profile Simulation, Appendix). Considering that, we can get 100μm displacement from piezoelectric device, applying a voltage around 30V, we could obtain a variation of the fiber radius in the order of 100μm. Though there are two piezo that squeeze the fiber, we supposed, that half displacement will affect the cannula and other half the fiber. The simulation is performed using a multimodal fiber with diameter of 200μm and NA=0.22. The light propagation occurs in a medium with refractive index n=1.36. The Figure 2.3 shows the irradiance profile (first Gaussian mode) of light coming from fiber with different core radius. What comes out from simulation is the possibility to modulate the light intensity spatial distribution, giving us the possibility to stimulate different nerve sites. Reducing the fiber diameter, light propagation distance decreases (28% @600μm distance, with 50% of fiber radius variation) due to the scattering and divergence.

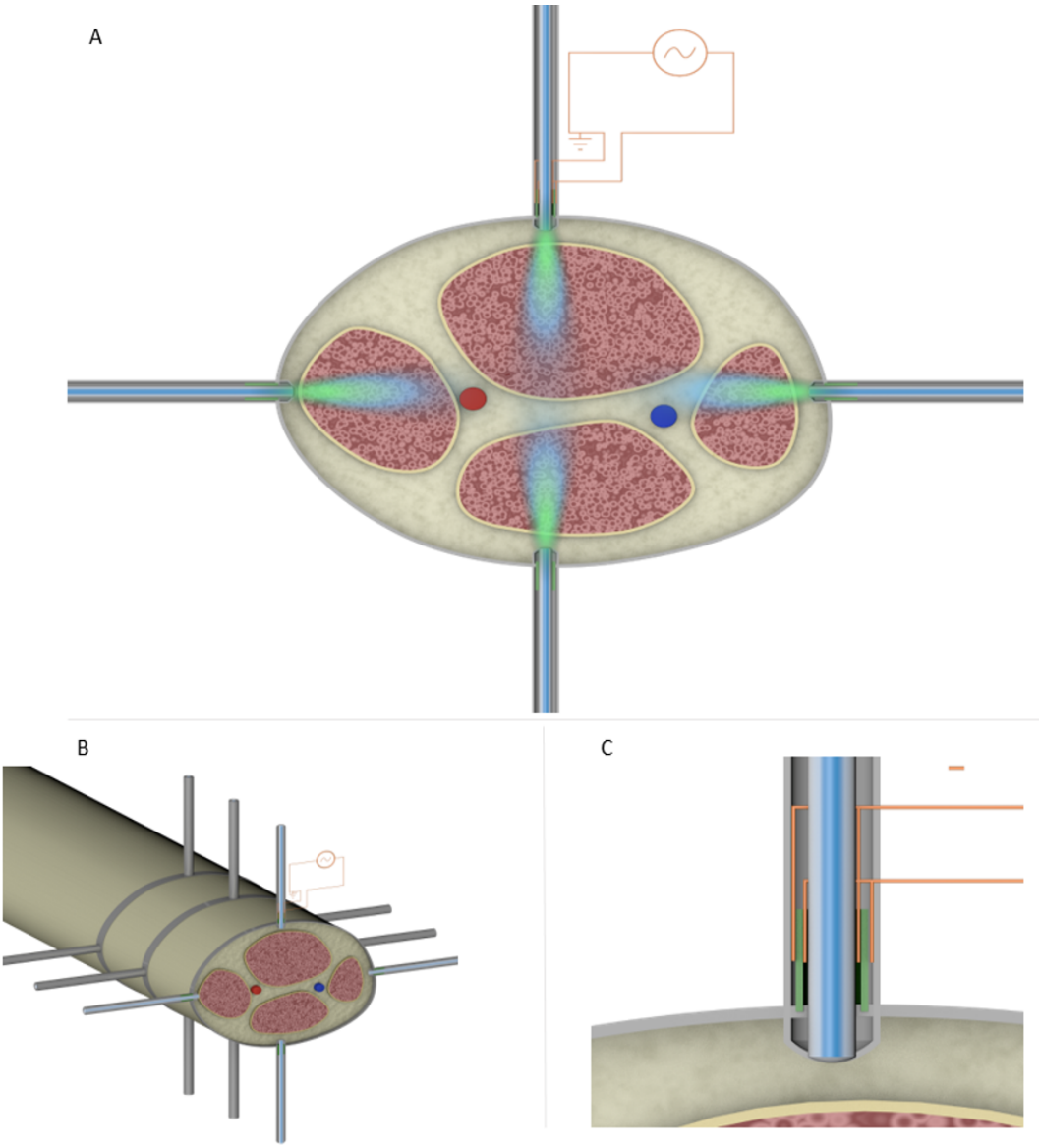

Figure 2.2: *Piezo-fiber squeeze Nerve Stimulator*
(A)The figure shows a model of piezo transversal nerve stimulator. The stimulator with a glass structure wraps the nerve and thanks to a cannula the optical fibers are inserted up to the nerve membrane. An electric piezoelectric system device driven by external voltage generators squeezes the fiber changing the focal length. An external laser as a light source and a controller chip for the piezo is needed. (B) Parallel model, to increase stimulation area and spatial modulation capability. (c) Zoom view of how piezo and fiber are arranged inside the cannula.

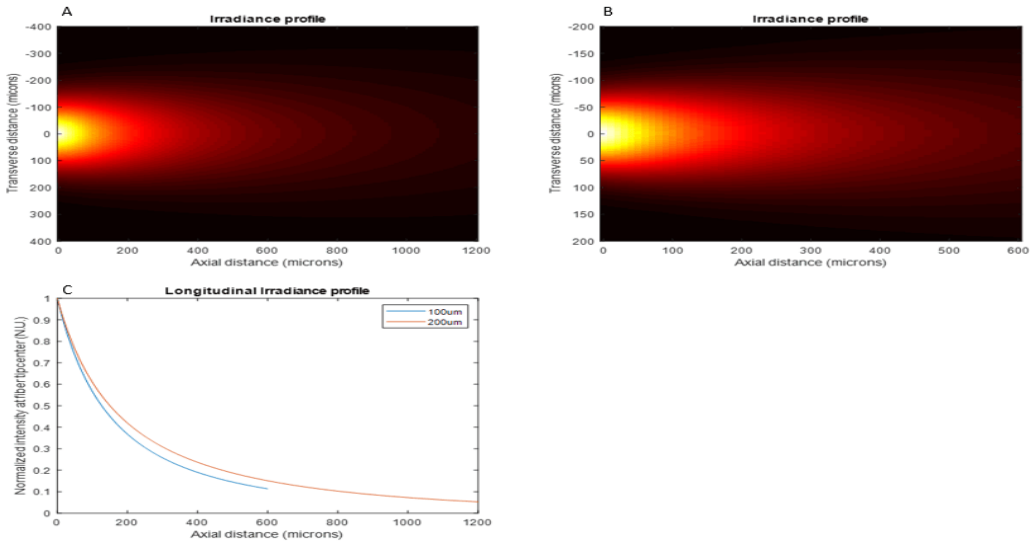

Figure 2.3: *Absorption and scattering light profile in the medium*
(A) Irradiance profile in the medium n=1.36, light coming from fiber with core diameter d=200µm. (B) Same of (A) but light coming from fiber with core diameter d=100µm. (C) Longitudinal irradiance profile in both case.

We also want to give a brief demonstration, of how electromagnetic energy causes an increase in temperature in the biologic tissues. Thermal transfer occurs according to the properties of the radiation model. From [30], we got the relationship between the optical power and the temperature gradient in the tissue:

$$q(x) = -kA\frac{dT}{dX}, \tag{2.1}$$

where q is the constant optical power, k the thermal conductivity of the tissue, A the cross-section of the incident beam with the matter and dT/dX the temperature gradient. From the section 1.3, we know that the light intensity propagation decays exponentially in the tissue. Considering the scattering coefficient equal to zero and taking into account the only absorption coefficient, we can write the optical power propagation like:

$$q(\mathrm{x}) = q_0 e^{-\mu_a(\lambda)x}, \tag{2.2}$$

where μ_a is the absorption coefficient and q_0 the initial optical power provided to the tissue. Replacing the (2.2) equation in the (2.1) and integrating for the temperature and the propagation axis (infinitely extended object) we get:

$$\Delta T = \frac{q}{\mu_a kA}, \tag{2.3}$$

where ΔT is the temperature variation of the tissue when constant optical power (q) is provided.

Since we want to get the tissue temperature variation given by our stimulator, we need to find the right values to insert in the (2.3) equation. From Table 1.2 is possible to obtain the absorption coefficient for white matter, μ_a =0.35mm^{-1} at 470nm. From [31], it is possible to get the thermal conductivity for hypodermis layer, k=0.69Wm^{-1}°C^{-1}. Regarding the cross-section A, it is a good approximation consider it equal to the cross-section of the fiber used for the previous simulation.

Therefore, A=0.031mm^2, calculated as the area of the radius circle equal to 100μm. Concerning the power q, a brief discussion has to be done. From section 1.3, we know the attenuation of the light propagation (90%@1mm) and the minimum threshold of light for optogenetic stimulation(1mW/mm^2). If with our system, we would like to go deeper in the tissue until 1mm, assuring photosensitive proteins activation, the initial intensity should be q_0=10mW/mm^2. Since we send pulse of light, (to mimic neuronal stimulation activity), we should perform an average on the instant power, in order to get the mean power value of light delivered to the nerve. To perform this calculation, we considered the worst case condition, that arises, when high frequency pulses of light has to be sent to the nerve. From [32], we got the information needed to compute the duty cycle of the spikes neuronal activity in this condition (D=8.87%). Thus, the mean power value q is equal to the pulse power multiplied by the duty cycle. Performing this calculation, and inserting all the values in the equation (2.3), we get a ΔT=3.35°C. From [33], we can see that the maximum temperature variation, before the patient perceives pain is 8-9°C. Therefore, we can say that our system is able to provide pulse of light at the highest spikes rate frequency, without pain perception from the patient. Of course, with the genetic progress the activation threshold is going to be lower and thus also the required power will be reduced. Consequently, also the temperature variation will decrease.

2.2 Employed devices for tactile prosthetic design

After we have shown two new possible topologies of PNS stimulator, we can move on and present all the materials involved in the design of an experimental tactile prosthetic for optical stimulation of the peripheral nerves. The optical part of the system approaches the stimulator model presented in the section 2.1.1. The overall system includes the electrical tactile sensor, neuronal signals decoding and opto-neural signals projection.

Being a fairly large and complex system that includes both a hardware and computational design, we try to divide it into small parts and eventually put them all together to create a final completed setup. Designing an artificial touch system, we have integrated all the components needed to achieve this goal (see Figure 2.4). Indeed, the system include: an artificial fingertip able to transform tactile stimuli into an electrical analog signal, a unit elaboration system for data acquisition and neuromorphic decoding, an optical pattern projector for optogenetics stimulation and an optics focusing system to scale down pattern of light in the same order of magnitude of nerve size. This new system is able to provide tactile sensing detection, real time neuromorphic decoding and spatial-temporal modulation of the light projected to stimulate body or axons of culture cells. In the following sections we are going to give a detailed description of what materials are used to build the overall setup and how the various components are connected to each other.

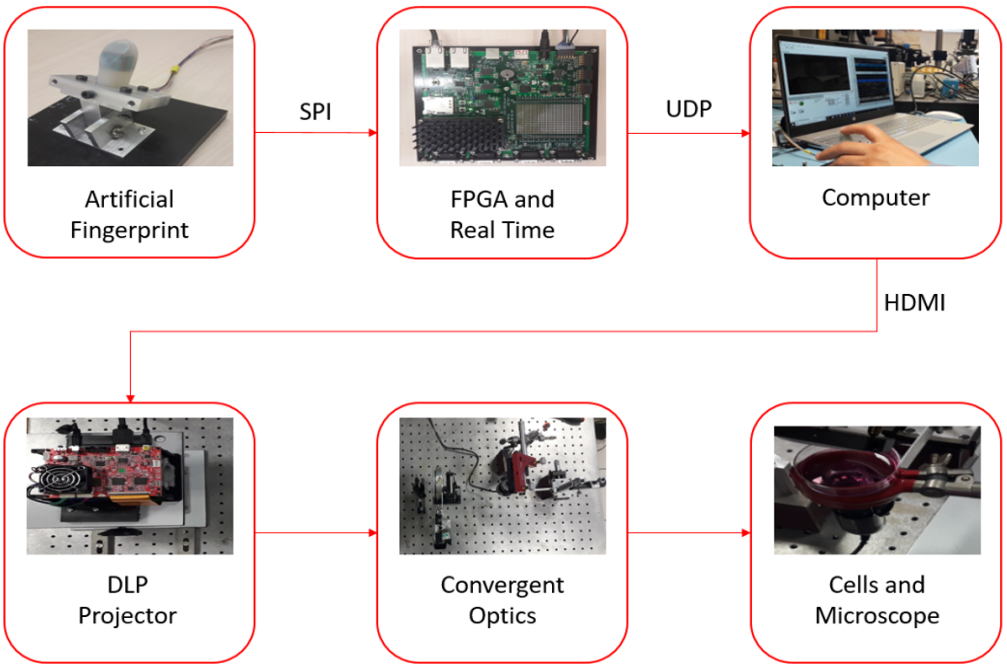

Figure 2.4: *Overall System design*
The figure shows in sequence the implementation of the system. Starting from the artificial fingertip up to the cell culture, used to study the characteristics of the tactile prosthesis. It is possible to note which communication protocols link all the system components.

2.2.1 Artificial Fingertip

The artificial fingertip is 2X2 array of a silicon-based three-axial force sensors [34]-[35]-[36] (MEMS) , where normal and shear forces are detected by four piezoresistors implanted at the roots of a cross shape, with a pillar-structure in its center acting as a force driver toward the transducers [37] (see Figure 2.5), fabricated through silicon micromachining technologies. The sensor can measure the normal and shear forces with high linearity (~=99%) and sensitivity SF = $\frac{\Delta R/R}{F} = 0.032 \pm 0.001 N^{-1}$, in the range between (0-2)N.

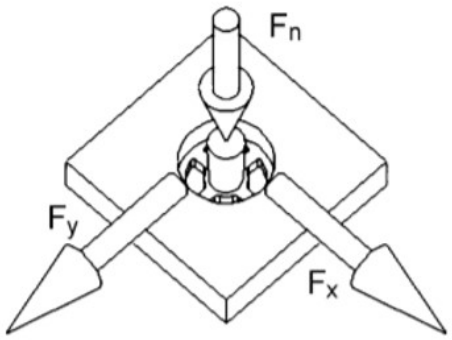

Figure 2.5: *Three axial force sensor* Mechanical structure of the sensor where the applied forces are indicated with Fn for the normal force, while Fx and Fy are the two components of the shear load. From [34].

The conditioning electronics guaranteed an output voltage proportional to the relative variation in resistance ΔR/R. The piezoresistor variation (R ~= 1kΩ) is recovered by means of half Wheatstone bridge configuration. The partition resistance is provided by a dummy piezoresistor implanted into the sensor and positioned at a point where it does not receive any strain. The polarization voltage of the circuit is V_{in} = 5V. The output sensor voltage is:

$$Vout = \frac{R+\Delta R}{2R+\Delta R} Vin \approx (\frac{1}{2} + \frac{\Delta R}{2R}) Vin. \quad (2.4)$$

Since each piezoresistor variation is independently readout, the total number of output channels are 16. The sample frequency of each output channel signal is 380 Hz. Sampling and conversion is made by means of an analog-to-digital converter ADC (ADS1258, Texas Instruments, USA) [38], integrated over a rigid-flex printed circuit board, which was arranged on a human-sized fingertip and covered with polymeric material (DragonSkin 10, Smooth-on, USA) [39]. The rigid parts of the board are linked one of each other using Kapton material. This particular material gives the possibility to print strip line for signal transmission and fold it to adjust rigid boards inside the fingertip. Each channel is multiplexed and buffered before to be converted in 24bits digital word by a fourth-order ΣΔ modulator (see Figure

2.6). The on board ADC gives the benefit to digitalize the channels very close to the sensor, avoiding to couple external disturbances to the signal and so improving the S/N. As a matter of fact, the output sensor signals are not filtered, in order to not occupy the amount of space required by analog filters, giving to the fingertip a real anatomic size (see Figure 2.7). Table 2.1 gives the description of inputs and outputs pins of the artificial fingertip.

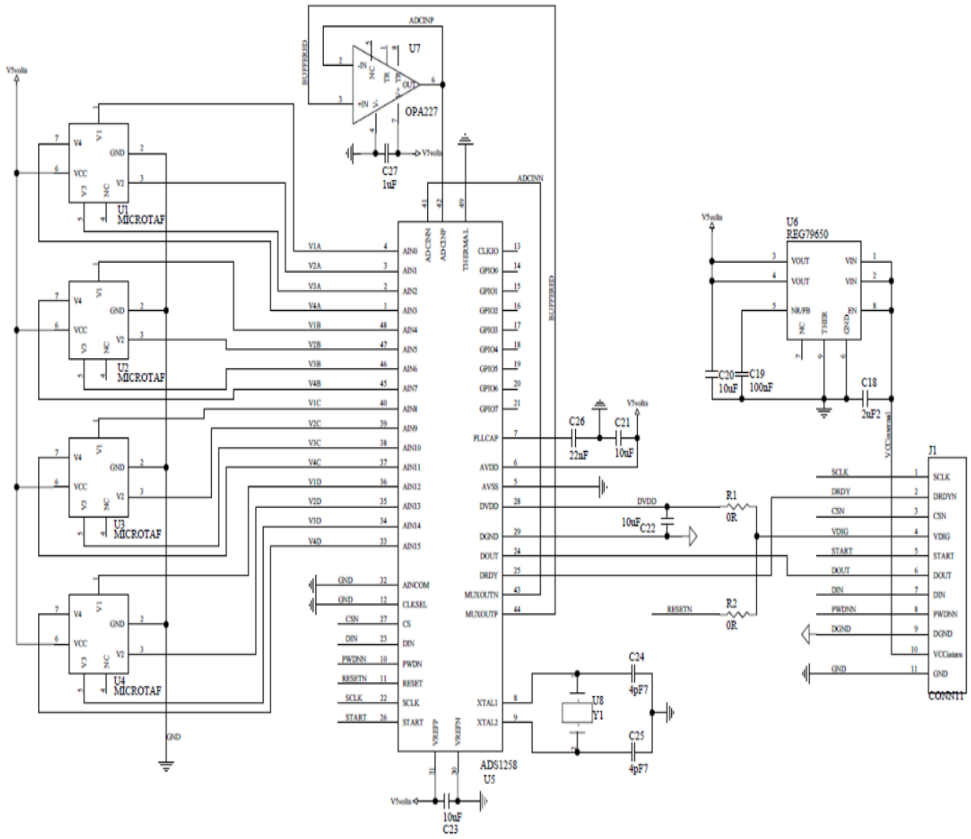

Figure 2.6: *Fingertip Schematic*
The figure shows the schematic circuit on board to the artificial fingertip. The 16 channels coming from the sensors are multiplexed and buffered to be converted by an ΣΔ fourth-order modulator followed by a decimator and a programmable low pass digital filter. Data are sent to the FPGA via SPI communication interface.
From [39].

Signals	Description
VCCinter	Battery voltage supply
AIN[0:15]	Inputs analog signals
DVDD	Digital Supply
GND	Analog ground
DGND	Digital ground
V5	Output voltage regulator
VREF(P/N)	Analog ADC voltage reference
MUXOUT(P/N)	Outputs multiplexer
ADCIN(P/N)	ADC inputs
XTAL1/2	Inputs Crystal Oscillator 32.768kHz
AINCOM	Common voltage reference single- ended inputs
SCLK	Input SPI clock signal
DRDY	Output data ready ADC
CSN	SPI chip select
DIN	SPI Digital input
DOUT	SPI Digital output
PWDNN	Power down ADC
START	Start conversion ADC
RESET	Hardware ADC reset

Table 2.1: *Inputs and Outputs description of the artificial fingertip*

2.2.2 FPGA and RT processor

The hardware components for acquisition and data processing are located on the same chip, SOM (System on Module), provided by National Instrument Corporation. Actually, the SOM has one FPGA and two Real Time processors. The FPGA manages the data acquisition from the ADC and a preliminary data processing. The Real Time processor performs all the neural computation model algorithm.

As we have seen the artificial fingertip used in our prototype has 16 output analog channels (see Figure 2.7), each of which is sampled and converted. Digital data communication, between the ADC and the FPGA is performed by a SPI interface. Also the ADC's registers are configured before start conversion by means of SPI. Each single channel is sampled at 380Hz; thus the total throughput of data coming out from the ADC is 24.329kbytes/s, acquired by the FPGA with a SPI clock at 2MHz.

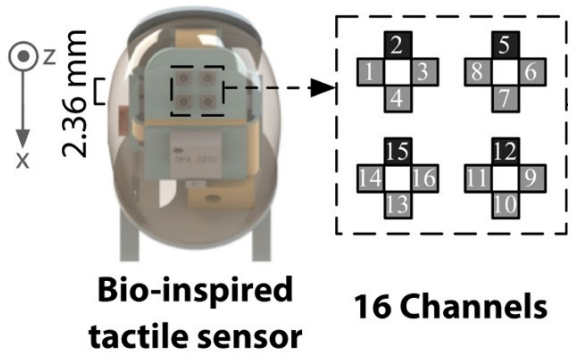

Figure 2.7: *Artificial fingertip 16 channels*
Mechanical structure of the fingertip, particularly focalized on the 2X2 array sensor, 16 channels output. From [34].

Still on FPGA, a moving average filter is applied to the received data and the polarization signal, common to all 16 channels, is subtracted, in order to obtain only the signal variation given by the applied strain on the piezoresistor sensor. After that, data are inserted in a FIFO (First Input First Output) memory buffer and sent to the Real Time Processor through DMA (Direct Memory Access) communication.

Two different processes are assigned to the two Real Time processors. As we said, the data acquired from the FPGA are sent via DMA to one of Real Time processor. In here, another FIFO is implemented to read the received data. DMA communication gives the possibility to transfer data only generate one single interrupt per single transfer block. In this way, the two units are free to carry out their tasks, without request any other resources. On RT, we performed a signal transformation, from digital data to neuronal spikes. This last process is implemented by means of a time variant model able to mimic neuron activity (see section 2.3). Also ISI (Interstimulus interval) is calculated, in the second Real Time

processor, with the purpose of detect the time interval between spikes. After processing, data are sent to the computer for further elaboration via UDP protocol. More information about this topic are going to be shown in the next chapter, where it is explained in detail, how everything has been implemented.

2.2.3 DLP projector system

The DMD (see section 1.2.3) is used in our system, to exploit the light spatial-temporal modulation that this device is able to provide. Each single micromirror can be depicted like a switch of light (see Figure 2.8.B) able to illuminate or to leave in the dark, regions of the matter. If an optics system is interposed between DMD and matter, we can also get high spatial resolution in the order of the axon diameter.

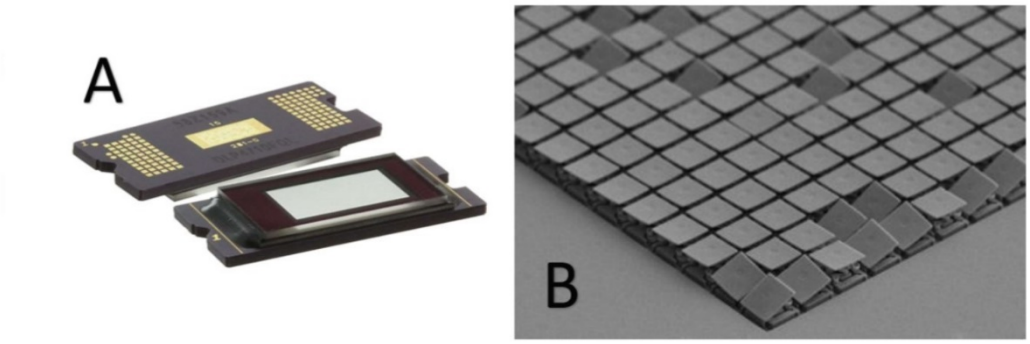

Figure 2.8: *DMD Chip*
(A) Top and down packaging view of DMD. The pads are in the bottom and micromirrors in the top, protected by a quartz glass slide. (B) SEM image of the micromirrors array. From [17].

The DLP 4710 (Digital Light Processing, Texas Instrument provider), shown in Figure 2.9, embeds: the DMD, all the electronics chips to drive it and the power light source. This device is used in our setup to generate different patterns of light, depending on the activity of the fingertip channels. The command instruction communication with the PC occurs by means of I2c interface and video communication again with the PC via HDMI. On board the DLP 4710 has: a Led Driver, three LEDs RGB power source, a DMD, two parallel DMD controller and an integrated projection optics (see Figure 2.10). In our system the projection optics has been removed and an external custom optics has been implemented to focalize light patterns in the same size of peripheral nerves.

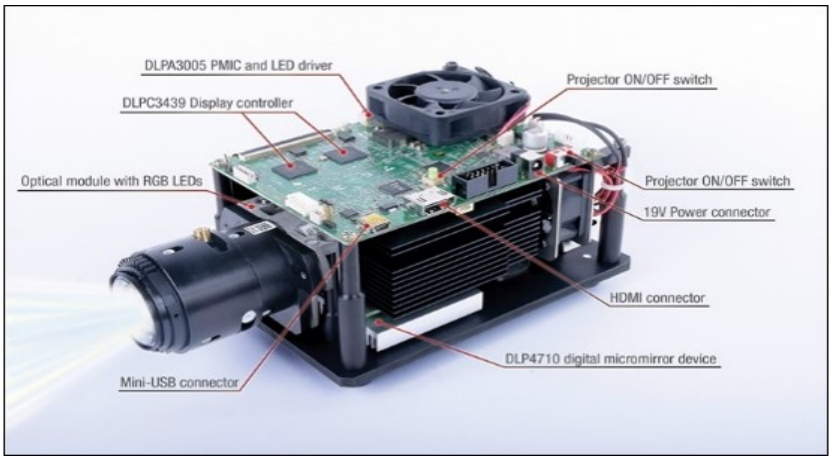

Figure 2.9: *DLP4710 EVM-G2*
The image shows the DLP device used in our experiments with on board: an electronics LED and a DMD controller, an optical LED's source and an optics system projection. During the experiments the projection optics has been removed and only the DMD, the controller and optical power integrated source have been exploited.

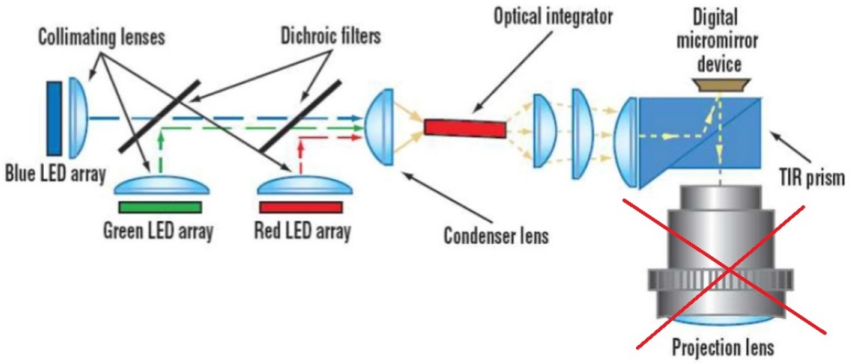

Figure 2.10: *DLP Optical System*
The figure shows exactly how the DLP optical system is implemented. Three LED's source are collimated in a single beam of light, using lenses, dichroic mirror, condenser lens and optical integrator. A TIR prism is used to change the direction of the beam towards the DMD and project the formed object through the optic axis. From [17].

2.2.4 Implemented optical setup

Since we are interested to project patterns of light generated by the DLP device to characterize the tactile prosthesis prototype, that makes use of this innovative method of optical stimulation and since we want to generate high spatial resolution patterns, for eventually in vitro cells opto-stimulation, we decided to implement a convergent optics able to give these feature to the system.

Being the DMD integrated inside the DLP and considering it like an extended object, we prefer deal the topic as image construction, having better approximation

of the project. Actually, DMD cannot be treated like a point source as a usual collimated laser beam.

The goal to be achieved in the optics design is get a high resolution system, for stimulate axons in culture cells. From datasheet, we know that the pitch of the DMD micromirror is 5.4μm and the myelinated axon has a diameter in the order of (5÷15)μm. Assuming to be in the absence of non-ideality, every single micromirror can intercept individual axons.

Actually, the DLP has been designed for projection purpose, the output light reflected by the DMD, integrated in the DLP, is divergent and thus, we need to cascade an external narrowing optics system to get 1:1 magnification of the projected pattern (same DMD dimension).

Using linear optics theory, we can easily understand that this goal can be reached putting a lens after the DLP device. From the thin lens (2.3) and magnification equations (2.6), we can calculate which distance the lens should be from the DMD, to have a real image of the same object size.

Thin lens and magnification equations:

$$\frac{1}{f} = \frac{1}{d1} + \frac{1}{d2}, \tag{2.5}$$

$$M = \frac{f}{f - d1}, \tag{2.6}$$

To have unit and negative magnification (real image), d1 must be equal to twice the focal distance of the lens and the real image (d2+d3) will be at distance two times the focal length. This quickly explains why the components have been arranged in this way in the setup.

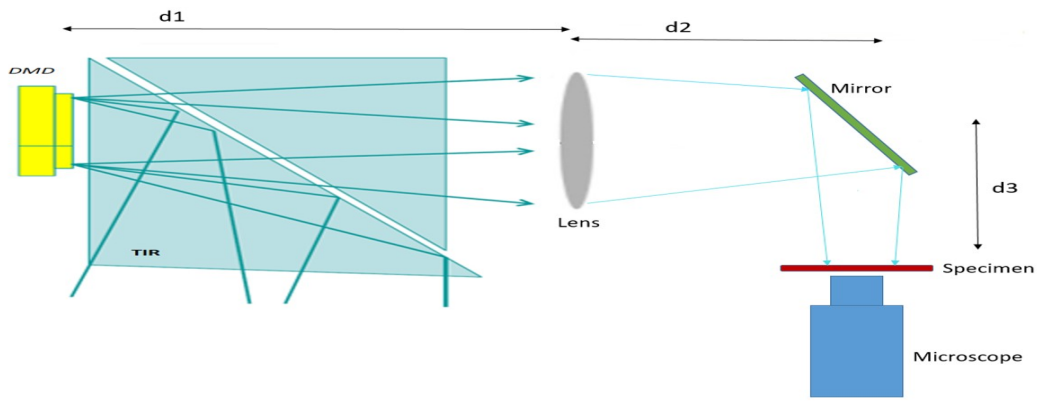

Figure 2.11: *Optical setup Model*
The figure shows a simple schematization of the setup. The light incidents on the DMD is reflected with a certain angle of divergence. Through a lens, a real image of the DMD will be created at distance d1=d2+d3=2*f.

Precisely, a plano-convex lens (BK7 material n=1.5236 @470nm) with 100mm focal length, diameter of 50mm and f/=f/D=2 is used, placed from the DMD at double of the focal distance. A silver mirror angled at 45 degrees is placed at the focal distance after the lens, to change the direction of light propagation and a Digital Microscope is placed at the same distance of the real image (2f distance, after the lens). To be precise, the Microscope focal plane is coincident with the real image plane (see Figure 2.12).

In order to improve the aberration limits, a diaphragm is placed before the lens to adjust the numerical aperture of the optical system. A neutral filter (T=15.2%) is placed after the lens, to attenuate the power emitted by the DLP, in order to avoid Microscope pixel saturation, when system resolution measures are carried out.

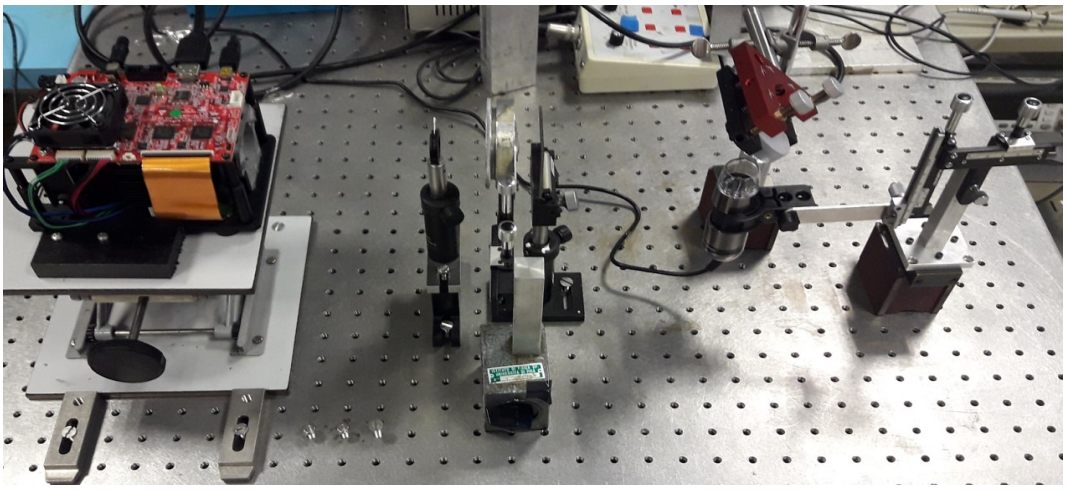

Figure 2.12: *Actually Implemented Optical Setup*
As we can see all the components are mounted on sledges that allow to improve the alignment. The whole setup is raised up to have a microscope view upwards, in case of in vitro experiments.

2.3 Spiking Neurons Model

Neuromorphic processing is developed on RT processor. In here, the raw digital data are transformed in physiological neuronal signals to mimic the behavior of the mechanoreceptors of the fingertip. Each channel could represent a different spatial site of the finger and thus, a precise mechanoreceptor to which a determined neuron is associated. The model used in this thesis work is the neuromorphic Izhikevich model able to simulate the generation of the action potential (neuronal activity, spiking and bursting behavior), making use of two time variant differential equations and a couple of conditions when the spike occurs. Furthermore, this model lends itself well to simulating the behavior of neurons associated with the sense of touch [40].

Below the two differential equations of the model:

$$\frac{dv}{dt} = 0.04v^2 + 5v + 140 - u + I \tag{2.7}$$

$$\frac{du}{dt} = a(bv - u), \tag{2.8}$$

with the auxiliary after-spike resetting:

$$\text{If } v \geq 30mV, then \begin{cases} v \leftarrow c \\ u \leftarrow u + d \end{cases} \tag{2.9}$$

Here, v and u are dimensionless variables and a, b, c, and d are dimensionless parameters. We would like to give a brief explanation of the two differential equations, introducing the meaning of each variable and parameter. The variable v represents the membrane potential of the neuron and u represents a membrane recovery variable, which accounts for the activation of K+ ionic currents and inactivation of Na+ ionic currents, providing a negative feedback on v. After the spike reaches its peak (+30 mV), the membrane voltage and the recovery variable are reset. Synaptic currents or injected currents (in case of electrical stimulation) are represented by the variable I, input variable of the system. The part $0.04v^2+5v+140$ has been chosen, to fit the neuronal dynamic and to scale potential and time respectively in mV and ms order. The neuron resting potential in this model is between (-70 ÷ -60) mV depending on the value of b. As most real neurons, the model does not have a fixed threshold. As a matter of fact, that depend on the history of the membrane potential prior to the spike. The threshold potential can be from -55mV to -40mV.

The other parameters have different meanings:

- a describes the time scale of the recovery variable u. Smaller values result in slower recovery.
- b describes the sensitivity of the recovery variable u to the subthreshold fluctuations of the membrane potential v. Greater values couple v and u more strongly resulting in possible subthreshold oscillations and low-threshold spiking dynamics.
- c describes the after-spike reset value of the membrane potential v caused by the K^+ ion hyperpolarization current.
- d describes the after-spike reset of the recovery variable u.

Different choices of the parameter result in different firing patterns (see Figure 2.13).

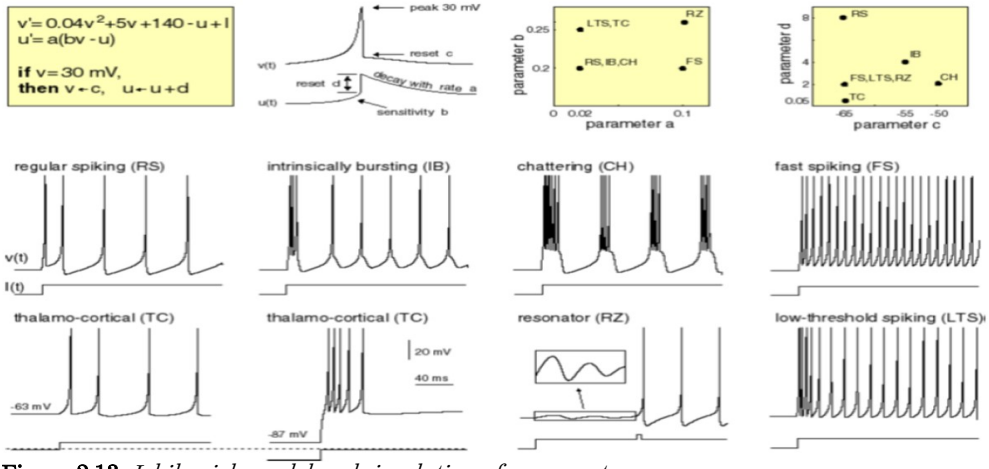

Figure 2.13: *Izhikevich model and simulation of neurons types*

Since the output sensors signals of the fingertip are voltage V_{sen}, it is necessary to convert them into input current for the differential equation. By multiplying for GF (Gain Factor) and dividing for a unit capacitance C_m only for unity matching system [41], we get the transformation. So, we can rewrite the two differential equations (2.7) (2.8) in this way:

$$\frac{dv}{dt} = Av^2 + Bv + C - u + \frac{V_{sen}GF}{C_m} \tag{2.10}$$

$$\frac{du}{dt} = a(bv - u), \tag{2.11}$$

after spike resetting:

$$\text{if } v \geq 30mV, then \begin{cases} v \leftarrow c \\ u \leftarrow u + d \end{cases} \tag{2.12}$$

The value parameters used in this specific case are in Table 2.2.

A	B	C	C_m	a	b	c	d	GF
0.04 $s^{-1}V^{-1}$	5 s^{-1}	140 Vs^{-1}	1 F	0.02 s^{-1}	0.2	-65 mV	8 mV	10000 S

Table 2.2: *Izhikevich value parameters*

This algorithm is applied to each channel, using the Runge-Kutta iterative method (Euler method), to approximate time discrete differential equation. In this way, we have 16 independent neurons, each with own temporal dynamics. Being the sensors spatially distributed on the fingertip, the channel number is an

important data to get the spatial localization of the tactile stimulus. Having available the channel number and its temporal response given by the signal processing with the neuronal model, we can generate at high level patterns of light for axons stimulation. In fact, as each group of axons maps a specific region of the human fingertip, what we want to do is stimulate group of axons that are interested in the transmission of tactile signal, from a region of the artificial fingertip where the perception occurs, to the first order neuron in the spinal cord. Thus, each channel or linear combination of channels will be a specific pattern of light that will illuminate specific areas of the nerve section for a time equal to the spike duration.

In this chapter, we presented two new topologies of peripheral nerve optical stimulator and all the materials employed to implement a new model of tactile prosthetic for upper limb. The optical setup inspired by the stimulator model, shown in the section 2.1.1, has been implemented for two reason. First of all, to use it like a demonstrator of the tactile prostheses system and second, to build a setup that can be used for in vitro optogenetics experiments. In the next chapter, we are going to present the methodologies adopted to combine all the devices together, to get a reliable system with excellent performances.

3 Methodologies

In this chapter, we present all the procedures and protocols for tactile prosthesis implementation. In addition, we show the setting of all the setups that have been used to characterize and test the system. Further tools and materials are provided in the Appendix chapter.

3.1 Stimulation Protocol Implementation

As we anticipated in the previous chapter, our goal is to associate a certain spatial stimulation region of the artificial fingertip with a specific pattern of light able to excite a particular site of the nerve. Furthermore, on base on the ISI (Interstimulus Interval) of the channel, we would like to modulate the optical power of the pattern by changing the intensity of light. Another possibility could be the modulation of the pattern projection area. In our system, we implemented both the possibility. Basically, we modulate the intensity of light or the area of the projected pattern, depending on the difference between the previous and the actual ISI value of the channel, calculated inside the Real Time loop.

In the next section, we are going to show how data acquisition and processing is managed on the Real Time and how somatosensory signals are elaborated in the computer station to generate patterns of light for peripheral nerve stimulation. The all chain elaboration system is show in the Figure 3.1.

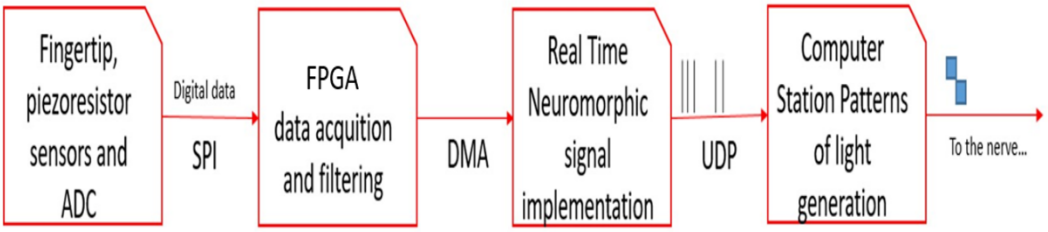

Figure 3.1: *Elaboration chain of the tactile prosthetic design*

3.1.1 ADC configuration and acquisition data

Before starting with acquisition and data transfer, we must set up a routine to configure the ADC registers. Essentially, we write 8 registers for setting up: data acquisition mode, data transfer rates and pins configuration between multiplexer and ADC. The routine runs on the Real Time module before data acquisition. Basically, we send the registers values to the target FPGA, placed on the same board, by means of DMA communication. The FPGA writes the received registers to the ADC, exploiting SPI communication. After writing, a request to read the ADC registers values is sent by RT. The FPGA takes care to get the information, transferring it to the RT module. In here, we do a comparison of the registers. If the acquired registers values are equal with the registers involved in the written phase, data sampling is allowed to start, otherwise, power reset device operation is needed. Data is continuously acquired within the timed loop of the Real Time processor using a state machine. In fact, if the data ready request get success, the data are read and the necessary calculations are made on them. Instead, if the data ready request has not success, the data ready request status will not be released until there will be a new data. The Figure 3.2 represents the flow chart of this first configuration and initialization parts followed by the acquisition data signal.

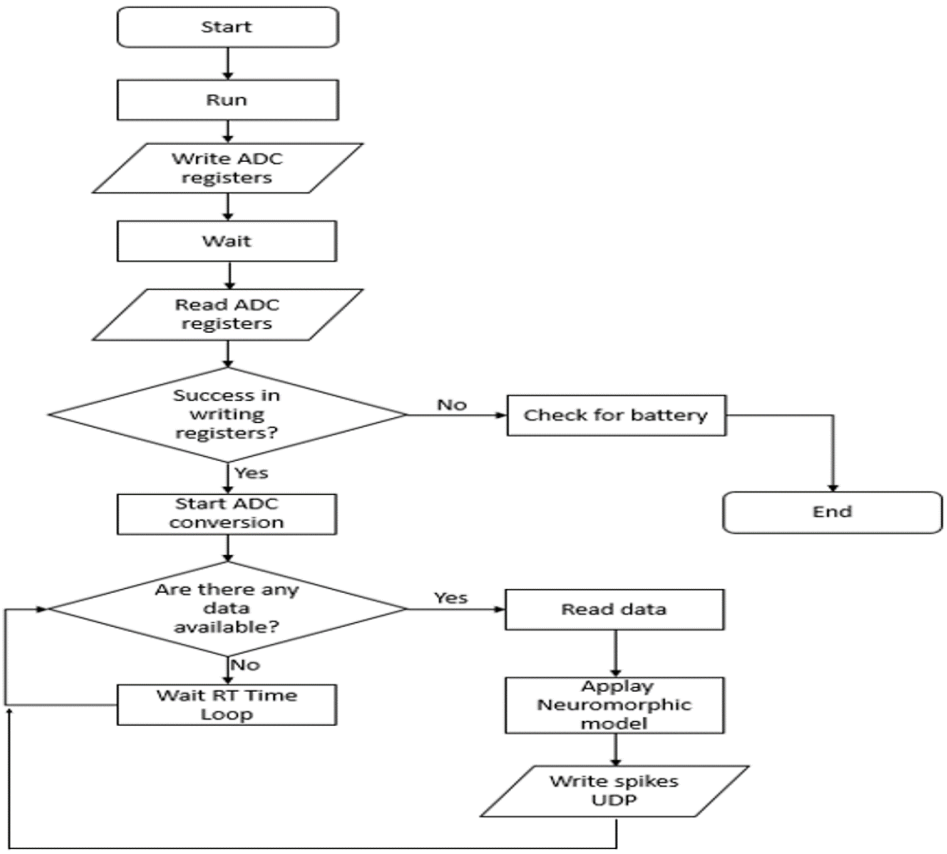

Figure 3.2: *RT flowchart for ADC configuration registers and data acquisition*

3.1.2 From analog to neuromorphic signal

In order to set a precise timing of events and data processing, both neuronal spikes and ISI are computed on Real Time processor. The SOM has two RT processor and to each one can be assigned a different process. We decided to divide the two tasks to each of them. In fact, two different timed loops are implemented each dedicated to different processor.

First processor (see Figure 3.3) manages the data acquisition from FPGA and elaboration using the neuromorphic model described in the previous chapter (see section 2.3). Since a state machine with two statuses is implemented inside the timed loop, in order to manage the communication data with the FPGA, the loop time period is set to be half of the acquisition time of all the channels. In this way, the acquisition time and elaboration has the same rate and the FIFO does not fill up and not require large amount of memory.

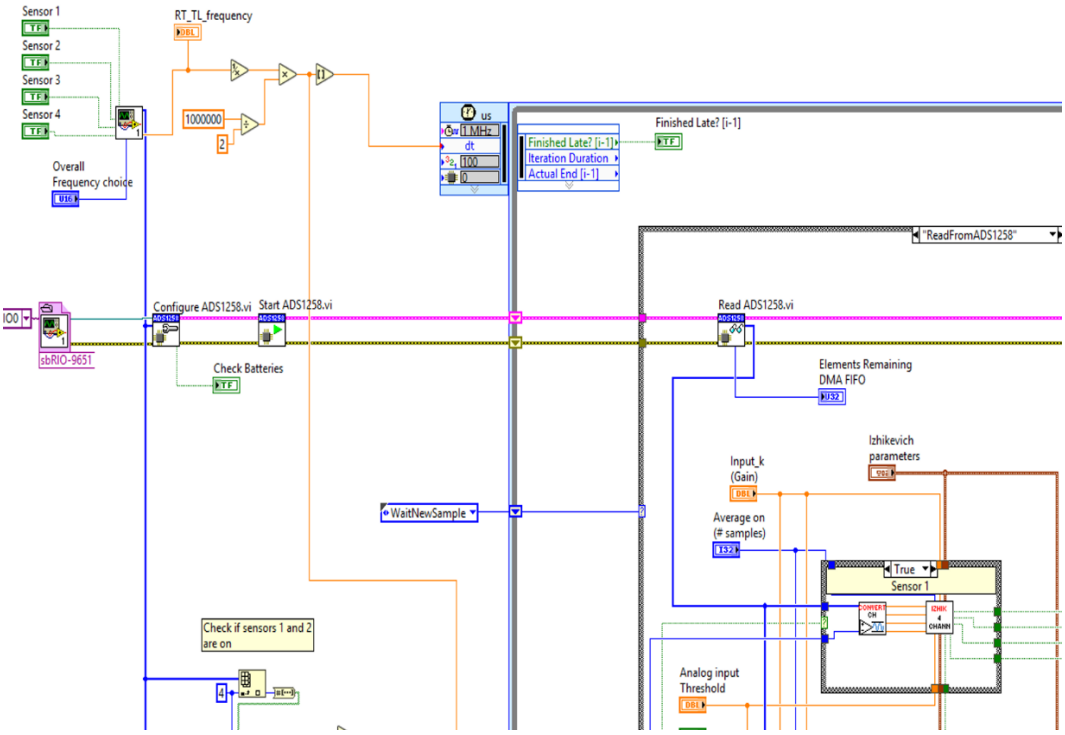

Figure 3.3: *RT Virtual Instrument acquisition and data process*
The screenshot shows the virtual instrument implemented in a Real Time processor for data acquisition from FPGA and elaboration, in order to get a neuromorphic signal compatible with neurons activity. On top left, it is possible to note, how time loop is computed depending on sample frequency channels.

From the Figure 3.3 we can see: the setting timed loop period depending on channels sampling frequency, the ADC configuration function for writing and checking registers values, the read data function and the split data and calculation neuromorphic model sub-functions. Another thing to note is the state machine implementation within the loop. There are two statuses: one depicted in the Figure 3.3 deals with the reading data from the FIFO and calculations for the neuronal model, the other state simply waits for a ready data, carrying out a check of how much data are inside the FIFO.

The data acquired by the RT is already digital filtered and also the polarization signal has been removed. The information is compacted into an array of size 4, equal to the number of sensors. The four channels associated with a sensor are unpacked by an element of the array, so that, we can get all the 16 channels signals by the entire array. After splitting, each channel is given in input to a sub-function that calculates the Izhikevich model. The output of this sub-function is an array of Boolean of size 4, where each element can be 1 or 0 depending on if the spike is or is not present for that channel respectively. Furthermore, the sub-function takes in input the various parameters for the neuromorphic model, thus allowing a real-time tuning of it. The Figure 3.4 shows the Izhikevich model implementation in LabVIEW.

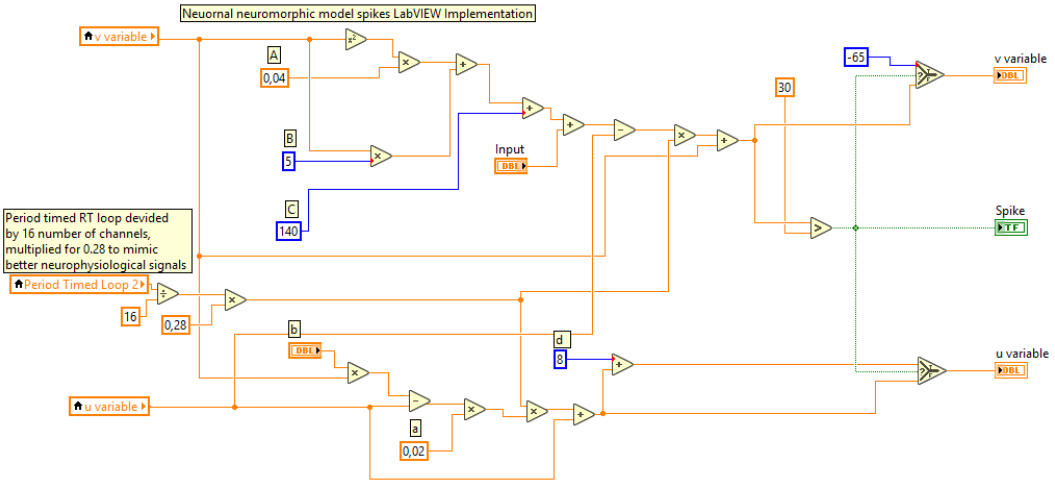

Figure 3.4: *Virtual Instrument Izhikevich model implementation*

3.1.3 Interstimulus interval (ISI) calculation

Regarding the ISI computation, another dedicated timed loop is implemented to get a precise calculation of the time between two different spikes of the same channel. The ISI is defined as:

$$ISI(spike_n) = t(spike_n) - t(spike_{n-1}), \tag{2.3}$$

The time period of the loop is half of the loop time period employed for acquisition and data processing. We decided to adopt this strategy to avoid not being able to count the exact time between the two spikes. Since the data between one loop and the other are shared by a local pointer variable, if the two loops have the same time period and if there is a certain phase shift between them, we could very well lose the synchronization and thus, failing in the time count between one spikes and another. Reducing the time period of this loop, we can reduce the probability of error. Doing like that, means apply the Nyquist theorem (see Figure 3.5).

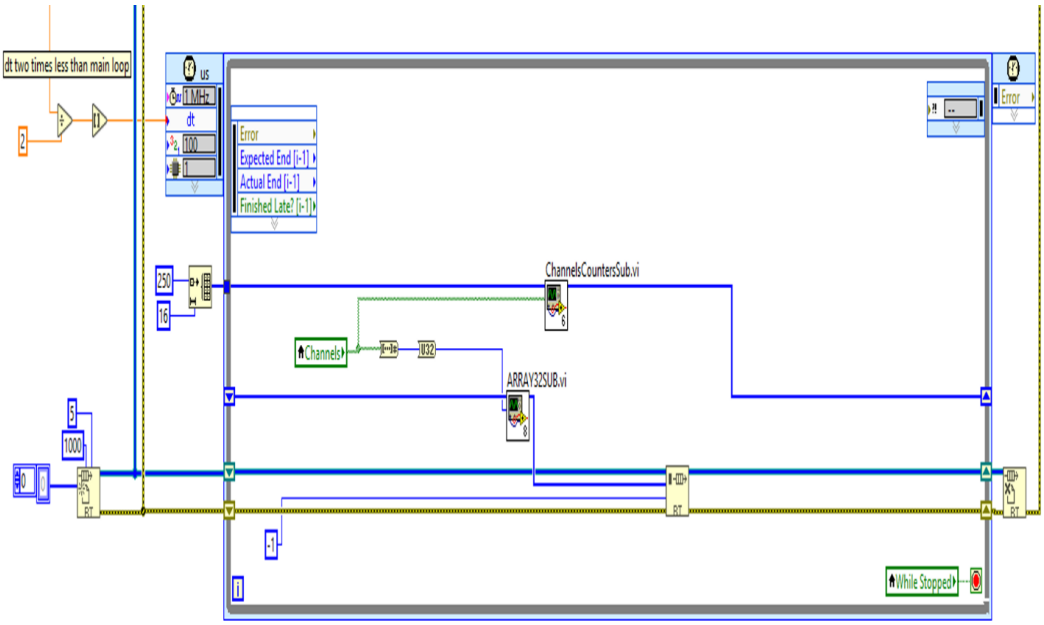

Figure 3.5: *RT Virtual Instrument ISI calculation*
The screenshot shows the second timed loop dedicated to compute the ISI (Interstumulus Interval) of each channel. Inside the loop we have two functions: the first implements 16 parallel counters, the other handles the packing data before being loaded on the RT FIFO and sent to the PC.

The loop implements 16 counters at 8 bits in parallel, maximum value is 255, each of them dedicated to each channel. When the spike occurs the counter is set to zero. In case, the counter reach the saturation, it remains at that value as long as a spike occurs and resets it to zero. At each cycle, the previous counters values are sent to the computer. Moreover, the value of the counter is halved before to be sent, in order to compensate the double speed of the loop. The values of four counters are packed in an array element at 32bits and thus, the total 16 channels are packed in an array of size 4. The array of counters is inserted in a RT FIFO to be sure to send all the value every moment. The FIFO is read in another not timed loop (see Figure 3.6) and data are sent via UDP protocol to the computer. Note, together with the counters, it is also sent the number of channels where spikes are occurred. Finally, with 5 packets at 32bits, all the necessary information to generate patterns of light are sent to the computer.

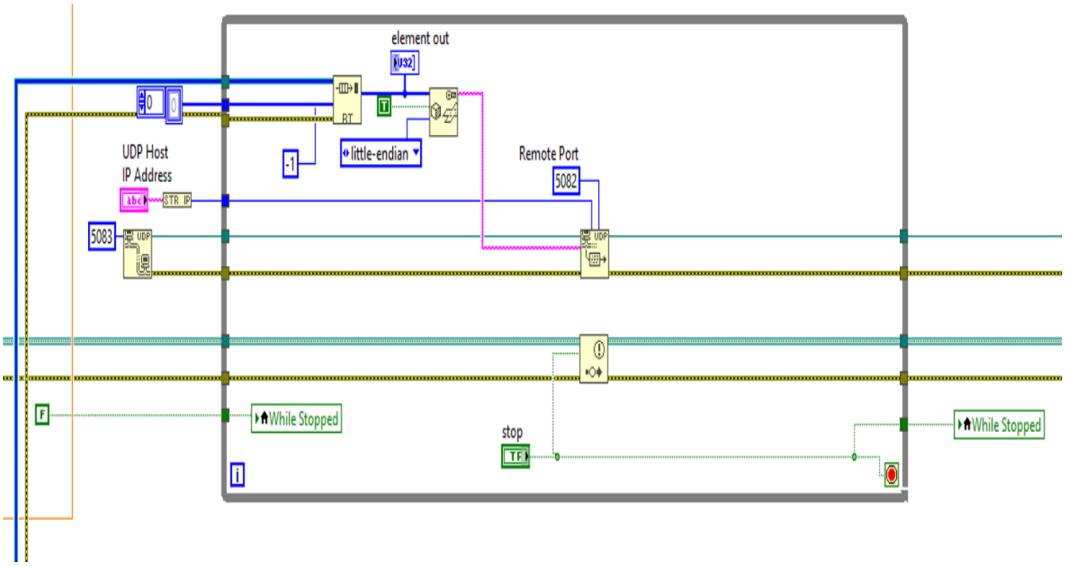

Figure 3.6: *Data transfer to the PC by means of UDP protocol*
The figure depicts the not timed loop implemented on RT for data reading from FIFO and sending to the computer via UDP protocol.

3.1.4 From neuromorphic signal to patterns of light

As we already know, 5 packets of 32bits data arrive to the computer via UDP protocol. Four of them are the counters, the other packet is the number of channels where stimulation occurred. It is important to understand, how we are going to use these received variables to generate different patterns of light. Basically, the number of active channels is employed to map the corresponding pattern in a specific region of projection area. The counters values are used to modulate power intensity or projection area of the associated pattern. We divided the projection area in 16 regions (different matrices) each of which has been assigned to a corresponding channel. Thus, each channel has a dedicated region of projection, activated only when spike is present.

Regarding the counters variables, the single byte is extracted from the 32bits data to restore the original value. After that, we implement a protocol to generate the equivalent pattern of light, depending on the ISI represented by the counter value. We decided to perform a subtraction between the current and the previously received counter value. The difference value is used to modulate the color intensity or the projection area of the associated pattern. All this is implemented in a sub-function that runs on the computer station. The counter value range goes from 1 to 127, thus, we can discretize 127 levels. Actually, we set, of our choice, only two thresholds and thus, we have only three levels of discretization. The Figure 3.7 shows the implementation of the pattern intensity variation. In Appendix, (see Figure A.3: *Patterns projection area modulation Virtual Instrument*) we can see the implementation for area projection modulation. In both cases, patterns are sent to the DLP like second monitor by means of HDMI communication.

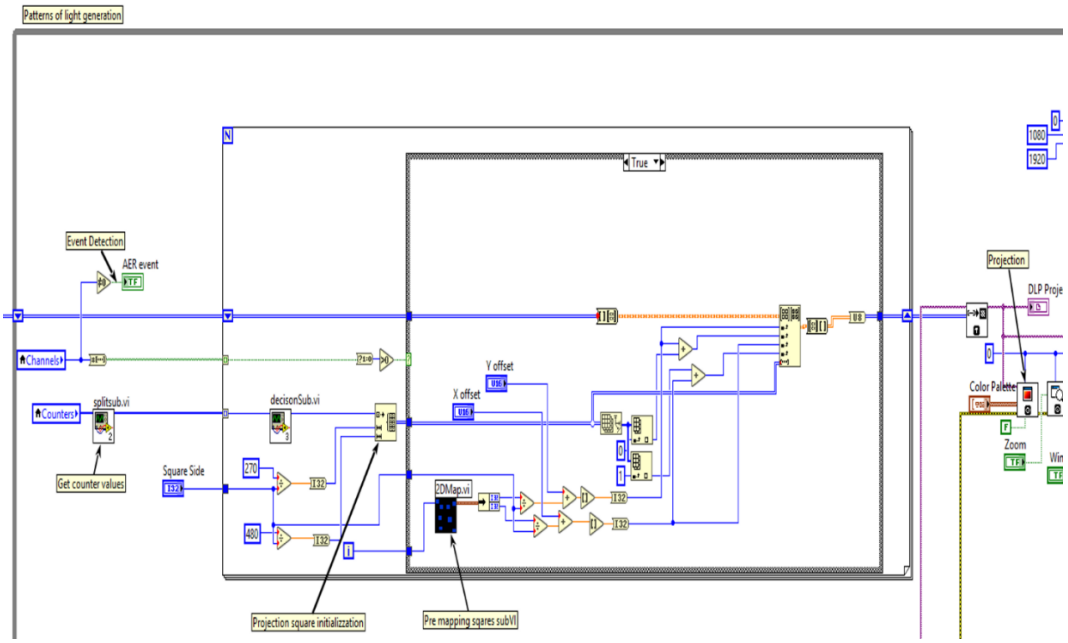

Figure 3.7: *Patterns projection and intensity modulation Virtual Instrument*
The screenshot shows the Virtual Instrument that implements a pattern projection and power modulation depending on spikes rate and ISI of each channel. Note, decisionSub is the subVI where the difference between the current and previous counters values is executed and the two thresholds are set.

Another loop, in parallel with the first one is implemented to manage communication with the RT processor and spikes visualization. Indeed, the last element of the received array is extracted to obtain spikes information and it is sent in input to a function that handles the data recovery and visualization in the front panel (see Figure 3.8).

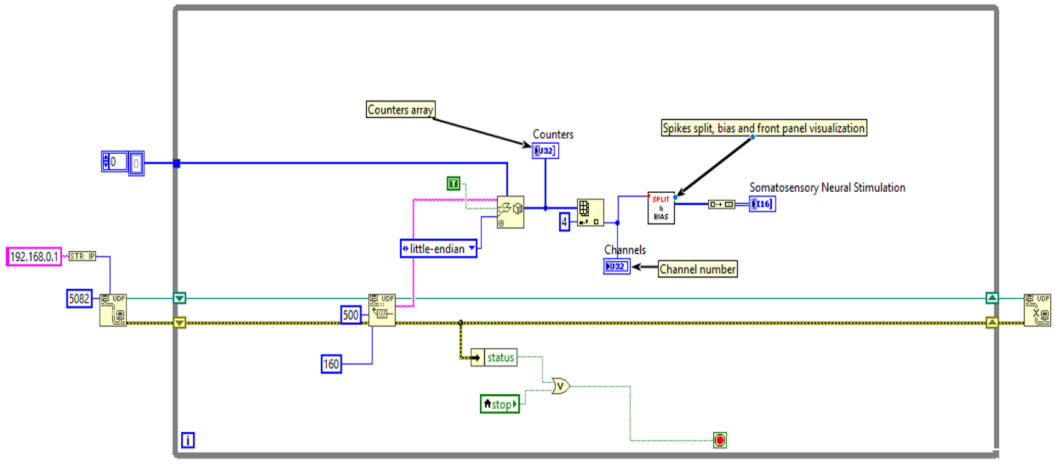

Figure 3.8: *Data acquisition via UDP and spike visualization*
The loop manages the data flow received by means of UDP communication protocol and implements a subVI for data visualization on the front panel.

3.2 Characterization tests

After introducing and explaining all the methodologies of system design, both at the hardware level with the presentation of the components employed and at integration level, showing how they have been combine all together, now we are going to explain which settings have been adopted to lead the experiments of system characterization.

At this point, we are interested to give a demonstration of the overall system designed. As we already know, the optical setup has been implemented to give a demonstration to the feasibility of tactile prosthetic system exploiting optogenetics for neuronal cell stimulation. In order to plan future experiments, first of all, we need to know the features of the optical setup and DLP projector. It is also interesting to understand the characteristics of this setup in order to extend applications fields, for example, using it as a possible optical stimulator for cell cultures. The main tests that has been carried out are on optical resolution, projection speed and optical output power.

3.2.1 Optical Pattern Resolution

To study the optical resolution, we projected different patterns of light useful to highlight the resolving power of the system. The patterns have been generated using a Virtual Instrument program (see Figure A.2: *Virtual Instrument Timed Pattern Generation*, Appendix) and projected by the DLP via HDMI communication. The setup is exactly the same as the one shown in Figure 2.12. Indeed, the projector is used without the own optics and an external custom convergent optics is added in cascade, with the goal to get 1:1 magnification.

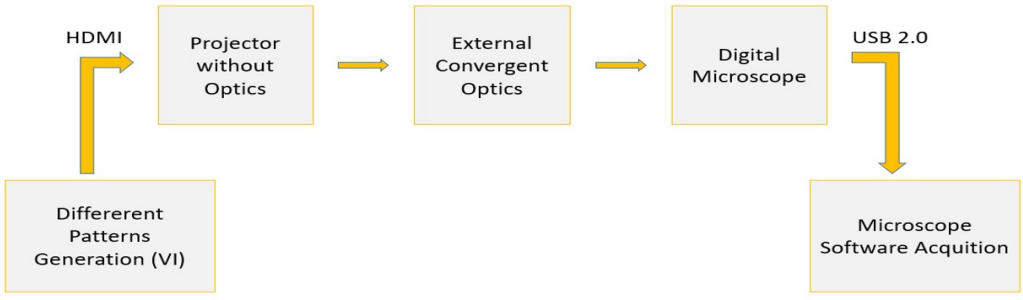

Figure 3.9: *Block diagram setup for optical resolution*

The patterns of light are acquired using a Digital Microscope (Dino Lite provider) with magnification of 250, a resolution of (1280*960) pixels and a field of view of (1564*1173)μm, thus, each single pixel of the microscope has a resolution roughly than 1μm. Resolution measures have been done using the software provided by Dino Lite and other data analysis and graphs extractions has been obtained in

MATLAB (see Table A.2: *Pattern resolution study*, Appendix). A neutral optical filter (15.2% Transmission) has been placed along the light way to attenuate power light, avoiding the saturation of the Microscope pixels' sensors. The focusing plane of the Microscope coincides with the image plane of the projector. Micromanipulators allow precise positioning of the optics components. The block diagram in Figure 3.9 shows how the optical resolution setup has been implemented.

3.2.2 Pattern Speed Projection

Regarding the patter speed projection, we decided to test the HDMI and I2C communication speed. HDMI communication sends pattern of light to the DLP like a video projection. Windows sees the DLP like a second monitor. Timed patterns are generated using a Virtual Instrument program (see Figure A.2: *Virtual Instrument Timed Pattern Generation*, Appendix).

Concerning the I2C communication, a very simple batch file has written and run by sending commands directly to the DLP (see Table A.4*: Batch file Timed Pattern Generation*, Appendix). The batch file contains the write command registers and the value to assign to them. For this application, simply, we set: the display size, the pattern to project and the time projection. After that a loop is implemented where only one LED (red) is turned on and off consecutively, in order to project the monochrome pattern.

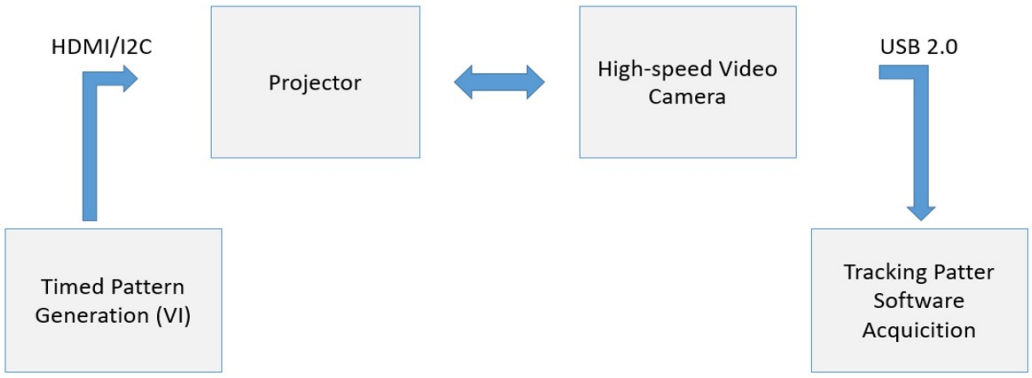

Figure 3.10: *Block diagram setup for speed patterns projection*

To study the projection speed, a HotShot 512 SC high-speed video camera (NAC Image Technology, Simi Valley, CA, USA) is used. This camera makes possible acquisitions from 50 to 200.000fps. In our case we sample at 3000fps, to be sure to be above the Nyquist frequency of the signal that drives the LED inside the DLP (switching driver LED). The HotShot 512 SC video camera stores images with a resolution of 512×256 pixels directly to its internal memory. These images were

downloaded into a dedicated computer for data analysis. The block diagram in Figure 3.10 shows how the pattern speed projection has been implemented.

3.2.3 Optical Output Power

A very important parameter to take into account is the optical output power of the system. Surely, it depends on the power of the incident light source on DMD but it is useful to understand which is the power variation by changing the number of micromirrors in the ON state. To conduct this experiment a Digital Optical Power Meter, provided by Thorlabas, has been used. A dedicated software deals with the data communication between the power meter device and the computer, giving the possibility to make a real time acquisition of the optical power data, sampled at 1Hz.

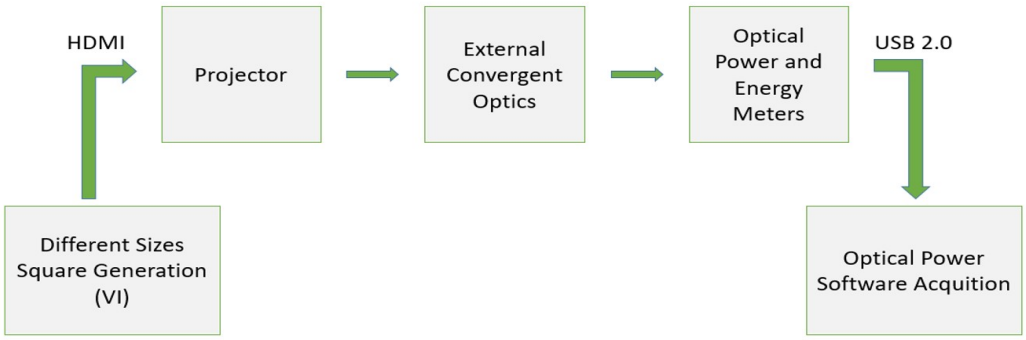

Figure 3.11: *Block diagram setup for optical output power*

The experiment was carried out in the dark and further mechanical coverage was interposed so that the shadows would not interfere with the experiment. The experiment consists in the projection of a square of variable side that goes from 1000 pixels per side to the single pixel on. A zero base line measurement without pixel on has been done and then subtracted from all other measures (CDS with Filtered Base Line).

3.3 Design Validation tests

After introducing the characterization methodologies for the optical setup, we want to proceed with methods description, used for the validation of the system designed.

In the first experiment, we have correlated the electrical response of the artificial fingertip with the equivalent optical pattern generated by the system. In this way, we tested the decoding protocol described in the section 3.1. In the second experiment, we have illuminated neuronal cells contained in a petri, to corroborate the use of our setup as a possible stimulator for optogenetic applications.

3.3.1 Tactile information processing

We would like to give a demonstration of how the overall projection looks like, when different stimuli are applied to the fingertip, showing the possibility to project patterns, modulating size and light intensity. To correlate the electrical fingertip response with the equivalent pattern of light, we thought to give precise stimuli to it. The recorded electrical signals have been analyzed and subsequently the equivalent patterns have been projected. Basically, we computed the average ISI value related to each channel and to each stimulus and then we computed the average ISI for each channel on the all stimuli applied. Note, the average of each experiment has been performed over the time shown in Table 3.1. Depending on the relative variation between the two value, we decided to project a matrix of spots with different radius. This could be just one of several protocols that correlates ISI with a given stimulus to the fingertip. The protocols may also depend on the patient on whom stimulation is taking place.

For precise fingertip stimulation, a motorized platform was used. The platform allows translational fingertip displacement along one direction, with a fixed sliding velocity, while a fixed normal force is applied (see Figure 3.12.A). Accuracy in speed is provided by the motors speed control of the platform and the force is established by means of load cell on which the fingertip is mounted. BioSkin material was used like texture to be intend. Three test were done, each with a different force and slide velocity (see Table 3.1). The fingertip stimulation occurs in three steps: indentation between fingertip and BioSkin material (z-axis), tangential sliding (x-axis), contact release between fingertip and BioSkin material (see Figure 3.12.A). In Figure 3.12.B is possible to see the overall system involved in the experiment. In particular, it is possible to notice how the 16 electrical channels coming out from the artificial fingertip are remapped like region of patterns projection. The activity of each individual output of the fingertip is transduced into a pattern that illuminates a respective region of the image plane of our optical setup. The total projection area is equal to the Microscope field of view, so that, we can make a detection of all patterns. Furthermore, the projection dimensions are exactly of the same order of magnitude of the nerve diameter.

Since the translation takes place on a single axis, the piezoresistors involved in the stimulation are only 8. From the acquired data, we can confirm what we have said. In Figure 3.12.B the green squares represent the number and position of channels, where spikes activity occur and the blue squares represent where they have been remapped for the projection. The acquired electrical signals of each channel are digitally converted and saved in a text file.

By setting thresholds on the relative variation, we get the parameters to be multiplied to the intensity of light or to the amount of area projected, associated to each channel. In here, we decided to modulate the number of micromirror in ON state. Results in section 4.2.1.

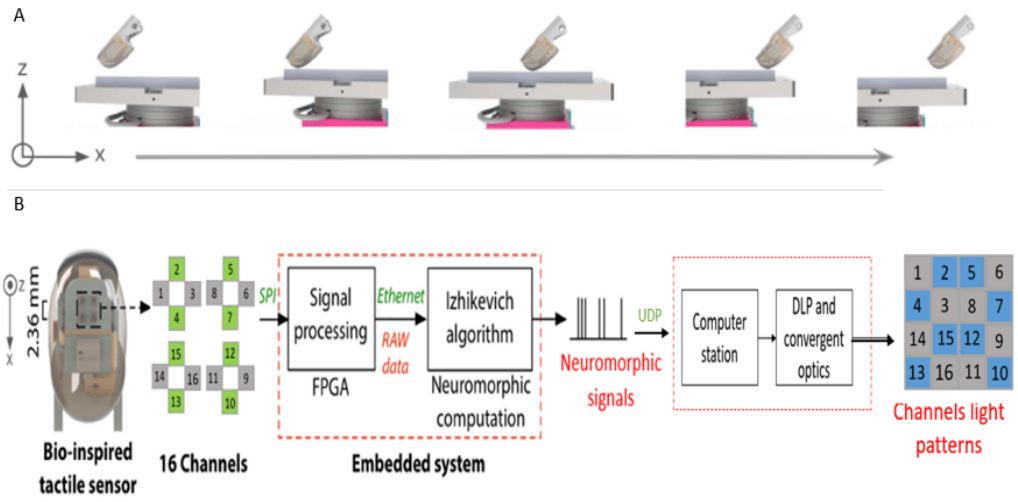

Figure 3.12: *Finger displacement on platform and acquisition and projection system*
(A) The figure shows how the fingertip is placed on the platform and how translation occurs along the x axis. (B) Overall acquisition chain. From the 16 electrical output channels of the fingertip to the 16 mapped region of projection.

# Test	Tangential sliding Velocity [mm/s]	Normal Force [mN]	Time window [s]
1	5	600	6,077
2	15	400	3,975
3	25	200	2,376

Table 3.1: *Speed and Force applied in tests and time average window*

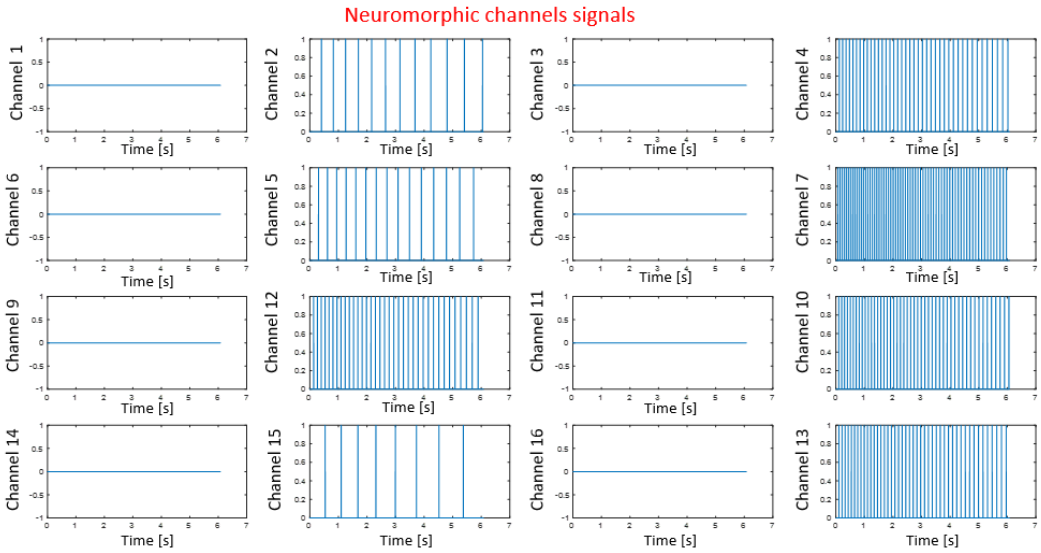

Figure 3.13: *Neuromorphic channels signals*
The figure shows the artificial neuronal activity of the 16 channels sensors of the fingertip, when test 1 is carried out.

3.3.2 Optical cells Stimulation

From the experimental results, shown in the section 4.1, we realized that our system has all the qualities to be used as an optical stimulator for in vitro cell experiments. As a matter of fact, the performances in terms of resolution, speed and power of the projected pattern are very high.

Since our optical system has been designed as a demonstrator of a tactile prosthesis that exploits the axons optical stimulation of peripheral nerve, we thought, it might be interesting to close the loop, using our prototype to stimulate neuronal axons in a cell culture. Actually, we did this experiment to give a true application to our optical setup, so that it can be used for optogenetic applications.

The overall setup is shown in Figure 3.14. The cells are contained within a petri dish and a mechanical ring supported by a pedestal holds the sample suspended above the Digital Microscope. This arrangement makes it possible to place the cell culture on the image plane, allowing the microscope to be positioned freely, so that its focal plane coincides with that of the sample. As we saw in the session 3.2.1, the microscope has a resolution of about 1μm. This is enough to visualize cultures of cells with a diameter in the order of a few microns. The Microscope has been interfaced with LabVIEW environment, making directly possible video acquisitions on the front panel of the virtual instrument.

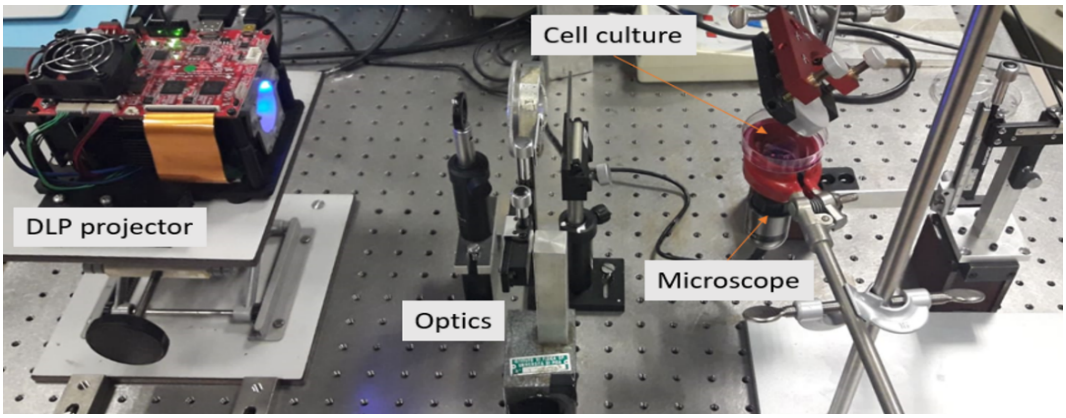

Figure 3.14: *Cell Stimulation Setup*
The system is the same as the one presented in the section 2.2.4, with the difference that here we have cell culture placed on top of the Microscope in order to be stimulated and detected at the same time.

Two types of experiments were conducted with cell culture. In the first one, we exploit the possibility to navigate with a projected beam of light along the cell culture. Besides the possibility to control beam trajectory, we can also change the size of the incident beam, by adjusting the number of micromirrors in ON state. All this makes possible to access particular sites of cells culture, giving the possibility to stimulate different parts in sequential manner. To perform this experiment a LabVIEW code has been implemented. From the front panel we have access to the Microscope and we can move the beam of light around the culture and increase or decrease the side dimension of it (see Figure A.4: *Virtual Instrument Navigation on the projection*, Appendix).

The second experiment exploits the parallel projection capability of the DLP projector, by illuminating in parallel all the cells under the Microscope field of view. Basically, the image acquired by the Microscope is given input to pattern recognition algorithm implemented on LabVIEW. Once the object is detected, it is loaded onto a projection matrix, scaled and if necessary rotated, in order to adapt the coordinate frame of the Microscope and DLP. In practice, we are able to recognize cells and illuminate them with the exact dimension from above. If there are any movements, we would be able to capture it and to follow the movement, so that the projection is able to fit again the recognized pattern. A quick manual calibration before conducting the experiment is necessary to obtain what has been described. For more information on implemented algorithms (see Figure A.5: *Pattern Detection Virtual Instrument*, Appendix).

Before to close this section, we are going to present briefly the cell involved in this two experiments. The scientific name is SH-SY5Y. These are human neuronal cells, of epithelial morphology of the bone marrow tissue, with 4-year age of a female species. In a culture environment they can be mixed, adherent and suspended. They have good biosafety level, equal to 1 and they are excellent for cell transfection applications. For our experiments they have not been transfected and they do not give any answer to the stimulation of light. In Figure 4.9 is possible to observe their morphology.

In this chapter, we have presented all the methodologies for the implementation of an innovative nerve stimulator, with the future goal to stimulate axons in the nerve, exploiting the new optogenetics stimulation technology. In particular, we have dealt with the processing of electrical signals coming from an artificial fingertip for the generation and projection of optical patterns in the same order of magnitude of axons in the nerve. Furthermore, we have shown all the methodologies for the characterization tests of the optical setup and for the validation of the whole elaboration and projection system.

4 Experimental results and Discussion

This chapter presents all the experimental results on the characterization and system validation tests, conducted according to the methodologies shown in the previous chapter. Excellent outcomes have been achieved, which revealed the feasibility of the prototype and contributed to the state of the art.

4.1 Characterization results

In the following section, we present the results obtained from the experimental optical setup used for testing and validation of the tactile prosthesis design for neuronal stimulation. We are going to show different graphs and tables, that highlight the outstanding system performances. We also discuss about the non-idealities that limit the system, presenting, new possible improvements that could be done in future works.

4.1.1 Pattern resolution

The Figure 4.1 shows the projection of a single micromirror in ON state. The beam reflected by the DMD, pass through the optics and it is focused on the image plane. By developing some algorithms for image processing in MATLAB, we obtained some useful data to define system features. The images taken from the Microscope are converted to grayscale and the FWHM (Full Width Half Maximum) is computed as the radius of the circle at half of the maximum pixel value, thus, the FWHM is referred to the pixel value.

The image acquired has been analyzed and we calculated a FWHM=9μm .

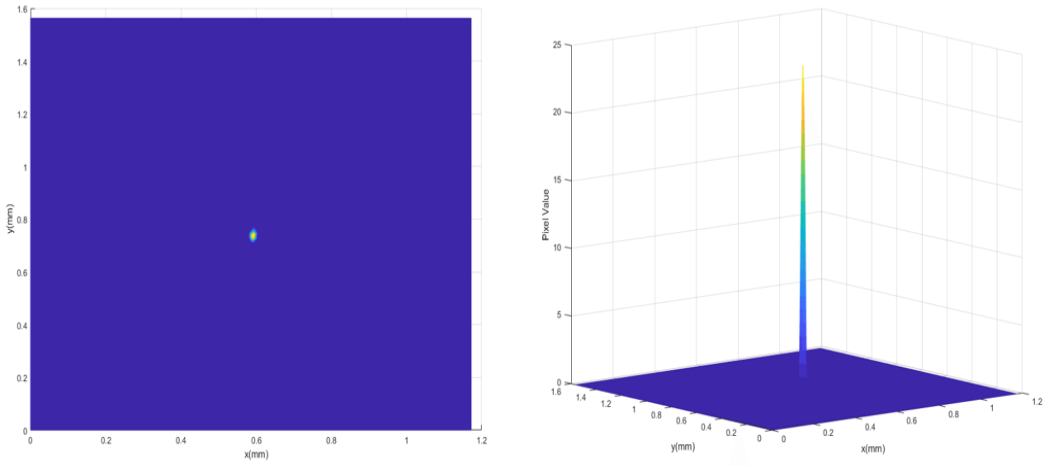

Figure 4.1: *Single micromirror projection*
(A) Single pixel ON projection, (B) 3D view of A. The image is taken by the Digital Microscope and a neutral filter with transmission equal to 15.2% is used to limit the saturation of the Microscope sensors.

As we can see, excellent optical resolution results have been achieved. Though we are using incoherent light source (LED), instead of coherent light source (Laser), we have exceeded the resolution quality presented in the works [18]-[19]-[42].

This result is really important for us, because we are exactly on the same order of magnitude of the axon diameter. Indeed, a myelinated axon, like that associated with the sense of touch, have a diameter around (5÷15)μm [43]. This demonstrate that our prototype exactly as it has been designed, it has all the characteristics to be able to stimulation single axons of neuronal cell culture.

A brief observation should be done, to see what we expected about the resolution and what we got from the results.

With 1:1 magnification, we expect, that the single micromirror projection has a dimeter of the same size of the side of micromirror (5.4μm). From the results, the beam diameter is a bit bigger. This makes us understand that some limitations could affect our system.

Being a real system, we should take into account two effects that can reduce the performance: diffraction and aberration. First of all, we can check the diffraction limit but should be not a problem, since the f/ of the lens and the wavelength (@470nm) are small. The light coming from the lens should have the first minimum (from diffraction theory), with an angle:

$$sin\theta = \frac{1.22\lambda}{d}, \tag{4.1}$$

for paraxial approximation and considering that, the image plane is at a distance twice the focal length, we have a beam radius:

$$r = 2f * \frac{1.22\lambda}{d}, \tag{4.2}$$

where f is the focal length of the lens and d is the lens diameter. Substituting the right numbers in the formula, we obtain a radius r =2.29μm. Since the micromirror pitch is 5.4μm, we can understand that diffraction resolution is higher and thus, it is not a limit for the system.

Since the blue LED has a quite narrow band, we can neglect the chromatic aberration. The most important contribute in focus limitation could be given by Coma and Spherical aberrations. We have Coma aberration, when lens and the object are not perfect aligned and spherical aberration, when the spherical shape of the lens has irregularities due to the margins of error during manufacture process.

The Figure 4.2.A well shows, how our system is affected by Coma aberration. Both coma and spherical aberration limits can be improved, using a lens with higher f/ and better manufacture.

To improve the system resolution, we inserted a diaphragm before the lens, in order to increase the f/ of the optics system. If the diaphragm has a small diameter, we risk to fall into problems related to the diffraction. A good result was obtained with a f/ equal to 5, thus, with a diaphragm diameter equal to 20mm. Therefore, the resolving power of the lens was found as optimal point between diffraction and aberration limits. The distance between two still distinguishable peaks (Rayleigh criteria) is about 9μm (see Figure 4.2.D). Note, the Figure 4.1 and the Figure 4.2.C have been taken after adding the diaphragm. The methodology and the setup setting are well described in the section 3.2.1.

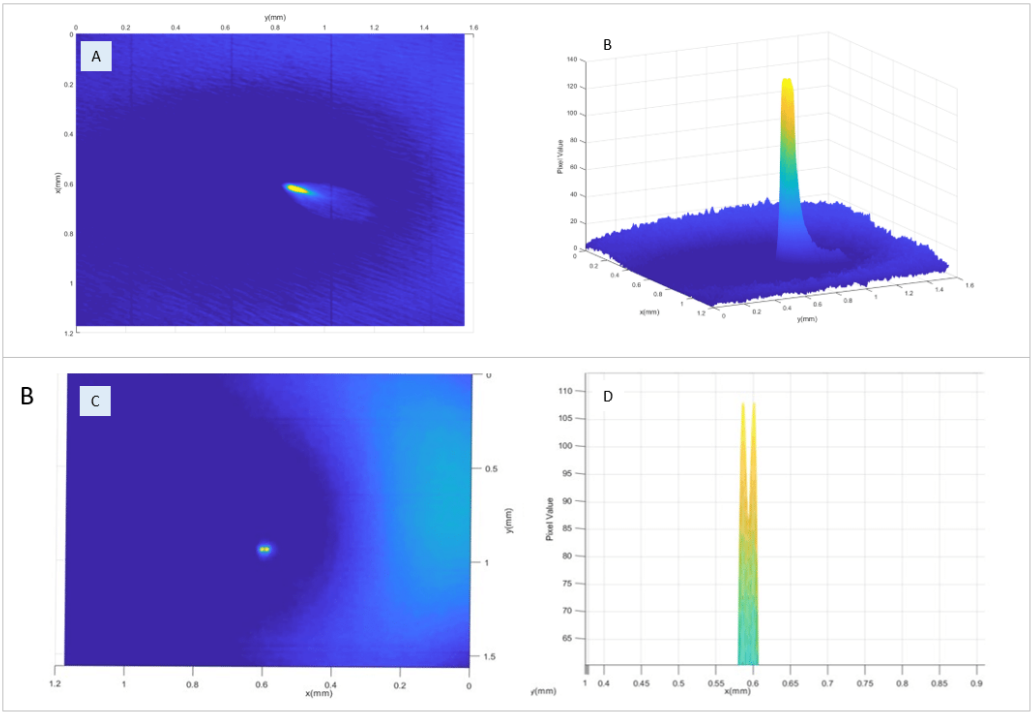

Figure 4.2: *Coma aberration and Resolving Power Resolution System*
(A) The figure shows the Coma aberration; it looks like a comet. This phenomenon together with spherical aberration are the limits of the system resolution. (B) 3D view A. (C) The figure shows the maximum resolving power resolution, 1 pixel ON e 1 pixel OFF. The distance between one micromirror ON and one OFF is more or less 9um, exactly the minimum distance between two peaks to be distinct. (D) 3D view of C.

4.1.2 Projection speed

In here, we are going to show the results obtained from the experiment on the pattern projection speed of the DLP system. In the section 3.2.2 is possible to get the information about the methodology and the setting of the setup. Basically, we tested the maximum frames per second projected by the device, exploiting HDMI and I2C communication. First pattern projection at 20fps has been sampled at 3Kfps from a high speed camera. Result are shown in Figure 4.3.

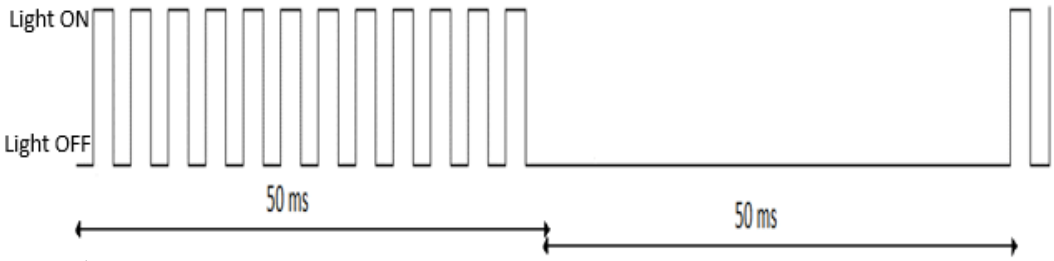

Figure 4.3: *Pattern projection at 20Hz*
The figure shows the sequence frames acquired by the high-speed camera. When pattern is projected by the DLP for 50ms, we see this strange switch ON-OFF (at 250 Hz) due to the driver LED. When a black pattern is projected, the frames acquired are all black. Note, sampling at 3Kfps, we get 150 frame per pattern projected by DLP.

The pattern of light is a red solid color projected for a time equal to 50ms. Sampling at high frequency is possible to see this square wave while pattern is in ON state projection when instead, we expected to see a square wave with a period of 100ms. This weird behavior is due to the LED driver. As a matter of fact, the power LED source is the load of a switch (Power mosFET), piloted by a PWM (pulse-width modulation) signal. This configuration is used to reduce power consumption and to be able to program the led current, modulating the duty cycle of the PWM. Since the drive led frequency is at 250Hz, our eyes do not see this effect. What is shown in Figure 4.3 is valid both for HDMI and I2C communication.

By increasing the projection frequency, we got the same kind of waveform with smaller period. Again, this is valid for HDMI and I2C communication (Figure 4.4).

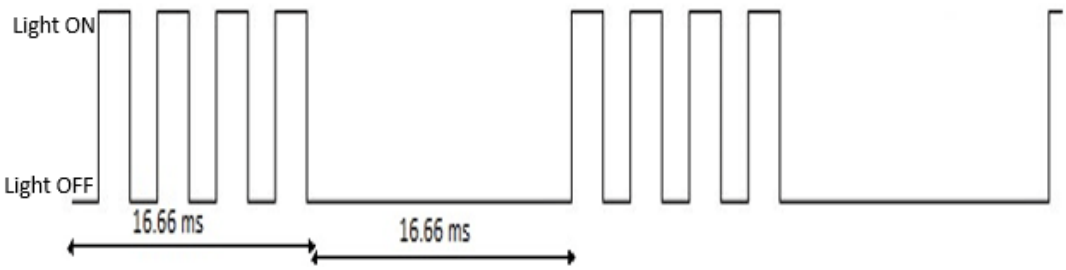

Figure 4.4: *Pattern projection at 60Hz*
The figure shows the sequence frames acquired by the high-speed camera. When pattern is projected by the DLP for 16.66ms, we always see the switch ON-OFF (at 250 Hz). Note, sampling at 3Kfps, we get 50 frames per pattern projected by DLP.

If we try to go above 60 fps frequency projection, from the high-speed camera we will see always the same equivalent waveform acquired for the 60fps.

This result was obtained for both communications, thus coming to the conclusion that the 60fps projection speed is a hardware limit and not a communication limit.

There are DLP technologies capable to reach very high frame rates (1Kfps), projecting gray scale image. Also for our optogentics stimulation application, we do not need to project color image at 24 bit. Employing, DMD controller for grayscale image projection, we can increase the projection speed of at least one order of magnitude, and thus, be able to reach projection frequency comparable with spike rates of the neuronal activity. However, our result is very good because we are not so far from activation speed of the optogenetics technique. Moreover, the possibility to project in parallel on more samples (in a time equal to 16.66ms), makes this system more efficient than many others with sequential illumination.

4.1.3 Output Power

In this section, we are going to show the result on the optical output power capability of our system. In section 3.2.3 is possible to see the setup setting to perform this test.

Obviously, the output power is a consequence of the optical power source. Nevertheless, our goal is see how the optical output power differs, when the number of micromirrors in ON state changes. The graph in Figure 4.5 shows the relation between the two quantity.

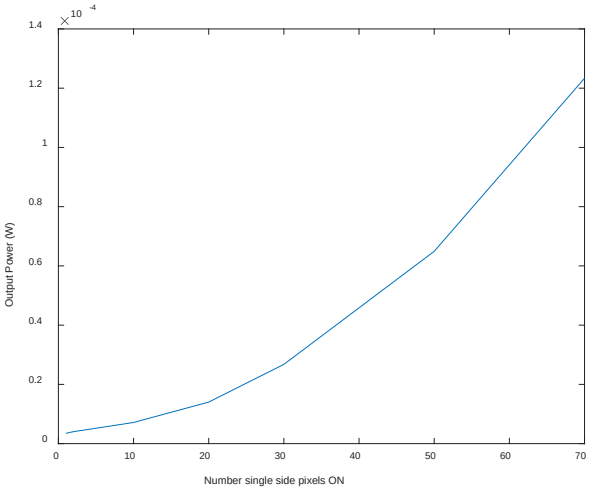

Figure 4.5: *Output Optical Power*
Output power from the DLP in function of the number of pixels in ON state. The X axis is the side of the square matrix projected.

One single pixel ON reflects an output power about 3.4μW with a light source at 470nm. The power density defined as the optical power divided by the area of the beam is J=P/A=2.7mW/mm². To compute the beam cross-saction we have considered the area of a circle with radius equal to the FWHM got in the section 4.1.1. This could be an overestimation of the effective power density but it is still a food approximation. Since the minimum power density required for optogenetic stimulation is 1mW/mm² [29], we can assert that our stimulation system could be employed for in vitro optical stimulation experiments.

The Table 4.1 is going to highlight the properties of our setup.

Optical Resolution	FWHM=9μm
Patter Time Projection	16.66ms
Power Intensity Single pixel ON	$2.7 mW/mm^2$

Table 4.1: *System Performances*

4.2 Design Validation Result

In this section, we are going to show the experimental results conducted according to the methodologies discussed in the section 3.3. These results highlight the potential of the optical stimulation system for tactile perception, demonstrating that the stimulation protocol presented in section 3.1 works well. Furthermore, we want to present the results about cellular illumination, validating our setup as an in vitro stimulator for optogenetic applications.

4.2.1 Optical patterns projection

For this test, we have correlated the electrical channel activity of the fingertip, associated with a precise stimuli provided to it, with the corresponding pattern projected by the optical stimulator.

The projection pattern assigned to each channel is a matrix of spots. When spike channel occurs, the corresponding pattern, it is going to be projected. The spatial distribution of the patters on the overall projection area is described in Figure 3.12 (see section 3.3.1). Note, the projection area is the sum of all the 16 patterns of channel. The possibility to project multiple spots for each channel, highlight the potentiality to spatial-time modulate the overall projection area.

In addition, we are able to modulate the spot area of the patterns related to each single channel. The modulation of the spot area depends on the protocol used to carried out this test. This protocol is well described in the section 3.3.1. Basically, the projection of the spot area is related to the relative variation of the channel's ISI mean value respect to the channel's ISI mean (see Figure 4.7). Practically, the average of the ISI of each channel has been computed for each test with different input stimulus. After, for each channel, the average of the mean values ISI has been calculated and a relative variation respect to that value has been performed. We fixed two thresholds and depending on the value of each relative variation (if is above, under, on in the middle of the two thresholds), we projected three different area of the spots related to that channel. The Figure 4.6 shows the results obtained from this protocol.

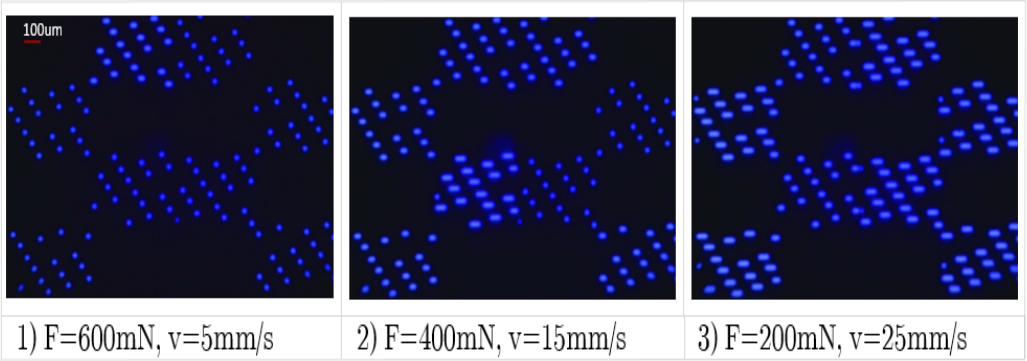

Figure 4.6: *Patterns of light related to the three conducted tests*
The image shows the three patterns of light correlated to the three tests performed according to the methodologies seen in the section 3.3.1. The illuminated area is associated with the active channels during the stimulation, the thickness of each dot is assigned depending on the ISI test mean value respect to the channel's ISI mean value.

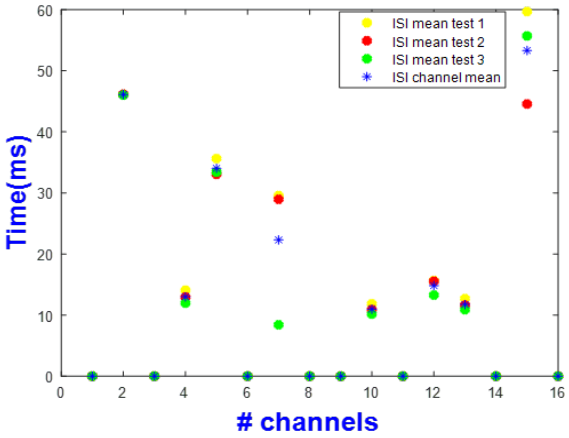

Figure 4.7: *Mean value ISI channels*
The figure shows the ISI mean value of each channel for each test. The blue star is the mean ISI value of the channel for all the three test.

From the Figure 4.7 is possible to see the mean ISI value of each tests(yellow, red and green dots) and the mean ISI value of each channel (blue stars) on the three tests. In most cases, the yellow dot, high ISI, is related to the projection of the small spots, the red with the intermediate and the green with the biggest spots. From the result looks like that increasing the speed and reducing the force of the relative stimulus given to the fingertip, the projection area of the spots increases. Furthermore, it is important to see that this protocol gives a differentiation in pattern projection when different input stimuli are applied, goal achieved.

In real time process, it is not possible execute all these calculations to implement this protocol, because performing an average, we introduce delay to the system, and thus, we lose synchronism of the process. Nevertheless, we can compute the difference between the current and the previous ISI of the same channel, when spike occurs. Depending on the value of the difference, a specific pattern of light will be projected. This could be a good protocol for real time stimulation. Performing this calculation, we are not so far from what we have done with the subsequent data

acquisition. Moreover, the overall projection will be uploaded at each single cycle. The overall pattern will have an appearance that depends on: the number of channel stimulated, the spike activity and the implemented ISI protocol.

The Figure 4.8 shows the Real Time execution of the tactile stimulator presented in the previous chapters. From the Figure 4.8.A, we can see the system response to a random stimuli applied to the fingertip. The direction, localization, speed and force of the tactile stimulus implies the activation of different channels and thus the projection of the corresponding patterns. In here, we decide to project solid rectangle pattern for each channel (not spots, like before). The Figure 4.8.B shows two graphs running real time through a LabVIEW interface. The first graph on the right represents the 16 somatosensory signals output channels from the artificial fingertip, processed Real Time. When the channel is not stimulated, it remains silent and does not generate any spikes. Regarding the graph on the left, it represents the zoom in of the overall patterns projection.

If in the precedent case (see Figure 4.6), we changed the projection area of the projected spots depending on the relative ISI variation, in here we change the intensity of the blue light, depending on the difference between the previous and the actual ISI value of each channel. Also here, we set two thresholds and depending on the value of the difference, respect to the thresholds values, different intensity patterns are assigned to the channel.

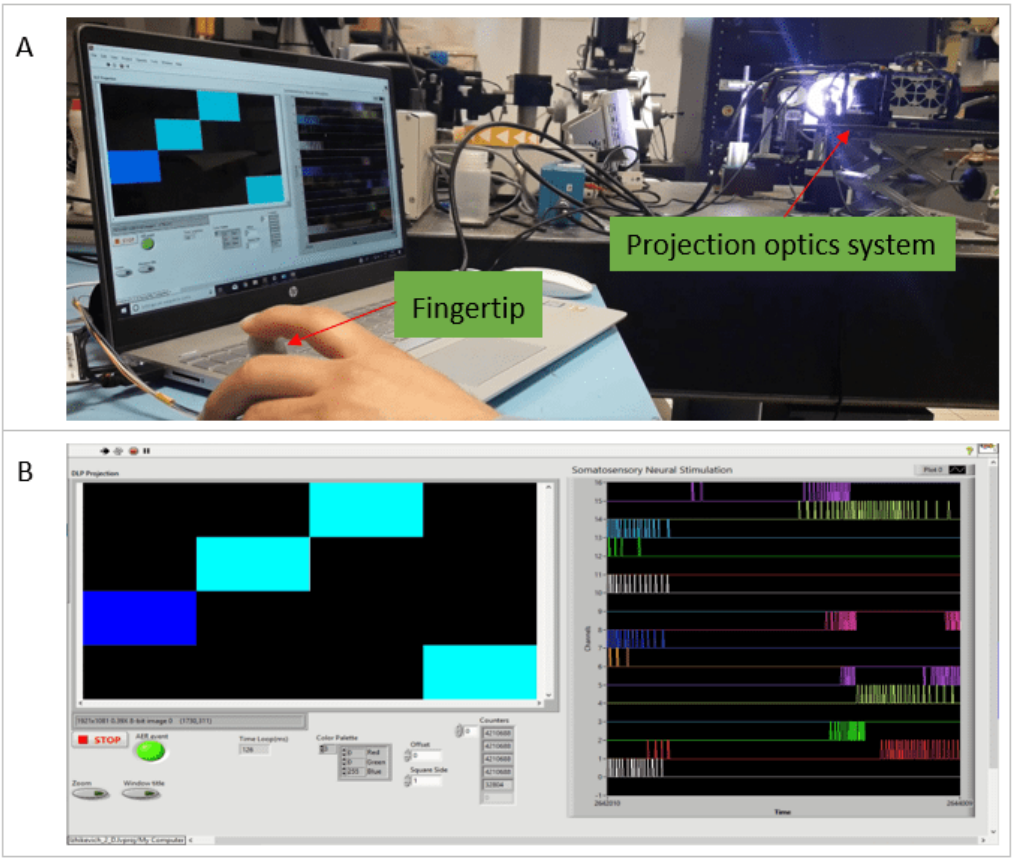

Figure 4.8: *Real time execution of the tactile stimulator system*
(A) The operator gives random stimuli to the fingertip, activating the corresponding channels and thus projecting the relative patterns. (B) LabVIEW front panel that shows the somatosensory signal and the relative patterns projected.

4.2.2 Cells Stimulation result

As expected, the results on cells culture experiments are excellent, making it clear that this setup can be used for in vitro optogenetic applications.

What we show are the results of two different stimulation modes, all the involved methodologies to carry out these experiments are well described in the previous chapter (see section 3.3.2), where it is also possible to find a brief description of the used cells. As for the cell stimulation mode we have: sequential and parallel. The Figure 4.9 shows the sequential mode. The three images in sequence give the idea of the possibility to navigate on the cell culture and to stimulate different cell regions, from the body to the axon. We can modulate the projected spot by changing the number of micromirror in the ON state. In this case, with a single micromirror ON, we have the possibility to stimulate single parts of axons.

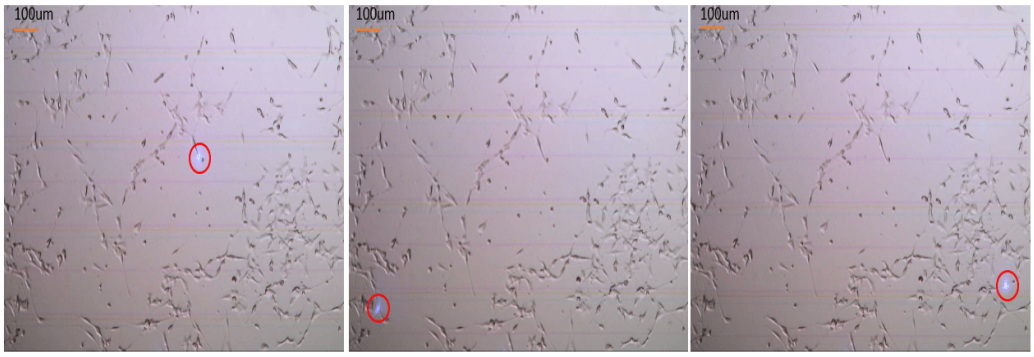

Figure 4.9: *Sequential Stimulation of a culture cell*
The figure shows three screenshots taken by the Microscope used in the acquisition. The red circles highlight the light beam, white ball, located in different regions of culture. In particular, it is possible to see the illumination of axon of three different cells.

The Figure 4.10 shows the parallel mode. From the first image, we can clearly see how light is superimposed over the cells in the culture, under the vision field of the Microscope. This describes the potential of our system capable of recognizing the position and size of cells and projecting light in parallel to all them. Moreover, if migratory movements of cells are presents, we are able to capture the movement and follow them with light.

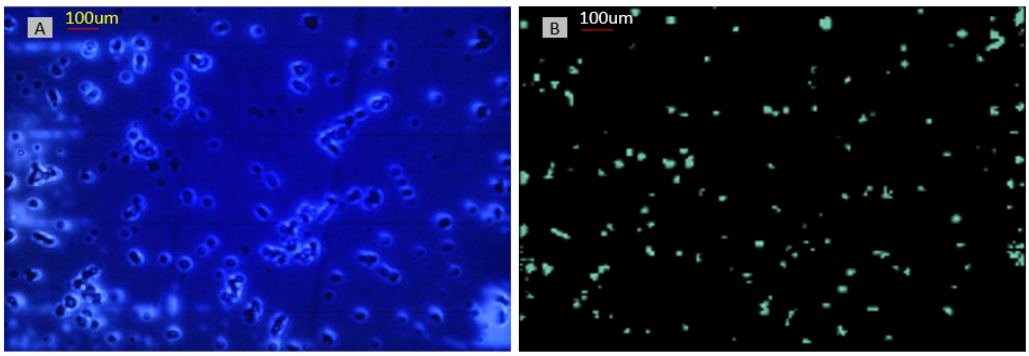

Figure 4.10: *Parallel Stimulation of a culture cell*
(A) Microscope video acquisition of cell culture parallel stimulated. We can note, how light precisely overlaps the cells. Stimulation occurs on top, image acquisition on the bottom. (B) Pattern projected by the DLP. The shapes present in the pattern are exactly those of the cells.

In this chapter we have presented the results came out from the experimental setup. In particular, we have discussed the optical properties of the system, the speed projection and the optical power capability. After that, we went ahead, showing the results of two other experiments: one application on tactile prosthesis and the other directed to the optical stimulation of cells in vitro. Also in this other two applications, we obtained very excellent outcomes, which they have demonstrated that our system works well, both from the hardware and software point of view. Moreover, we have deliberated the possibility to use this setup for in vitro experiments in optogenetics.

Conclusion

This thesis develops an innovative optogenetic stimulation system for bionic tactile prostheses. This goal has been achieved thanks to the coexistence of an artificial electronic fingertip and an optical pattern projection system. The analog signals of the artificial fingertip are digitally converted by means of ADC and sent to a FPGA.

Part of this thesis work has been devoted to the acquisition and elaboration data on a Real Time processor, interfaced with LabVIEW development environment. On RT module a time variant neuronal model has been applied, decoding digital data in somatosensory signals. The processed data are sent to the laptop, where an original conversion protocol between neuromorphic signals and optical patters projection are implemented.

To demonstrate and apply the operation of the acquisition and elaboration chain, we implemented an optical pattern projection system. In particular, we dealt with a DMD device integrated in a DLP system. This device, together with a convergent optics, gave the possibility to generate and project pattern of light at dimensions in the same order of magnitude of the cells axons. Characterization tests were made to evaluate the optical performance of the system, getting really good results in terms of optical resolution, speed projection and optical output power capability.

Consequently, we carried out two validation test to verify the implemented optogenetic stimulator system for peripheral nerve stimulation. The first test correlates the neuronal spikes activity of 16 channels of the fingertip with the overall pattern projected. A really interesting result came out from this test. The stimulation system is able to differentiate different stimuli applied to the artificial fingertip. This capability is mirrored in the projection of different patterns of light. Moreover, this makes it clear, that the implemented conversion protocol could be employed for optical tactile stimulation system. The second test demonstrates the possibility of using this setup for in vitro stimulation of cells in optogenetic applications. Indeed, we performed an experiment with culture cells. Taking a video acquisition by means of a digital Microscope, we saw in real time where the stimulation occurred. From obtained images, we realized that this setup is able to illuminate single axons of neuronal cell, giving the possibility to navigate with the light beam around cell culture. Furthermore, exploiting a LabVIEW pattern recognition function, we performed the cellular tracking and parallel cells stimulation.

We have also devised two new possible scale modeling of optogenetic stimulators for the peripheral nerves. The first one, exploits the DMD system to get spatial and time modulation of light with high optical resolution and the second one, exploits the shape modulation of the optical fiber tip, in order to tune its optical

focal distance. The goal of both devices is to stimulate different regions of the peripheral nerve with a certain spatial and time precision, in order to activate different nerve sites, to restore tactile perception to an amputee patient. For both the devices calculations on implementation and optical simulations have been carried out.

The development of this thesis has led to the resolution of challenges for the design of tactile prosthetic. In particular, we have dealt with the decoding of tactile stimuli into neural opto-physiological signals, developing the entire demonstrator system, having as initial basis of an artificial fingertip. As a result, this brought new challenges that could be developed in future endeavors.

Since the future goal is the implantation of this system in amputee patient, to restore tactile perception, in future, researchers should include many improved aspects of this technique.

In particular, we need to resize the prosthesis system to the human anatomical dimension. In this step, we have to emphasize to design a stable system, biocompatible with the anatomic tissue. Furthermore, we should design a mechanical model that can be implanted with a minimal invasive surgical operation. The proposed architectures of PNS stimulator could be used for this purpose but they still require in-depth studies of a mechanical and medical nature.

Moreover, from an electronic point of view, the first goal is reducing the power consumption of all the system, in order to have an autonomy for a certain number of hours. Another goal will be the design of an electronics dedicated for the control of the portable prosthesis.

From the optical point of view, the evolution of new high efficiency, low diffraction integrated laser sources can give a boost to the evolutions of new prostheses, avoiding the use of fragile optical fibers but directly integrating the light source in situ. Also the 2 photon stimulation and the holography 3D pattern generation could be the key points for the development of a stimulator at high spatial-temporal resolution, with a good capability of penetration in tissues.

Another critical aspect is the genetic progress. Indeed, all this makes sense only if the genetics improvements are positive for our applications.

As a matter of fact, the continuous genetic development is giving us the right motivations to aim higher and move forward, in the design of an implantable tactile prosthesis for optogenetic stimulation of the peripheral nervous system.

Bibliography

[1] K. Deisseroth, "H I S TO R I C A L C O M M E N TA RY Optogenetics : 10 years of microbial opsins in neuroscience," vol. 18, no. 9, pp. 1213–1225, 2015.

[2] E. Melin, E. E. Group, and W. N. Centre, "Optogenetic kindling," no. October, 2013.

[3] F. Zhang *et al.*, "The microbial opsin family of optogenetic tools," *Cell*, vol. 147, no. 7, pp. 1446–1457, 2011.

[4] K. L. Montgomery, S. M. Iyer, A. J. Christensen, K. Deisseroth, and S. L. Delp, "Beyond the brain: Optogenetic control in the spinal cord and peripheral nervous system," *Sci. Transl. Med.*, vol. 8, no. 337, 2016.

[5] C. Towne, K. L. Montgomery, S. M. Iyer, K. Deisseroth, and S. L. Delp, "Optogenetic Control of Targeted Peripheral Axons in Freely Moving Animals," *PLoS One*, vol. 8, no. 8, 2013.

[6] B. A. Hierlemann *et al.*, "Growing Cells Atop Microelectronic Chips: Interfacing Electrogenic Cells In Vitro With CMOS-Based Microelectrode Arrays," *Proc. IEEE*, vol. 99, no. 2, pp. 252–284, 2011.

[7] X. Li *et al.*, "Fast noninvasive activation and inhibition of neural and network activity by vertebrate rhodopsin and green algae channelrhodopsin," *Proc. Natl. Acad. Sci.*, vol. 102, no. 49, pp. 17816–17821, 2005.

[8] M. Welkenhuysen *et al.*, "An integrated multi-electrode-optrode array for in vitro optogenetics," *Sci. Rep.*, vol. 6, no. December 2015, pp. 1–10, 2016.

[9] L. A. Gunaydin, O. Yizhar, A. Berndt, V. S. Sohal, K. Deisseroth, and P. Hegemann, "Ultrafast optogenetic control," *Nat. Neurosci.*, vol. 13, no. 3, pp. 387–392, 2010.

[10] F. Zhang *et al.*, "Optogenetic interrogation of neural circuits: Technology for probing mammalian brain structures," *Nat. Protoc.*, vol. 5, no. 3, pp. 439–456, 2010.

[11] A. J. Christensen *et al.*, "In Vivo Interrogation of Spinal Mechanosensory Circuits," *Cell Rep.*, vol. 17, no. 6, pp. 1699–1710, 2016.

[12] M. Watanabe *et al.*, "The Cellular and Synaptic Architecture of the Mechanosensory Dorsal Horn," *Cell*, vol. 168, no. 1–2, p. 295–310.e19, 2017.

[13] S. Dufour, "Optrodes for combined optogenetics and electrophysiology in live animals electrophysiology in live animals," 2018.

[14] L. Sileo, M. Pisanello, M. De Vittorio, and F. Pisanello, "Fabrication of multipoint light emitting optical fibers for optogenetics," *Prog. Biomed. Opt. Imaging - Proc. SPIE*, vol. 9305, p. 93052O, 2015.

[15] G. Shin *et al.*, "Flexible Near-Field Wireless Optoelectronics as Subdermal Implants for Broad Applications in Optogenetics," *Neuron*, vol. 93, no. 3, p. 509–521.e3, 2017.

[16] K. L. Montgomery *et al.*, "Wirelessly powered, fully internal optogenetics for brain, spinal and peripheral circuits in mice," *Nat. Methods*, vol. 12, no. 10, pp. 969–974, 2015.

[17] B. Lee, "Introduction to ±12 Degree Orthogonal Digital Micromirror Devices (DMDs)," no. July 2008, pp. 1–13, 2008.

[18] J. Cha, D. Kim, G. W. Cheon, and J. U. Kang, "Spatially Multiplexed Fiber-optic SLM Microscopy for Applications of Optogenetics," *Imaging Appl. Opt. 2015*, p. IM4A.2, 2015.

[19] A. M. Leifer, C. Fang-Yen, M. Gershow, M. J. Alkema, and A. D. T. Samuel, "Optogenetic manipulation of neural activity in freely moving Caenorhabditis elegans," *Nat. Methods*, vol. 8, no. 2, pp. 147–152, 2011.

[20] P. Zhu, O. Fajardo, J. Shum, Y.-P. Zhang Schärer, and R. W. Friedrich, "High-resolution optical control of spatiotemporal neuronal activity patterns in zebrafish using a digital micromirror device," *Nat. Protoc.*, vol. 7, no. 7, pp. 1410–1425, 2012.

[21] S. Mohanty and V. Lakshminarayanan, "Optical Techniques in Optogenetics Optical techniques in optogenetics," no. May, 2015.

[22] N. Grossman, V. Simiaki, and C. Martinet, "The spatial pattern of light determines the kinetics and modulates backpropagation of optogenetic," no. November, 2012.

[23] D. Oron, E. Papagiakoumou, F. Anselmi, and V. Emiliani, *Two-photon optogenetics*, 1st ed., vol. 196. Elsevier B.V., 2012.

[24] "ENP summer school, 2017," 2017.

[25] K. Feldbauer, D. Zimmermann, V. Pintschovius, J. Spitz, C. Bamann, and E. Bamberg, "Channelrhodopsin-2 is a leaky proton pump.," *Proc. Natl. Acad. Sci. U. S. A.*, vol. 106, no. 30, pp. 12317–22, 2009.

[26] G. Nagel *et al.*, "Channelrhodopsin-2, a directly light-gated cation-selective membrane channel," *Proc. Natl. Acad. Sci.*, vol. 100, no. 24, pp. 13940–13945, 2003.

[27] R. L. Arlow, T. J. Foutz, and C. C. McIntyre, "Theoretical principles underlying optical stimulation of myelinated axons expressing channelrhodopsin-2," *Neuroscience*, vol. 248, pp. 541–551, 2013.

[28] S. Billakota and L. D. Hobson-Webb, "Standard median nerve ultrasound in carpal tunnel syndrome: A retrospective review of 1,021 cases," *Clin. Neurophysiol. Pract.*, vol. 2, pp. 188–191, 2017.

[29] T. J. Foutz, R. L. Arlow, and C. C. McIntyre, "Theoretical principles underlying optical stimulation of a channelrhodopsin-2 positive pyramidal neuron," *J. Neurophysiol.*, vol. 107, no. 12, pp. 3235–3245, 2012.

[30] M. L. Cohen, "Measurement of the Thermal Properties of Human Skin. a Review," *Journal of Investigative Dermatology*, vol. 69, no. 3. pp. 333–338, 1977.

[31] D. Ratovoson, F. Jourdan, and V. Huon, "A study of heat distribution in human skin: use of Infrared Thermography," *EPJ Web Conf.*, vol. 6, p. 21008, 2010.

[32] B. Wang *et al.*, "Firing Frequency Maxima of Fast-Spiking Neurons in Human, Monkey, and Mouse Neocortex," *Front. Cell. Neurosci.*, vol. 10, no. October, 2016.

[33] K. R. L. Hall, "RELATION OF SKIN TEMPERATURE TO PAIN," pp. 74–81, 1951.

[34] L. Beccai *et al.*, "Design and fabrication of a hybrid silicon three-axial force sensor for biomechanical applications," *Sensors Actuators, A Phys.*, vol. 120, no. 2, pp. 370–382, 2005.

[35] C. M. Oddo, M. Controzzi, L. Beccai, C. Cipriani, and M. C. Carrozza, "Roughness encoding for discrimination of surfaces in artificial active-touch," *IEEE Trans. Robot.*, vol. 27, no. 3, pp. 522–533, 2011.

[36] C. M. Oddo, L. Beccai, M. Felder, F. Giovacchini, and M. C. Carrozza, "Artificial roughness encoding with a bio-inspired MEMS- Based tactile sensor array," *Sensors*, vol. 9, no. 5, pp. 3161–3183, 2009.

[37] U. B. Rongala, A. Mazzoni, and C. M. Oddo, "Neuromorphic Artificial Touch for Categorization of Naturalistic Textures," *IEEE Trans. Neural Networks Learn. Syst.*, vol. 28, no. 4, pp. 819–829, 2017.

[38] N. M. Codes *et al.*, "16-Channel , 24-Bit Analog-to-Digital Converter," 2011.

[39] C. M. Oddo, L. Beccai, J. Wessberg, H. B. Wasling, F. Mattioli, and M. C. Carrozza, "Roughness encoding in human and biomimetic artificial touch: Spatiotemporal frequency modulation and structural anisotropy of fingerprints," *Sensors*, vol. 11, no. 6, pp. 5596–5615, 2011.

[40] E. M. Izhikevich, "Simple model of spiking neurons," vol. 14, no. 6, pp. 1569–1572, 2003.

[41] U. B. Rongala, A. Mazzoni, D. Camboni, C. Carrozza, and C. M. Oddo, "Neuromorphic artificial sense of touch : bridging robotics and neuroscience," pp. 617–630, 2018.

[42] S. Sakai, K. Ueno, T. Ishizuka, and H. Yawo, "Parallel and patterned optogenetic manipulation of neurons in the brain slice using a DMD-based projector," *Neurosci. Res.*, vol. 75, no. 1, pp. 59–64, 2013.

[43] A. P. Santos, C. A. Suaid, V. P. S. Fazan, and A. A. Barreira, "Microscopic anatomy of brachial plexus branches in wistar rats," *Anat. Rec.*, vol. 290, no. 5, pp. 477–485, 2007.

[44] R. S. Weiss, A. Voss, and W. Hemmert, "Optogenetic stimulation of the cochlea—A review of mechanisms, measurements, and first models," *Netw. Comput. Neural Syst.*, vol. 27, no. 2–3, pp. 212–236, 2016.

[45] P. Kubelka and F. Munk, "Ein Beitrag zur Optik der Farbanstriche," *Zeitschrift für Tech. Phys.*, vol. 12, pp. 593–601, 1931.

[46] F. Mapping, "Viviana Gradinaru."

Appendix A

In this appendix, we present an integration of the software materials used for the development of the thesis work. Since many of these codes present original novelties of development for applications in image processing and study of the optical properties of the system, we deem it appropriate to add them. The purpose of this thesis is also share the right knowledge and materials, to those who want to get into the world of optogenetics.

The MATLAB function, shown in Table A.1, is exploited to simulate 2D irradiance profile of the light coming from a fiber and incident in the medium, taking into account scattering and absorption of the matter. The function takes in input the NA and the core radius of a fiber and gives in output the irradiance profile as a 2D matrix. In [44] and [45] is possible to find a detailed explanation of the formulas used in the model. Moreover, the coefficient used in the model are taken from [46]. For the absorption and scattering effects, this function implements the Kubelka-Munk model.

```
function B = Intensity_profile(NA, r0)
%------initialization variables------
n0 = 1.36; % Tissue refractive index
rmax = 2*r0; % Transverse plot dimensions (micrometers)
zmax = 6*r0; % Longitudinal plot dimensions (micrometers)
dz = 10; % z increment (micrometers)
dr = 0.5; % r increment (micrometers)
K = 0.0001;% absorption coefficient (um^-1)
S = 0.005;% Scattering coefficient (um^-1)
l=0; j=0; %indices
theta = asin(NA/n0); % Divergence half-angle

%-------computing profile------
for z = 0:dz:zmax
z0(l+1)=l*dz;
l=l+1;
for r = -rmax:dr:rmax
j=j+1;
C = r0/(r0 + z*tan(theta)); % Geometric factor
G = (1/(2*pi))*exp(-2*(r/(r0 + z*tan (theta)))^2); % Gaussian factor
a = 1+(K/S);
b = ((a^2)-1)^0.5;

%Absorption and scattering
M = b/((a*sinh(b*S*((r^2+z^2)^0.5))) +(b*cosh(b*S*((r^2+z^2)^0.5))));
B(j,l)=C*G*M;
end
j=0;
end

%-----plots----------
imagesc(0:zmax,-rmax:rmax,B);
colormap(hot);
xlabel('Axial distance (microns)');
```

```
35  ylabel('Transverse distance (micons)');
36  title('Irradiance profile');
37  figure();
38  [m,n]=size(B);
39  B0=B(round(m/2),:)/max(B(round(m/2),:));
40  % Normalized value of the longitudinal profile for r=0;
41  plot(z0,B0);
42  xlabel('Axial distance (microns)');
43  ylabel('Normalized intensity at fiber tipcenter (N.U.)';
44  title('Longitudinal Irradiance profile');
```

Table A.1: *2D Irradiance Profile Simulation*

The MATLAB script, shown in Table A.2, has been implemented to analyze the screenshot taken by the Digital Microscope. The script takes in input the image and the Microscope field of view. The image is converted from RGB to gray scale and a low pass Gaussian filter is applied to dull the discontinuities, the average background is extracted and subtracted from the image. The area of the beam, its radius and the FWHM is calculated.

```
1   %---------clean before run-------------
2   clc
3   clear all
4   %close all
5
6   % --------Variable declaration-----------
7   Xres=1.564; %X dimension image in (mm)
8   Yres=1.173; %Y dimension image in (mm)
9   threshold=0;% FWHM for getting resolution
10
11  %image acquisition and get size
12  I1=imread('1PER1.bmp');
13  Dim=size(I1);
14
15  %create new matrix image
16  Im=zeros(Dim(1),Dim(2)-1,'uint8');
17  %remove the zero row in the matrix, the camera gives us this artifact
18  Iresize=I1(1:Dim(1)-1,1:Dim(2)-1,1:3);
19  %gray scale transform
20  Im=rgb2gray(Iresize);
21  % gaussian filter
22  Im = imgaussfilt(Im,2);
23  %show image
24  imshow(Im)
25
26  %computation of the zero level offset, to remove the background
27  Mode=mode(Im);
28  Mean=mean(Mode);
29  %X and Y generation
30  X=[0:Xres/(Dim(1)-1):Xres-Xres/(Dim(1)-1)];
31  Y=[0:Yres/(Dim(2)-1):Yres-Yres/(Dim(2)-1)];
32
33  % remove the back ground
34  Im=Im-Mean;
35
36  -------FWHM------------
```

```
Max=max(Im(:));
% half of the max will be the FWHM threshold
threshold=Max/2;

%plot
mesh(Y,X,Im)
xlabel('x(mm)');
ylabel('y(mm)');
zlabel('Pixel Value');

%-------area computation--------
countArea=0;
for i=1:Dim(1)-1
for j=1:Dim(2)-1
if Im(i,j)>threshold;
countArea=countArea+1;
end
end
end
%finding the ratio between the lmbeam area and the overall microscope area
Ratio=countArea/((Dim(1)-1)*(Dim(2)-1));
Area= Xres*Yres*Ratio;
% approximation it is a circle so we get the radius
Radius=sqrt(Area/pi);
%----------end--------
```

Table A.2: *Pattern resolution study*

The MATLAB script, shown in Table A.3, is a simple and fast implementation of the Izhikevich model. Useful, if we want to analyze how the spikes rate changes when model parameters are modified. The script takes as input all the model parameters and gives as output the plot of the related spikes.

```
% E M Izhikevich: Simple Models of Spiking Neurons
%equations
%dv/dt=0.04v^2+5v+140-u+I
%du/dt=a(bv-u)
%If v≥30mV then v←c
% and u←u+d
%close all
clc
clear all

% Input parameters-------------------------------
N = 5000;    % number of grid points
tMax = 100;  % max time [ms]
% model parameters a b c d I
a = 0.02;
b = 0.4;
c = -65;
d = 2;
I = 10;

% solve equation---------------------------------
cc(1) = 0.04; cc(2) = 5; cc(3) = 140;    % D.E. coefficients
```

```
22  t = linspace(0,tMax,N);                % time steps [ms]
23  v = zeros(N,1); vM = zeros(N,1);
24  u = zeros(N,1); uM = zeros(N,1);       % recovery variable
25  Iext = zeros(N,1);
26  Iext(N/10:end) = I;
27  dt = t(2)-t(1);
28  v(1) = -65;
29  vM(1) = -65;
30  u(1) = b * v(1);
31  uM(1) = u(1);
32  for n = 1 : N-1
33  v(n+1) = v(n) + dt*( cc(1)*v(n)^2 + cc(2)*v(n) + cc(3) + Iext(n) - u(n) );
34  u(n+1) = u(n) + dt*a*( b*v(n) - u(n) );
35  if v(n+1) > 30;
36  vM(n+1) = 30;
37  v(n+1) = c;
38  u(n+1) = u(n+1) + d;
39  else
40  vM(n+1) = v(n+1);
41  uM(n+1) = u(n+1);
42  end
43  end

44  %plot----------------------------------------
45  figure(2)
46  set(gcf,'units','normalized','Position',[0.3 0.32 0.32,0.38]);
47  set(gca,'fontsize',12);
48  hSubplot = subplot(2,1,1);
49  set(hSubplot,'position',[0.13 0.46 0.78 0.45]);
50  xP = t; yP = vM;
51  plot(xP,yP,'b','lineWidth',2);
52  ylabel('v_M [mV]');
53  grid on
54  set(gca,'fontsize',12);
55  hSubplot = subplot(2,1,2);
56  set(hSubplot,'position',[0.13 0.15 0.78 0.20]);
57  xP = t; yP = Iext;
58  plot(xP,yP,'r','lineWidth',2);
59  xlabel('time t [ms]');
60  ylabel('c_5 I_{ext} [mV]');
61  axis([0 tMax 0 1.2*max(Iext)]);
62  grid on
63  set(gca,'fontsize',12);
```

Table A.3: *Izhikevich model MATLAB Script*

The Virtual Instrument program, shown in Figure A.1, has been implemented to study the optical resolution of the system. Basically, we projected different patterns of light useful to highlight the resolution capabilities, like: dots, different size squares, segments, circles of different radius.

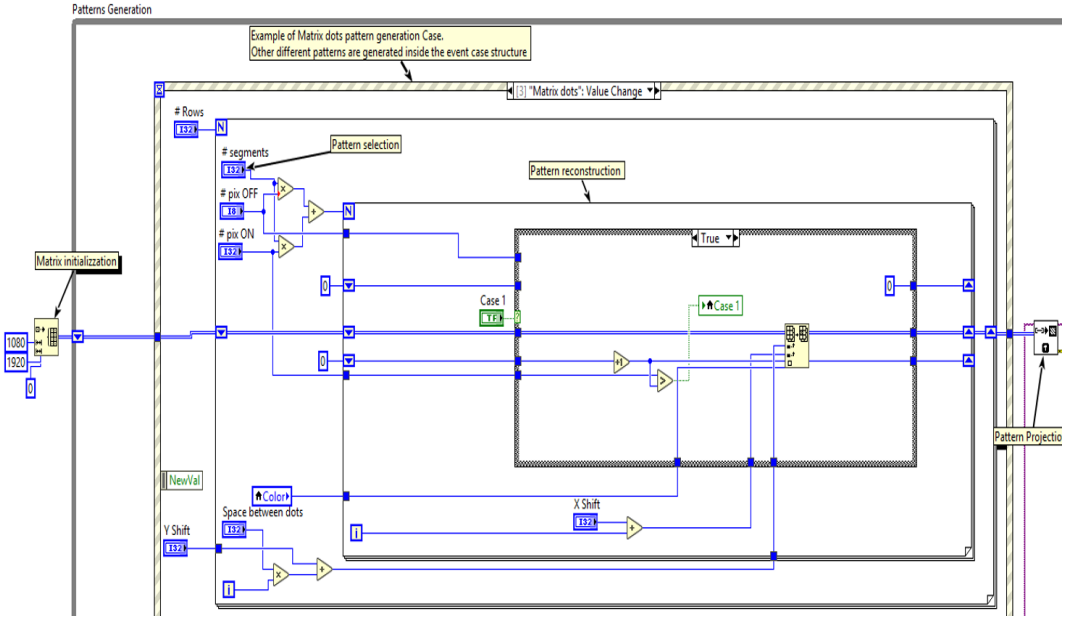

Figure A.1: *Virtual Instrument Patterns Generation*
This VI projects multiple pattern selecting them using an event structure. The pattern is projected in a second window and sent to the DLP system via HDMI communication.

The Virtual Instrument program, shown in Figure A.2, is used to test the DLP projection speed. The program implements a timed sequence of solid patterns (red and black) and HDMI communication.

The Table A.4 shows the batch file used to implement the same task of the previous VI, sending instructions direct to the DLP by means of I2c communication

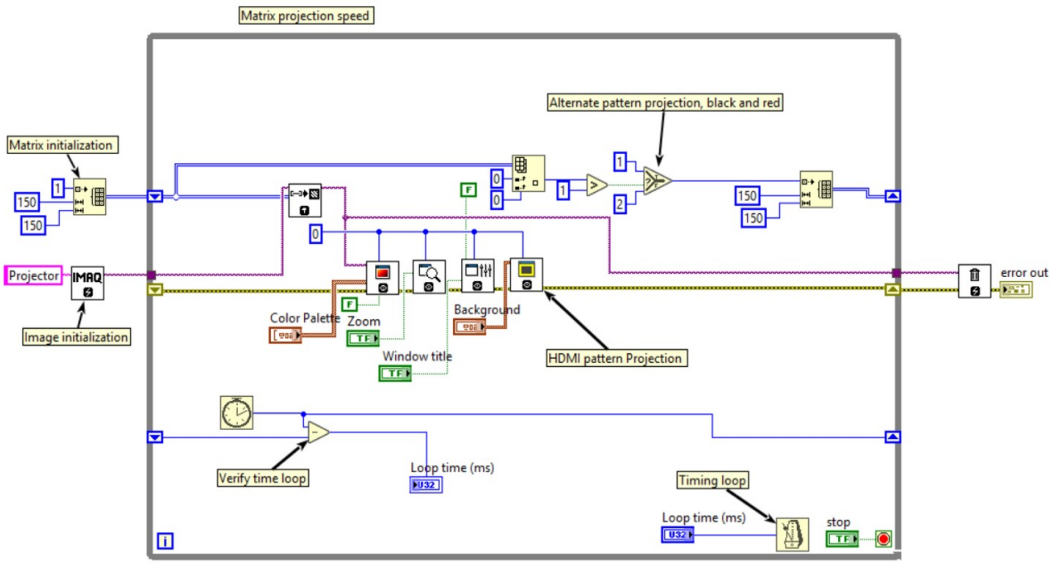

Figure A.2: *Virtual Instrument Timed Pattern Generation*
This VI projects timed pattern in sequence. The pattern is a solid color (red LED) follow by a black pattern. The loop generation is timed by the user and it is possible go fast until 500fps. The pattern is projected in a second window and sent to the DLP system exploit the HDMI communication.

```
.#####################################
#       PATTERN PROJECTION
#####################################
# Write: DisplaySize
W 36 12 80 07 38 04

#Write Test Pattern Select (solid color pattern)
W 36 0B 00 03

# Write: InputSourceSelect (Test pattern generation)
W 36 05 01

#Loop LED ON-OFF
:LOOP

# Write: WRITE RED LED ENABLE
W 36 52 02

# delay
W 36 DB 64 00

# Write: WRITE LED DISABLE
W 36 52 00

# delay
W 36 DB 64 00

GOTO LOOP
```

Table A.4*: Batch file Timed Pattern Generation*

The Figure A.3 shows how we can modulate the projection area of the pattern depending on the value of the difference between the current and previous ISI. A counter is implemented to count the number of pix on and off at the same time, exploiting the overflow of U8 data. A matrix, divided in 16 parts gives the information related to the ISI of the channels. The matrix created is scaled to projection dimension and sent for visualization.

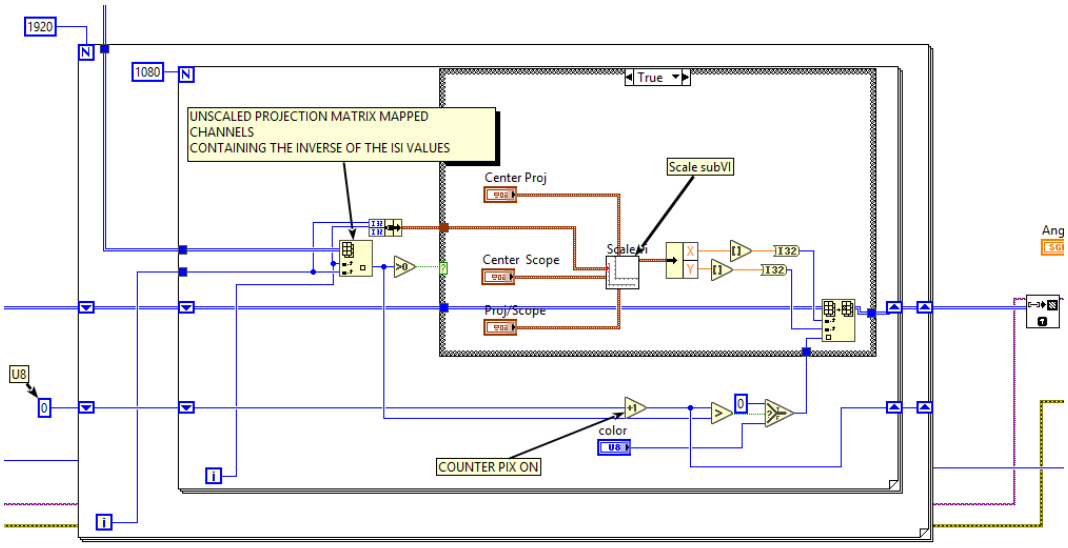

Figure A.3: *Patterns projection area modulation Virtual Instrument*

The Figure A.4 shows the Virtual Instrument to navigate with a beam of light on cell culture. After projection matrix initialization, we project a beam of light. During execution the beam can be shifted around the projection matrix to illuminate different region of cell culture. By modulating the number of micromirror in ON state, we can also tune the beam radius.

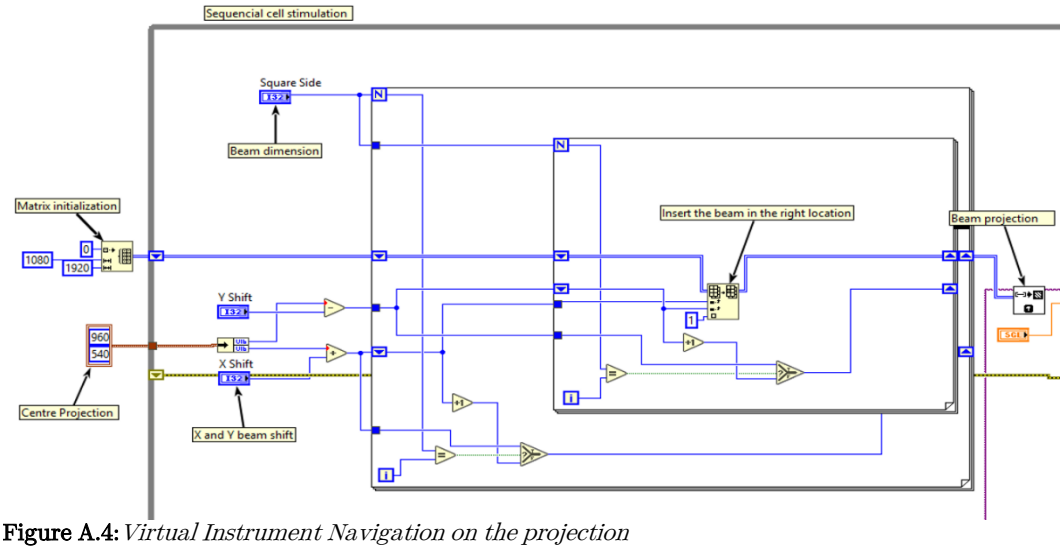

Figure A.4: *Virtual Instrument Navigation on the projection*

The Figure A.5 shows the Virtual Instrument for cells detection and tracking. The images sequence acquired by the Microscope are given as input to a function for color threshold detection (LabVIEW function). Basically, this function detects the difference of a single color on the image. If the color is above or below the threshold, the function returns a matrix of 1 or 0 of the same image input size. If the color is above the threshold is 1, otherwise 0. Background light is important for this algorithm, in order to increase contrast and thus the detection probability. The out matrix is going to be scaled by a factor equal to the ratio between the projection dimension and the Microscope acquisition field of view. We also have the possibility to rotate the projection respect to the center of projection and make the symmetric of it. In this way, the projection image can be perfectly aligned with the acquisition field of view. A fast manual calibration is needed before starting with a known sample.

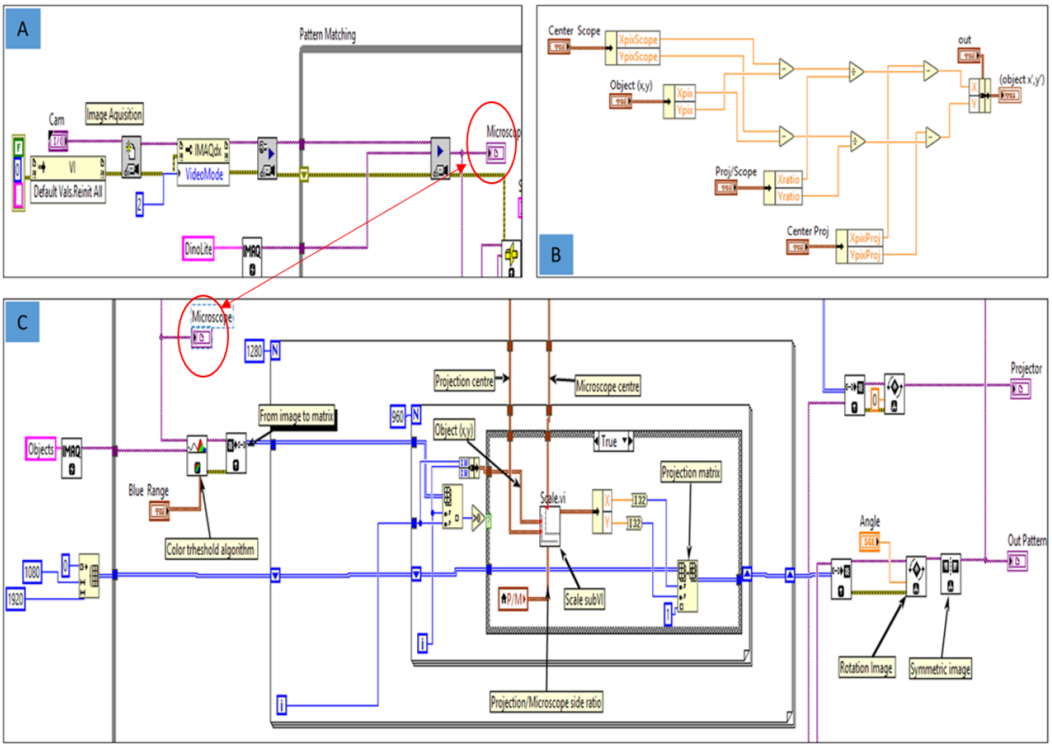

Figure A.5: *Pattern Detection Virtual Instrument*
(A) These function allow a Real Time image acquisition from the Microscope. (B) Scale subVI function, used to match the projection matrix with the acquired matrix form the Microscope. (C) Color threshold function and projection matrix generation.